Gradstein F. M., Ludden, J. N., et al., 1992
Proceedings of the Ocean Drilling Program, Scientific Results, Vol. 123

1. DEPOSITIONAL HISTORY, NANNOFOSSIL BIOSTRATIGRAPHY, AND CORRELATION OF ARGO ABYSSAL PLAIN SITES 765 AND 261[1]

Julie A. Dumoulin[2] and Paul R. Bown[3]

ABSTRACT

Sediments from the Argo Abyssal Plain (AAP), northwest of Australia, are the oldest known from the Indian Ocean and were recovered from ODP Site 765 and DSDP Site 261. New biostratigraphic and sedimentologic data from these sites, as well as reinterpretations of earlier findings, indicate that basal sediments at both localities are of Late Jurassic age and delineate a history of starved sedimentation punctuated by periodic influx of calcareous pelagic turbidites.

Biostratigraphy and correlation of Upper Jurassic–Lower Cretaceous sediments is based largely on calcareous nannofossils. Both sites yielded variably preserved nannofossil successions ranging from Tithonian to Hauterivian at Site 765 and Kimmeridgian to Hauterivian at Site 261. The nannofloras are comparable to those present in the European and Atlantic Boreal and Tethyan areas, but display important differences that reflect biogeographic differentiation. The Argo region is thought to have occupied a position at the southern limit of the Tethyan nannofloral realm, thus yielding both Tethyan and Austral biogeographic features.

Sedimentary successions at the two sites are grossly similar, and differences largely reflect Site 765's greater proximity to the continental margin. Jurassic sediments were deposited at rates of about 2 m/m.y. near the carbonate compensation depth (CCD) and contain winnowed concentrations of inoceramid prisms and nannofossils, redeposited layers rich in calcispheres and calcisphere debris, manganese nodules, and volcanic detritus. Lower Cretaceous and all younger sediments accumulated below the CCD at rates that were highest (about 20 m/m.y.) during mid-Cretaceous and Neogene time. Background sediment in this interval is noncalcareous claystone; turbidites dominate the sequence and are thicker and coarser grained at Site 765.

AAP turbidites consist mostly of calcareous and siliceous biogenic components and volcanogenic smectite clay; they were derived from relatively deep parts of the continental margin that lay below the photic zone, but above the CCD. The Jurassic–Lower Cretaceous section is about the same thickness across the AAP; turbidites in this interval appear to have had multiple sources along the Australian margin. The Upper Cretaceous–Cenozoic section, however, is three times thicker at Site 765 than at Site 261; turbidites in this interval were derived predominantly from the south.

Patterns of sedimentation across the AAP have been influenced by shifts in sea level, the CCD, and configuration of the continental margin. Major pulses of calcareous turbidite deposition occurred during Valanginian, Aptian, and Neogene time—all periods of eustatic lowstands and depressed CCD levels. Sediment redeposited on the AAP has come largely from the Australian outer shelf, continental slope, or rise, rather than the continent itself. Most terrigenous detritus was trapped in epicontinental basins that have flanked northwestern Australia since the early Mesozoic.

INTRODUCTION

The Argo Abyssal Plain is underlain by the oldest oceanic crust (Late Jurassic) yet recovered from the Indian Ocean (Veevers, Heirtzler, et al., 1974; Sager et al., this volume). Sediments of the Argo Abyssal Plain have been recovered from two deep-sea drilling sites: Site 261 (Leg 27) and Site 765 (Leg 123) (Fig. 1). Sediments directly overlying basement at Site 261 include nannofossils of Kimmeridgian–early Tithonian age, and these data have constrained subsequent interpretation of the seafloor magnetic anomaly patterns across the basin (Fullerton et al., 1989). Site 765 was drilled on magnetic anomaly M26 (Oxfordian) but basal sediments were essentially barren of age-diagnostic microfossils, and initially, their age was interpreted as Early Cretaceous (late Berriasian–early Valanginian) (Ludden, Gradstein, et al., 1990). Detailed sedimentologic and biostratigraphic analyses presented here include considerable new data as well as reinterpretations of earlier findings (Veevers, Heirtzler, et al., 1974; Ludden, Gradstein, et al., 1990) and have led us to conclude that the basement at both sites is Late Jurassic.

This study presents sedimentologic description and environmental interpretation of the abyssal plain pelagic and redeposited sedimentary sequences at both sites, with particular emphasis on the Upper Jurassic–Lower Cretaceous strata. This is followed by nannofossil biostratigraphy of the lower cores of both sites and a review of additional biostratigraphic data. Last, a biostratigraphic and lithologic correlation of the two sites is presented, and implications for the tectonic evolution and sedimentary development of this region of the Indian Ocean are discussed.

The AAP sedimentary succession described below is divided into lower and upper sequences, based on differences in seismic character and depositional environments. Upper Jurassic–Lower Cretaceous sediments make up the lower sequence, which is acoustically transparent and conformably draped over basement (Robinson et al., 1974). It was deposited during a "juvenile ocean phase" characterized by more condensed, less calcareous sedimentation (Veevers and Johnstone, 1974; von Rad et al., 1989). The upper sequence consists of flat-lying, acoustically layered Upper Cretaceous–Cenozoic sediments. These strata accumulated during the "mature ocean phase" of Veevers and Johnstone (1974), von Rad et al. (1989), and others, a time marked by "mature" thermohaline circulation in the Indian Ocean and dominantly calcareous sedimentation along the northwest Australian margin.

---

[1] Gradstein, F. M., Ludden, J. N., et al., 1992. *Proc. ODP, Sci. Results,* 123: College Station, TX (Ocean Drilling Program).

[2] Earth Sciences Board, University of California, Santa Cruz, CA 95064, U.S.A. Present address: U.S. Geological Survey, 4200 University Drive, Anchorage, AK 99508-4667, U.S.A.

[3] Department of Geological Sciences, University College London, London WC1E 6BT, U.K.

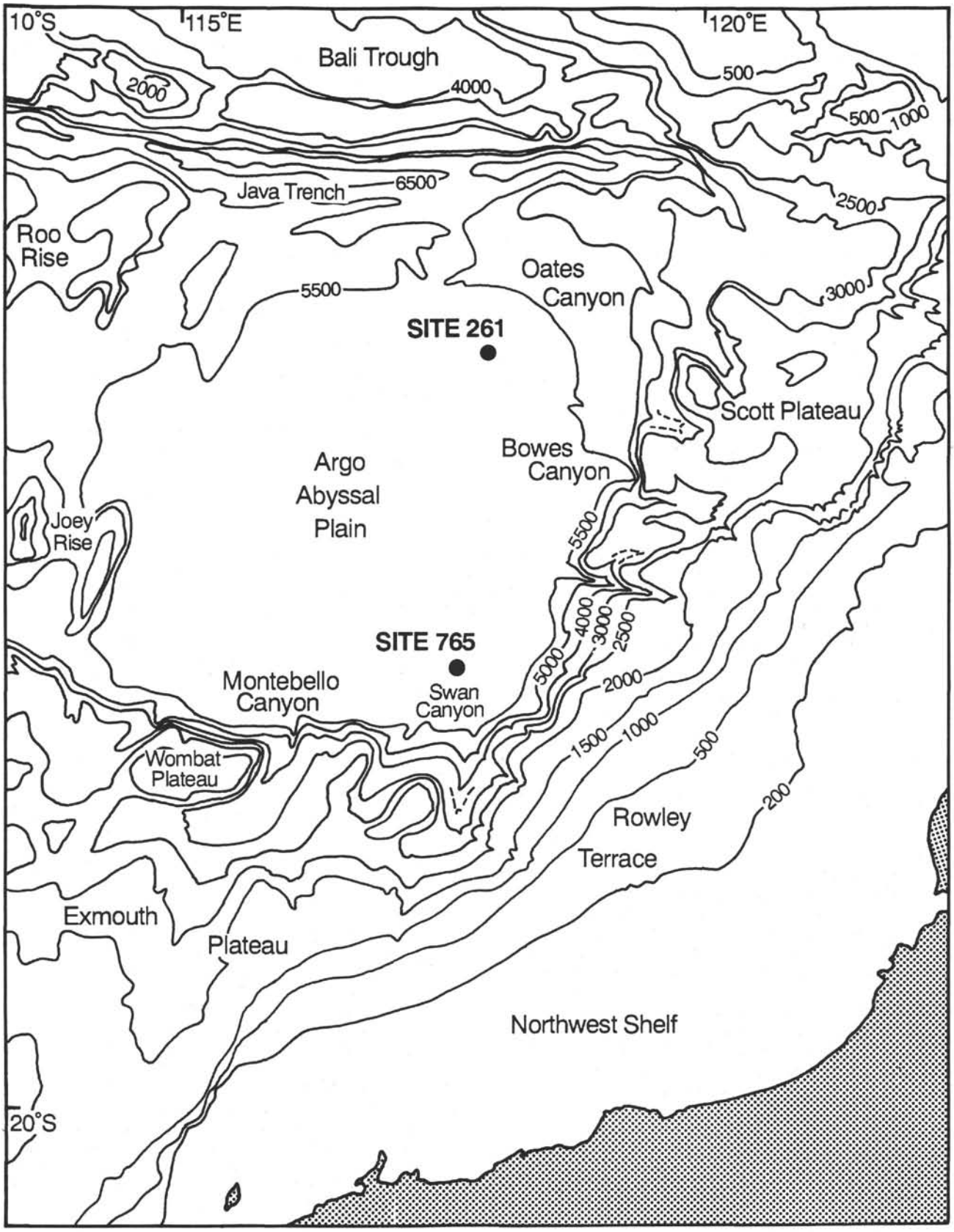

Figure 1. Regional setting and location of Sites 765 and 261. Contour interval in meters.

METHODS, DATA SOURCES, AND DEFINITIONS

The authors examined and sampled Site 765 cores aboard the *JOIDES Resolution* and subsequently at the ODP Gulf Coast Repository; Site 261 cores were studied and sampled at the DSDP West Coast Repository. Petrographic descriptions are based on examination of all cores recovered from both sites, more than 300 smear slides and 210 thin sections made from these cores, and scanning electron microscope, electron dispersive (EDS), and X-ray diffraction analyses of selected samples. Carbonate content of sediment samples analyzed for this chapter was determined by total combustion with a LECO CS/125 elemental analyzer, after subtraction of organic carbon (which was determined for acid-washed samples by the same method). Biostratigraphy relies largely on calcareous nannofossils from the two sites. These were studied using both the light and scanning electron microscopes. Routine biostratigraphy was performed using the light microscope and smear slides.

All SEM and EDS data and some carbonate content analyses in this chapter are new. XRD and additional carbonate content and microfossil data originally included in the initial reports of Sites 765 and 261 are summarized and cited where appropriate.

For Site 765, the sedimentology of the lower sequence presented here is based largely on detailed thin section observations performed after completion of shipboard studies. Sedimentology of the upper sequence is a summary of shipboard studies and is included here so that the sediments may be correlated with those at Site 261.

Only a brief, generalized description of the Site 261 sediments has been previously published (Veevers, Heirtzler, et al., 1974). We reexamined the entire section and performed additional petrographic studies to facilitate detailed correlation with the section at Site 765; all thin section data from Site 261 presented below are new.

The ODP classification scheme (see Ludden, Gradstein, et al., 1990, "Explanatory Notes" chapter) is used for most sediments described here. However, "marl" is used in place of "mixed sediment" for fine-grained sediment that contains less than 60% pelagic grains and less than 60% siliciclastic grains. Marl is also used for limy sediment that has an imprecisely known or highly inhomogeneous (on a small scale) carbonate content. "Calcareous sediment" is used here for limy sediment with a range of textural grades and carbonate contents (generally 20% $CaCO_3$ or greater). Calcareous sediments are dominantly turbidites, texturally and compositionally graded, and include sand-, silt-, and clay-sized material. Radiolarite refers to a firm, silt- to sand-sized sediment composed of at least 60% pelagic skeletal grains, of which more than 50% are radiolarians. Radiolarian claystone contains at least 60% clay and 10% or more radiolarians.

SITE 765 SEDIMENTS

Sedimentary Sequence

A 935-m-thick sedimentary section was drilled at Site 765 (Fig. 2); our study focuses on the 270-m-thick lower sequence (Cores 123-765C-62R through -34R; Units VII through IVC of Ludden, Gradstein, et al., 1990). We subdivided this interval into four lithologic units, L1 to L4 (one unit was further split into two subunits), distinguished chiefly by the presence or absence of calcareous material. Units are numbered stratigraphically upward and given the prefix L to distinguish them from units of the upper sequence. The lowest unit, 1.5 m of noncalcareous silty claystone, directly overlies igneous basement. The second unit, 10 m of inoceramid-bearing sediment, contains local concentrations of calcispheres and calcisphere debris. About 75 m of noncalcareous claystone with subordinate layers of radiolarite, bentonite, and redeposited calcareous sediment makes up the third unit, which was divided into two subunits based on the absence of calcareous sediment from the lower 27 m. The fourth unit constitutes most of the lower cores and is 180 m thick; it consists primarily of radiolarian claystone. Ages of the units given below are based on biostratigraphic and lithostratigraphic evidence discussed later in the chapter.

The upper sequence (Cores 123-765C-33R through -1R and 123-765B-41X through -1H; Units IVB–I of Ludden, Gradstein, et al., 1990) consists of calcareous material redeposited by gravity flows intercalated with various pelagic clays and claystones. Three units are recognized, U1 through U3, based primarily on changes in color and composition of "background" pelagic claystones through the section. This subdivision differs slightly from that used by Ludden, Gradstein, et al. (1990), which was based primarily on changes in grain-size and composition of the redeposited calcareous sediments.

Lower Sequence (Cores 123-765C-62R through -34R)

Unit L1, Silty Claystone ([?]Tithonian or older; Section 123-765C-62-4, 28 cm, to 62R-3, 35 cm; 931.2–929.7 m sub-bottom)

Description

The deepest sediment at Site 765 is 150 cm of essentially noncalcareous silty claystone (lower part of Subunit VIIB of Ludden, Gradstein, et al., 1990) that immediately overlies basalt. The contact between volcanic basement and sedimentary cover was recovered intact and consists of a few centimeters of basalt hyaloclastite, altered to celadonite, with a matrix of white sparry calcite and red-brown claystone. Aphyric pillow basalt occurs directly below the contact and dominates the 247-m-cored basement interval (Ludden, Gradstein, et al., 1990). No sediment was found intercalated within the volcanic rocks at this site.

The basal 7 cm of Unit L1 is firm, dusky red claystone like that interstitial to the basalt hyaloclastite; the rest of the unit is reddish-brown, locally silty claystone with a firm to sludgy texture. The claystone appears homogeneous and lacks megascopic sedimentary structures. It contains 5% to 20% silt and lesser sand, largely disseminated, but locally concentrated into grain-supported millimeter-scale lenses and laminae.

Clays in this unit are randomly interstratified illite/smectite (I/S) that contains about 33% illite layers, and lesser discrete illite (Compton and Locker, this volume). Angular quartz makes up much of the coarse fraction, but volcanic detritus is also notable (Fig. 3). Volcanic lithic clasts include lathwork grains and altered volcanic glass, and much of the smectitic I/S may have been derived from mafic volcanic material (Compton and Locker, this volume). Plagioclase, microcline, white mica, and phosphatic debris occur in trace amounts. Abundant agglutinated foraminifers are the only microfossils observed (Ludden, Gradstein, et al., 1990).

Opaque material is common and occurs as disseminated, typically oval micronodules (10–200 μm in diameter) and coatings on sand-sized grains. Rare larger nodules (to 4 mm) occur toward the top of the unit. Most of these opaques are probably manganese; similar micronodules in the overlying inoceramid-rich claystone are known to consist of manganite, and 2.33% MnO was detected in XRF analysis of a bulk sediment sample from Section 123-765C-62R-3 (Ludden, Gradstein, et al., 1990).

Carbonate content in this interval is negligible—0.3% to 0.5% (Table 1; Ludden, Gradstein, et al., 1990). Thin section observa-

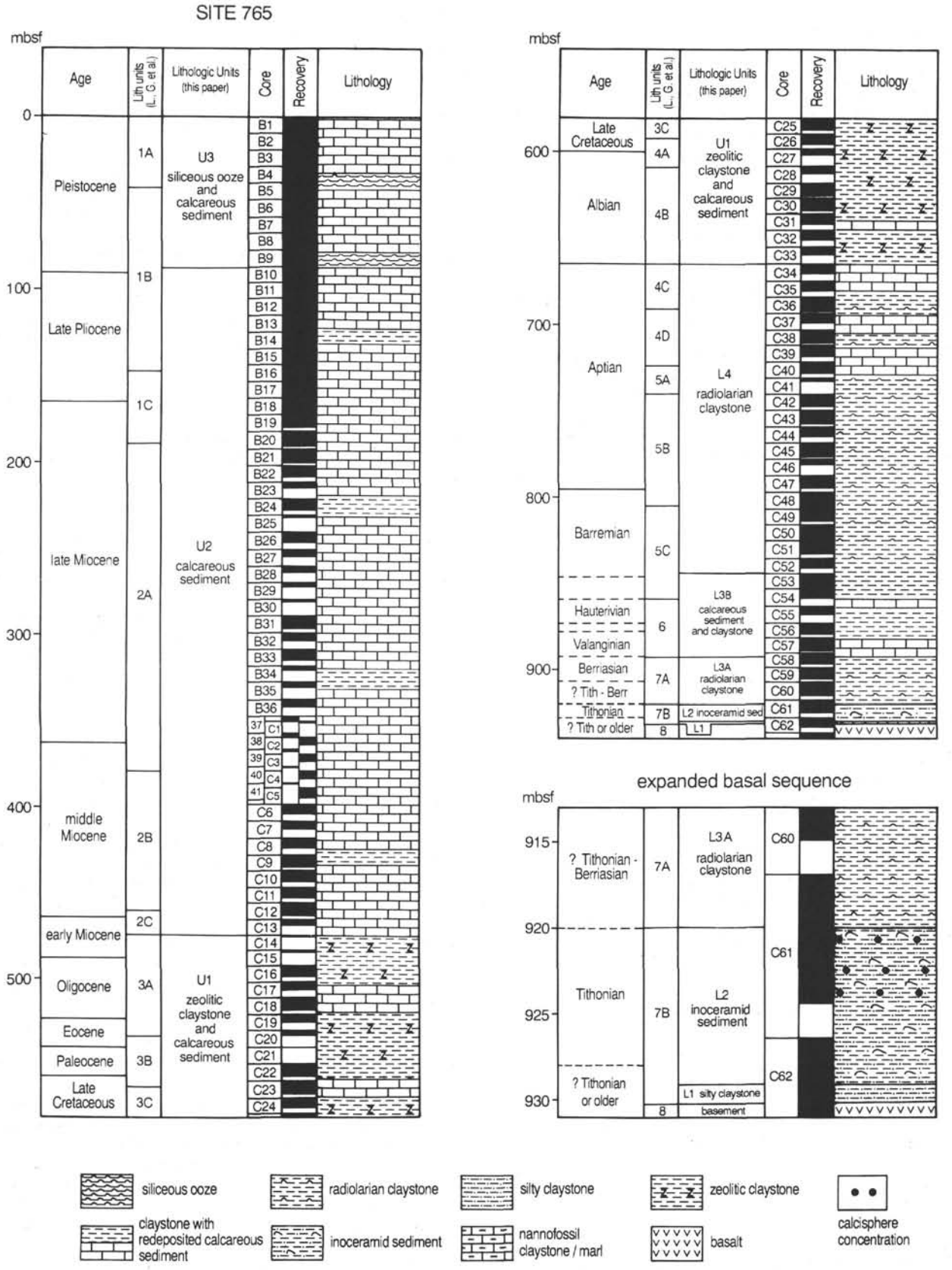

Figure 2. Stratigraphic section at Site 765; depths are in meters below seafloor. Age determination after Kaminski, Baumgartner, et al. (this volume), modified in the lower cores based on nannofossil data presented here.

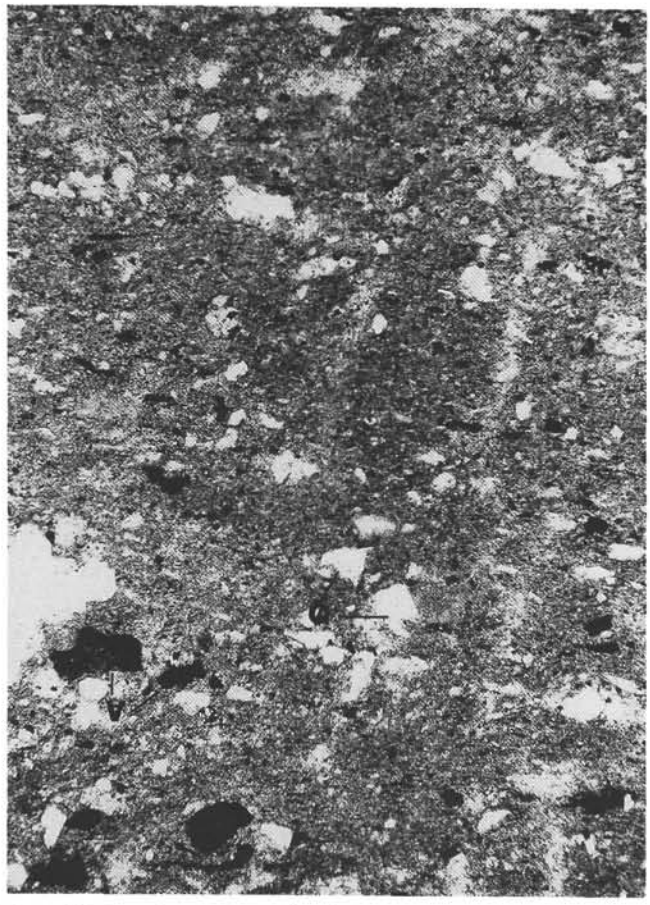

Figure 3. Photomicrograph of abundant angular quartz (Q) and manganese-coated volcanic lithic clasts (V) in silty claystone (Sample 123-765C-62R-3, 134–136 cm; scale bar is 0.2 mm).

tions indicate that calcite occurs as rare small grains (strongly etched, probable inoceramid prisms) and irregular diagenetic patches.

Interpretation

These sediments represent the first material deposited above the mid-ocean spreading center. The fauna is limited to agglutinated foraminifers of the *Trochammina quinqueloba* Assemblage, which appear autochthonous and signify bathyal or greater water depths (Kaminski, Gradstein, et al., this volume). The virtual absence of calcium carbonate indicates that sedimentation took place beneath the CCD, and the pervasive reddish-brown color denotes an oxic depositional environment. Volcanic detritus was likely derived from the spreading center itself, but the abundance of angular quartz grains reflects influx from the continental margin. Some terrigenous material in this unit might be eolian (Compton and Locker, this volume). Ludden, Gradstein, et al. (1990) suggested that the presence of abundant detrital material in this unit indicates relatively rapid rates of sedimentation. However, the abundance of manganese as nodules and grain coatings implies slow sedimentation, as does the magnetostratigraphy (Ogg et al., this volume).

Unit L2, Inoceramid Sediment (Tithonian; Sections 123-765C-62R-3, 35 cm, through -61R-3, 0 cm; 929.7–919.9 m sub-bottom)

Description

General features. Overlying the noncalcareous claystone is 10 m of dominantly brown to reddish-brown calcareous claystone to clayey sandstone; the calcareous component is largely inoceramid bivalve shell debris and lesser calcispheres and nannofossils. This facies also contains notable noncalcareous detritus (volcanic clasts and quartz), manganese nodules, and a few bentonite layers. The base of the inoceramid sediment unit is not obvious in core without applying hydrochloric acid, but is readily apparent in thin section or smear slide. We place the lower boundary at the abrupt appearance of abundant inoceramid prisms (detected in smear slide); nannofossils first appear slightly higher (Section 123-765C-62R-2, 13 cm). Calcispheres and calcisphere debris occur mostly in the upper part of the unit (Sections 123-765C-61R-5 through -3). The inoceramid sediment unit is equivalent to the upper part of Unit VIIB of Ludden, Gradstein, et al. (1990).

Texture throughout the lower half of Unit L2 (Core 123-765C-62R) is strikingly heterogeneous; claystone alternates with calcareous siltstone or sandstone on a scale of millimeters to centimeters (Fig. 4A). Sand-sized grains are largely inoceramid prisms and occur dispersed throughout the mud matrix or, more commonly, concentrated into thin laminae, lenses, and pods. The shell material is white and where most abundant imparts a speckled appearance to the core. Distinct white lenses 1 to 5 mm thick are most evident in intervals 123-765C-62R-1, 120–150 cm, -62R-2, 80–100 cm, and -62R-3, 0–6 cm.

The upper half of the unit (Core 123-765C-61R) appears more homogeneous; sand is less abundant and mostly disseminated. Several intervals rich in silt (calcispheres and calcisphere debris) are distinguished by their lighter color (reddish or pale green) and irregularly mottled aspect (Fig. 4B). This mottled texture may reflect pervasive bioturbation, but discrete burrow structures are rare. Small vertical to oblique brown tubes (*Trichichnus*? *Chondrites*?) are locally evident in core and thin section and may be filled with mud or sand.

Unit L2 is calcareous throughout, but carbonate is unevenly distributed on a microscopic scale and in general decreases upward. Shipboard (Ludden, Gradstein, et al., 1990) and shore-based (this study) carbonate content analyses (Table 1) found 41% to 61% calcium carbonate in inoceramid sediment samples from Core 123-765C-62R, and 10% to 27% in samples from Core 123-765C-61R. Low values (9%–10%) occur in impure bentonites and high values (46%–67%) characterize the zones rich in calcisphere debris. Thin section and smear slide observations indicate that carbonate grains make up 60% to 99% of layers and lenses a few millimeters to several centimeters thick throughout the inoceramid sediment facies; finer-grained interlayers generally contain much less calcareous material. Coarse calcareous layers decrease in abundance and thickness upward within the unit.

Inoceramid concentrations. Inoceramid remains are found throughout Unit L2, chiefly as discrete individual prisms. No complete inoceramid shells were observed, but fragments several millimeters in size (made up of 10 or more still articulated prisms) occur locally (Plate 1, Fig. 1). The highest prism concentrations (60% or more) are in lenses and laminae 0.1 to 1.0 cm long and 0.3 to 1.0 mm thick (Plate 1, Figs. 2, 3). Such lenses make up 3% to 30% of this unit and are thickest, most abundant, and richest in inoceramid grains in Section 123-765C-62R-1. Within these lenses, prisms are grain-supported and somewhat size-sorted;

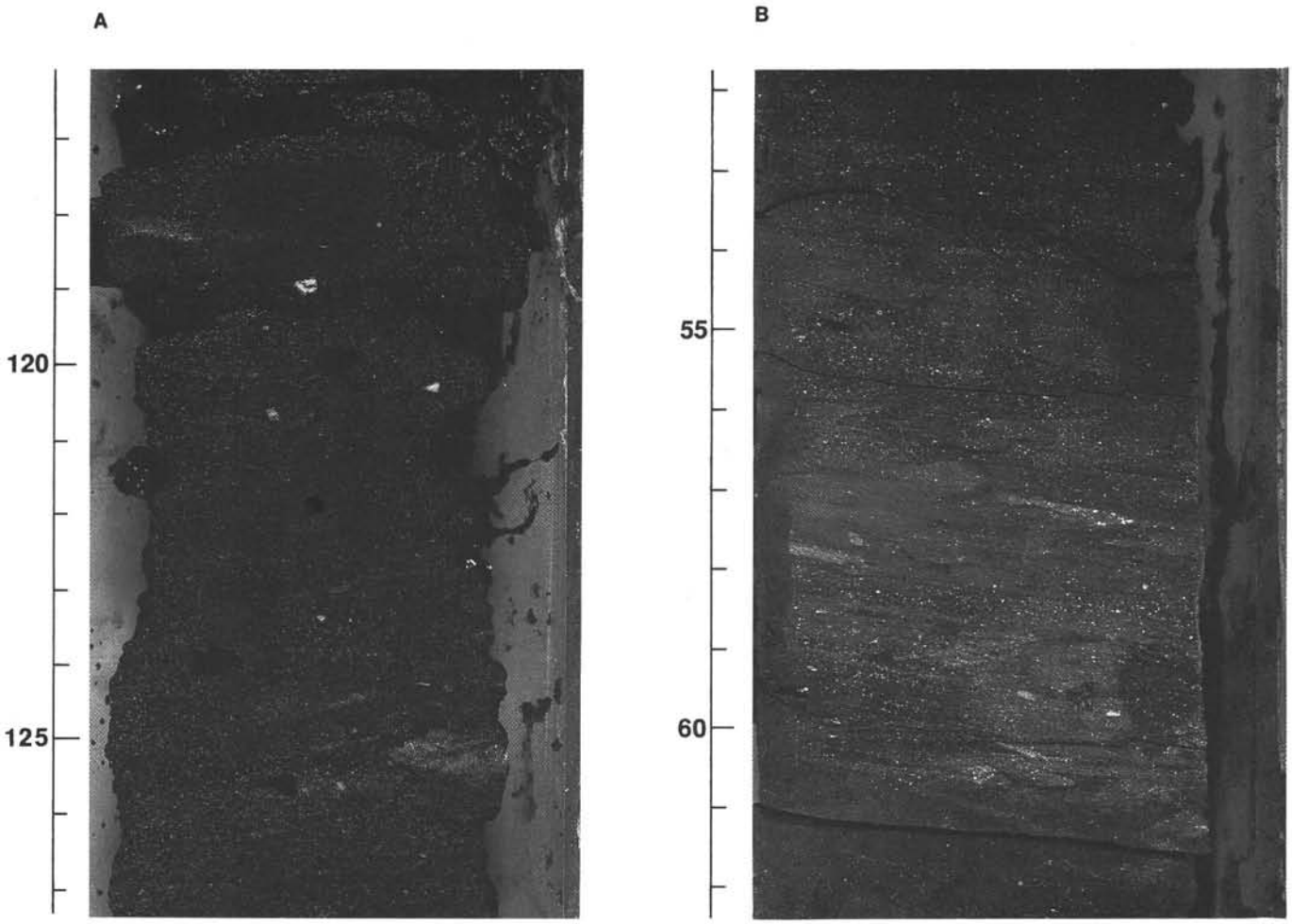

Figure 4. Macrotextures of inoceramid sediment (Tithonian). **A.** Concentrations of inoceramid prisms form white lenses and layers in brown calcareous claystone; manganese nodules are most abundant where prisms are most numerous (interval 123-765C-62R-1, 116–127 cm). **B.** Irregularly mottled calcareous claystone; white lenses are concentrations of inoceramid prisms; lighter areas contain abundant calcisphere debris (interval 123-765C-61R-5, 52–62 cm).

elongate prisms are dominantly aligned parallel to bedding, but less commonly occur at high angles to the overall fabric (Plate 1, Fig. 4). Many of the prism-prism contacts are sutured and/or interpenetrative (Plate 1, Fig. 5). Between the concentrated sand lenses, which are spaced a few millimeters to centimeters apart, clayey sandstone to sandy claystone contains 10% to 50% prisms, rarely in grain-support. Subordinate (10%–30%) clay-rich interlayers include less than 5% disseminated prisms.

Individual prisms are 0.05 to 0.2 mm × 0.3 to 2.5 mm in size, have a rounded hexagonal to rectangular cross section, and consist of a single calcite crystal. Most grains have smooth, relatively euhedral outlines and do not appear abraded. Some prisms, however, have strongly irregular, etched outlines (Plate 1, Fig. 3); these textures are most abundant in the upper part of the unit.

The prisms exhibit several types of internal texture, differentially distributed through the unit (Plate 1, Figs. 6–8). Rare grains are clear and featureless. Others have a clouded, murky appearance throughout the grain, or show cloudy bands a few tens of micrometers thick (Plate 1, Fig. 6). Still other grains contain abundant pits, generally filled with red clay identical to that making up the matrix between the prisms (Plate 1, Fig. 7). These pits are typically ovoid to cylindrical in form; many have an expanded, bulbous termination and a few are complexly curved or branched (Plate 1, Fig. 8). The pits are 2 to 40 μm (most 10–20 μm) wide and 20 to 50 μm (rarely, as much as 250 μm) long and are probable microborings. Pitted grains are most abundant (and most thoroughly pitted) toward the base (Section 123-765C-62R-3) and top (Sections 123-765C-61R-3 through -5) of the unit. Grains that have a cloudy texture dominate Sections 123-765C-62R-1 and -2.

Calcareous nannofossils. Calcareous nannofossils have a more restricted distribution within Unit L2 than does inoceramid debris. Coccoliths are found in two main intervals (Section 123-765C-61R-3, 0 cm, to -61R-5, 58 cm, and Section 123-765C-62R-1, 0 cm, to -62R-2, 13 cm) separated by a barren zone. The assemblages consist mostly of several species of a large, solution-resistant genus, *Watznaueria;* individual specimens are strongly etched. Coccoliths are more numerous in the lower interval (where they may make up 10%-15% of the total sediment) than in the upper interval (abundances 3% or less). Within the lower interval, nannofossils are most common in clay-rich layers between the inoceramid-rich lenses.

Calcisphere concentrations. Calcispheres and their debris are a local, minor component of the inoceramid sediment in Core 123-765C-62R, but occur persistently above Section 123-765C-61R-5, 70 cm. They are especially abundant in three intervals 8 to 12 cm thick.

The lowest of these calcisphere-rich intervals (interval 123-765C-61R-5, 54–62 cm) is reddish-orange calcareous claystone that has a streaky, mottled appearance and diffuse upper and lower

boundaries (Fig. 4B). The interval contains rare whole calcispheres, but consists largely of calcite needles, most likely derived from the breakdown of calcisphere tests. The needles form white nodular layers and lenses, 1 to 2 mm thick, and rounded to irregular clasts, 50 μm to 1.0 mm in diameter (Plate 2, Figs. 1, 3). In some layers, clasts are so abundant and closely packed that they coalesce into a microflaser texture.

The clasts consist almost exclusively of needles 1 to 2 μm × 3 to 10 (rarely, to 30) μm in size, commonly oriented in jackstraw fashion (Plate 2, Figs. 2, 4). These needles are the same size and shape as the individual calcite prisms that make up thick-walled calcisphere tests, and EDS analyses of individual needles and of whole calcispheres show identical composition (low magnesian calcite with no Sr). Further support for the inference that the calcite needles are disaggregated calcispheres is provided by the occurrence in this interval of curved stacks of needles that resemble calcisphere rim fragments.

Matrix to the clasts also consists of needles, as well as a larger component of noncarbonate material (clays, hematite) than is found in the relatively pure clasts. Matrix material typically "wraps around" the more resistent clasts, and SEM observation indicates that the clasts have been more thoroughly cemented, and retain less porosity, than the surrounding matrix (Plate 2, Fig. 3). Interpenetrative and sutured grain contacts occur in many of the clasts. Rare nannofossils and 15% to 30% coarse detritus (mainly inoceramid prisms and volcanic lithic grains) occur in both matrix and clasts, and the nodular needle-rich layers have clearly been burrowed (Plate 3, Fig. 1).

The middle calcisphere concentration is least distinctive megascopically; pale wispy lenses occur throughout the upper half of Section 123-765C-61R-4, but make up 50% of the interval 123-765C-61R-4, 15-25 cm. The lenses are concentrations of whole calcispheres and/or inoceramid prisms and are separated by muddier zones (Plate 3, Figs. 2, 3). Volcanic clasts are again notable. The most diverse nannofossil assemblage found in Unit L2 occurs at the base of this layer.

The uppermost calcisphere-rich interval (Section 123-765C-61R-3, 13–25 cm) is pale green calcareous claystone with a reddish halo; it is similar in color to bentonites (described below), but is not waxy. The upper red/green color boundary is relatively smooth, while the lower one is irregular; the color shifts do not coincide with any change in texture or primary composition in the sediment and probably formed during diagenesis. The layer consists mostly of closely packed calcispheres, all of which appear to be the same species, in a matrix of calcisphere debris, clay, and minor coccoliths. Other grains are rare (5%), and are mostly inoceramid prisms and quartz (1%).

Other fossils. Other fossils found in Unit L2 are agglutinated and calcareous benthic foraminifers, thin-shelled bivalves, and rare belemnite fragments and radiolarians (Ludden, Gradstein, et al., 1990). Agglutinated foraminifers occur throughout the inoceramid-bearing claystone, but (based on thin-section observations) are more abundant in the upper half of the unit. The agglutinated foraminifer assemblage includes some forms that require coarse particles (such as inoceramid prisms) as substrate or for construction of their test walls (Kaminski, Gradstein, et al., this volume). Calcareous benthic foraminifers are nowhere as abundant as the agglutinated forms, but were noted in thin section in both the inoceramid-rich lower half of the unit and in the concentrations of calcisphere debris in Sections 123-765C-61R-4 and -61R-5.

Rare, thin-shelled bivalves up to 1 cm in diameter occur throughout the lower part of this unit; they are especially abundant from Section 123-765C-62R-1, 99 cm, to -62R-2, 7 cm, and form a relatively concentrated 2-cm-thick layer in Sample 123-765C-62R-2, 4-6 cm. Shells are dominantly convex upward, aligned parallel to bedding, and float in the finer-grained matrix. Epifaunal overgrowths (serpulid worm tubes) occur on some shells (Ludden, Gradstein, et al., 1990).

Both the calcareous foraminifers and the thin-shelled bivalves locally contain clay-filled pits similar to those in the inoceramid prisms.

Noncalcareous component. Fine-grained, noncalcareous material in the inoceramid sediment consists largely of smectitic I/S, lesser illite, and microcrystalline to cryptocrystalline quartz (Compton and Locker, this volume). Terrigenous and volcanic sand and silt similar to that in the underlying unit makes up 1% to 15% of the total sediment. Both fine and coarse noncalcareous detritus increase in abundance in the upper part of the unit; volcanic clasts are especially notable in the intervals rich in calcisphere debris (Sections 123-765C-61R-4 and -5). Quartz grains are 0.02 to 0.4 mm in diameter; most are angular, but rare grains are rounded, and distinctly embayed quartz of volcanic origin occurs in several samples from Section 123-765C-61R-5. Clasts of undoubted volcanic origin are mostly mafic lathwork grains or altered glass; locally abundant orange to reddish-brown fine-grained clasts might be altered volcanic grains and/or sedimentary intraclasts. Other grains, present only in trace amounts, are plagioclase, microcline, white mica, tourmaline, glauconite, and phosphatic debris.

Black manganese nodules occur throughout Unit L2, but are especially abundant in Sections 123-765C-62R-1 and -2 (Fig. 4A). Nodules range from 0.1 mm to 1.0 cm in maximum diameter and are mostly ovoid in form, with the long axis horizontal. The nodules are largest and most numerous in the intervals richest in inoceramid debris; nodules 1.0 mm or more in size are common in Core 123-765C-62R but rare in Core 123-765C-61R. The nodules consist of manganite (XRD analysis in Ludden, Gradstein, et al., 1990) and some contain subordinate amounts of iron (EDS analysis, this study). Microtextures of these nodules indicate that they formed *in situ;* some nodules incorporate inoceramid prisms similar in size and shape to those in the surrounding sediment, and other nodules are surrounded by halos of fine-grained, disseminated manganite (Ludden, Gradstein et al., 1990; this study, Plate 3, Fig. 4). Manganese also coats sand-sized detritus in Sections 123-765C-61R-4 and -5.

Several layers of pink or green, waxy claystone as much as 13 cm thick are intercalated in the inoceramid sediment; these layers are altered ash (bentonite) that has been reworked and mixed with pelagic sediment by bottom currents (Thurow and von Rad, this volume). Two pink layers 0.5 to 1 cm thick occur in Section 123-765C-61R-4 (at 104 and 108 cm). Thicker pale to medium green layers (Sections 123-765C-61R-4, 79–92 cm, and -62-1, 59–62 cm) have sharp sandy bases with locally well-developed cross-lamination and are surrounded by orange to red diagenetic halos several centimeters thick. Sand in these layers consists of detrital material and microfossils, including quartz, volcanic lithics, plagioclase, altered glass, inoceramid prisms, agglutinated foraminifers, and phosphatic debris; the fine-grained fraction is largely smectite and rare nannofossils. Carbonate content of these intervals is lower than that of the surrounding sediment (Table 1).

Interpretation

Unit L2 formed through slow pelagic accumulation in a well-oxygenated, current-scoured setting near the level of the CCD. The compositional and textural variety that characterize the inoceramid sediment unit reflect a diversity of source materials and a combination of depositional and diagenetic processes. Pelagic and benthic biogenic material and volcanic and terrigenous detritus are all present in significant amounts.

The most distinctive aspect of the inoceramid sediment is its calcareous component; the rest of the unit resembles in color, composition, and texture the reddish-brown, locally silty clay-

Table 1. Carbonate content of selected samples from lower sequence at Site 765.

Core, section, interval (cm)	Unit	Lithology	$CaCO_3$ (%)
123-765C-55R-3, 0	L3B	Calcareous sediment	[a]21
56R-2, 108	L3B	Claystone	[a]1
57R-4, 4	L3B	Calcareous sediment	33
57R-6, 111	L3B	Calcareous sediment	8
61R-3, 18	L2	Calcisphere concentration	63
61R-4, 21	L2	Calcisphere concentration	46
61R-4, 58	L2	Inoceramid sediment	[a]10
61R-4, 102	L2	Inoceramid sediment	12
61R-5, 57	L2	Calcisphere concentration	67
61R-5, 81	L2	Inoceramid sediment	[a]27
61R-5, 74	L2	Inoceramid sediment	26
61R-5, 118	L2	Inoceramid sediment	[a]19
62R-1, 58	L2	Bentonite	9
62R-1, 120	L2	Inoceramid sediment	[a]41
62R-1, 131	L2	Inoceramid sediment (calcareous sand lens)	61
62R-2, 91	L2	Inoceramid sediment	47
62R-3, 0	L2	Inoceramid sediment	[a]43
62R-3, 68	L1	Silty claystone	[a]0
62R-4, 25	L1	Claystone	[a]0

[a] From Ludden, Gradstein, et al. (1990).

stones found above and below. The robust nature of the calcareous material and its relatively poor preservation (etching) indicate deposition took place near the CCD; changes in the type of calcareous grains and their overall abundance throughout the unit most likely result from changes in the position of the CCD relative to the depth of deposition, but could also reflect shifts in bottom current intensity.

The Inoceramidae are a family of extinct epibenthic bivalves; their remains are the most common macrofossils found in Mesozoic sediments drilled by the DSDP/ODP (Kauffman, 1976; Barron et al., 1984). This reflects the wide environmental tolerance and high dispersal potential of the Inoceramidae, as well as the resistance to destruction and dissolution of their thick, largely calcite shells (Kauffman, 1976). Inoceramids were adapted to soft mud substrates and poorly oxygenated bottom waters, but have also been found in well-oxygenated settings (Thiede and Dinkelman, 1977). They have a worldwide distribution that includes isolated oceanic islands, but they occur most frequently near continental margins (Thiede and Dinkelman, 1977). Inoceramids are most common in upper bathyal to neritic environments, but have been noted, apparently *in situ*, to paleodepths of 3500 to 4500 m (Barron et al., 1984).

The depositional setting of Site 765 is compatible with what is known of inoceramid paleoecology, and the bivalves could have been living at or near the site. The reddish-brown color of the inoceramid sediment indicates that it was deposited under oxidizing conditions (e.g., Potter et al., 1984), and Site 765 is within 75 km of the northwest Australian margin. The paleodepth postulated for this unit, based on backtracking of sediment/basement level, is about 2800 m (Ludden, Gradstein, et al., 1990). Although no whole inoceramid shells were recovered from Unit L2, the abundance and condition of the inoceramid prisms suggests a local origin. Inoceramid shells have a coarsely crystalline ostracum made of vertically oriented calcite prisms, which disaggregate easily along crystal boundaries (Thiede and Dinkelman, 1977). Oxic conditions enhance dissolution of the organic template binding the prismatic layer (E. Kauffman, pers. comm., 1990) and probably facilitated the disaggregation of inoceramid prisms at Site 765. Most prisms in Unit L2 are poorly sorted and unabraded, implying minimal transport.

It is possible that some of the inoceramid prism-rich layers in Unit L2 were deposited by turbidity currents (Ludden, Gradstein, et al., 1990), but the lack of features such as grading or Bouma (1962) sequences and the virtually monomictic composition of the layers argues against such an origin. Upper Cretaceous turbidites rich in inoceramid debris occur in the Angola Basin (Stow and Miller, 1984) and turbidites higher in the section at Site 765 (Subunit L3B) locally contain abundant inoceramid prisms. However, in both these instances, the inoceramid sediment contains a variety of other sand-sized fossils and lithic clasts, grades upwards into nannofossil claystone, is parallel- and cross-laminated, and occurs in layers that have sharp bases and distinctly burrowed tops. If the inoceramid prisms at Site 765 were introduced by turbidity currents, any textural evidence of such an origin has been destroyed (perhaps by bioturbation?) and the currents must have eroded a source that contained almost no sand-sized material other than inoceramid debris.

The inoceramid prisms in Site 765 sediments have largely clay-filled, cylindrical to ovoid pits that are probably microborings; some borings may have been enlarged by later dissolution. A variety of cyanophytes, algae, and fungi can produce borings 1 to 100 μm in diameter with diverse tunnel and baglike shapes; in their upper size range, these borings overlap similar structures formed by endolithic sponges (Golubic et al., 1975). Both fungi and sponges can invade substrates at depths well below the photic zone. In shallow, warm seas, vacated borings typically fill with aragonite or magnesian calcite, but in colder, deeper water, borings tend to remain empty and may be selectively leached (Golubic et al., 1975). Pit shapes in Site 765 inoceramid prisms are not distinctive enough to attribute to a specific organism, but the lack of cement fillings strongly suggests that the pits formed in colder, deeper water. Some pit shapes may have been controlled by the position of cleavage planes within the calcite substrate; such pits also may have been modified and enlarged by seco-ndary leaching (Plate 1, Fig. 8).

Some prisms also have alternating zones a few tens of micrometers thick of more or less clouded appearance, which may be growth bands (Plate 1, Fig. 6). Dark growth lines are a common feature of inoceramid shells (Kauffman, 1976) and reflect seasonal and yearly changes in the amount of organic matter incorporated into the shell (E. Kauffman, pers. comm., 1990).

The presence of inoceramid debris in Unit L2, and the inference that this debris is essentially autochthonous, is consistent with other evidence indicating a muddy, relatively deep-water, oxygenated depositional environment near the continental margin. Although the robust nature of inoceramid prisms makes them resistant to dissolution, the sheer abundance of inoceramid debris (if it has not been introduced by turbidity currents) suggests that deposition of Unit L2 took place above the CCD. Other fossils in these sediments help to delineate more precisely the depositional setting relative to the CCD.

Nannofossil assemblages, for example, suggest that the inoceramid sediment was deposited primarily above the CCD, but below the lysocline. Nannofossils occur through most of the unit, but are never abundant. This sparse but persistent distribution strongly contrasts with that shown by nannofossils in the calcareous sediment and claystone unit (L3) at Sites 765 and 261. In the L3 unit, nannofossils are confined to, but abundant and well-preserved within, certain intervals characterized by turbidity current structures, and thus have clearly been redeposited. In the inoceramid sediment unit, turbidity current structures were not noted, nannofossils occur within various sediment types (brown claystone, lenses rich in inoceramid prisms, calcisphere concentrations), and assemblages are everywhere strongly etched, incomplete, and composed only of robust, solution-resistant forms.

The sparse, poorly preserved, and relatively evenly distributed nannofossil assemblages of the inoceramid sediment do not appear to have been redeposited, but have definitely undergone dissolution. They thus imply that most of the unit was deposited just above the CCD. Intervals lacking nannofossils, such as the lower half of Section 123-765C-61R-5, may have formed when the site was just below the CCD; these zones also contain the most strongly etched and pitted inoceramid prisms. The most calcareous interval (Section 123-765C-62R-1) may have been deposited when the site was farthest above the CCD.

The other important biotic components of Unit L2 are benthic foraminifers and calcispheres. The foraminiferal fauna is dominated by agglutinated forms that lack calcite cement and are, in the absence of calcareous benthic foraminifers, characteristic of settings undersaturated with respect to calcite (Kaminski, Gradstein, et al., this volume). However, calcareous foraminifers are a minor, but persistent, part of the assemblage, which supports our supposition that sedimentation took place just above the CCD.

Calcispheres and their debris occur largely in the upper half of Unit L2 and are most abundant within discrete intervals a few centimeters thick in which they constitute the bulk of the sediment. Calcisphere floods appear to form in response to unusual (stressful) oceanographic conditions (e.g., Thierstein, 1981) and are particularly common in shelf and shelf-margin settings (Masters and Scott, 1979). The calcisphere material in this unit could have been derived from blooms at the sea surface above Site 765, or from blooms above the continental slope or outer shelf. In the latter case, the calcispheres must then have been brought into the abyssal plain environment of Site 765 by gravity flows and/or bottom currents, but as in the case of the inoceramid-rich layers described above, there is no textural evidence to indicate such an origin (e.g., grading, Bouma sequences). However, the calcisphere concentrations are finer grained than the inoceramid debris layers, and thus less likely to display Bouma sequence structures, and are also less monomictic (they contain as much as 30% other fossil and lithic grains). Therefore, a turbidite origin is considered more likely for the calcisphere concentrations than for the inoceramid prism layers.

The breakdown of calcisphere tests into individual calcite needles, observed in Section 123-765C-61R-5, 54–62 cm, might be the result of corrosive bottom-water conditions; this interval overlies a zone barren of nannofossils, contains particularly pitted (etched?) inoceramid prisms, and may have formed during a period of relative elevation of the CCD. The clasts and microflaser textures characteristic of the needle-rich interval probably formed in a manner analogous to that proposed by Garrison and Kennedy (1977) to explain similar but slightly larger-scale features in chalks. These authors invoked a combination of early and late diagenetic processes, including early cementation and development of hardgrounds, and later compaction and pressure dissolution, to explain the genesis of microflaser bedding in Cretaceous chalks of England.

The needle-rich interval contains features indicative of both early cementation and later dissolution. Early cementation of the needle-rich clasts is demonstrated by compaction of matrix around the clasts, and by concentration of clasts within a burrow. Most clasts were not completely lithified prior to deposition, however, as indicated by their rounded and irregular shapes. Relatively early calcite precipitation is also inferred from the size of a few of the needles (20–30 μm); this is greater than the thickness of a typical calcisphere test wall and suggests enlargement of needles during diagenesis by growth of calcite cement along the ends of the needles. Pressure dissolution also shaped the microtexture of the sediment, as shown by interpenetrative, sutured grain contacts within many clasts.

Volcanic detritus, notable throughout Unit L2, was presumably derived from the nearby spreading center; clast types and abundances are similar to those in directly underlying and overlying units. Intervals of discrete bentonite attest to the periodic input of relatively pure ash (Thurow and von Rad, this volume); in addition, much of the smectite component of the clay throughout the unit is probably a product of the breakdown of volcanic material (Compton and Locker, this volume). Terrigenous material, mostly angular quartz, testifies to continuing, but relatively minor, input from the continental margin.

Once deposited, the biogenic and detrital components described above were winnowed and reworked by intermittent bottom currents. The grain-supported inoceramid concentrations are best explained as lags from which bottom currents episodically removed fine material. The finer-grained, poorly sorted material between the inoceramid concentrations was deposited during periods of less vigorous current action and consists largely of hemipelagic material (clays, coccoliths) and lesser inoceramid debris.

Sediment texture in Unit L2 was modified further by bioturbation. Thorough bioturbation should tend to homogenize the two end-member sediment types (coarse shell lags and finer-grained hemipelagites). However, most of the inoceramid sediment unit appears to have been only partially bioturbated, as indicated by preservation of discrete burrow structures. Local intervals, such as the calcisphere needle concentration in Section 123-765C-61R-5, have a smeared and mottled appearance, which suggests more pervasive bioturbation.

Sedimentation rates for the inoceramid sediment were low (less than 2.5 m/m.y.; Fig. 5). Slow, discontinuous accumulation of this facies is supported by the occurrence of abundant manganese nodules, particularly in the unit's lower half. Manganese nodules typically form where sediment input is low, bioturbation common, and currents winnow bottom sediments (Scholle et al., 1983).

Small-scale compositional and textural heterogeneities in Unit L2 have been enhanced by compaction and pressure solution. The effects of compaction include laminae of fine-grained material draped over coarser grains, such as shell fragments and manganese nodules. Compaction and subsequent pressure solution have produced overly close packing and sutured grain contacts in many of the densest inoceramid prism concentrations. As would be expected, such textures are best developed in the more calcareous lower half of the unit.

Subtle changes in texture and composition through the inoceramid sediment unit result from a complex interaction of factors including position of the CCD, sedimentation rate, current strength, and sediment supply. The CCD appears to have been lowest during deposition of Section 123-765C-62R-1; this interval contains the most abundant and best-preserved carbonate material. Overall sediment accumulation rates may also have been lowest at this time, perhaps due to extensive removal of finer grained material by particularly strong bottom currents; winnowed shell lags and large manganese nodules are most numerous in Section 123-765C-62R-1. The rarity of pits within inoceramid grains in this interval (compared to sediments above and below) probably reflects both stronger currents and a lower CCD; boring is less intensive in high-energy environments (Golubic et al., 1975) and borings that were produced farther above the CCD would be exposed to less corrosive bottom water and therefore would be less etched.

Thus, the inoceramid sediment unit represents a mixture of biogenic, volcanic, and lesser terrigenous material that accumulated chiefly above the CCD, but below the lysocline. Biogenic material was derived both from autochthonous benthic organisms (inoceramid bivalves, agglutinated and rare calcareous foramin-

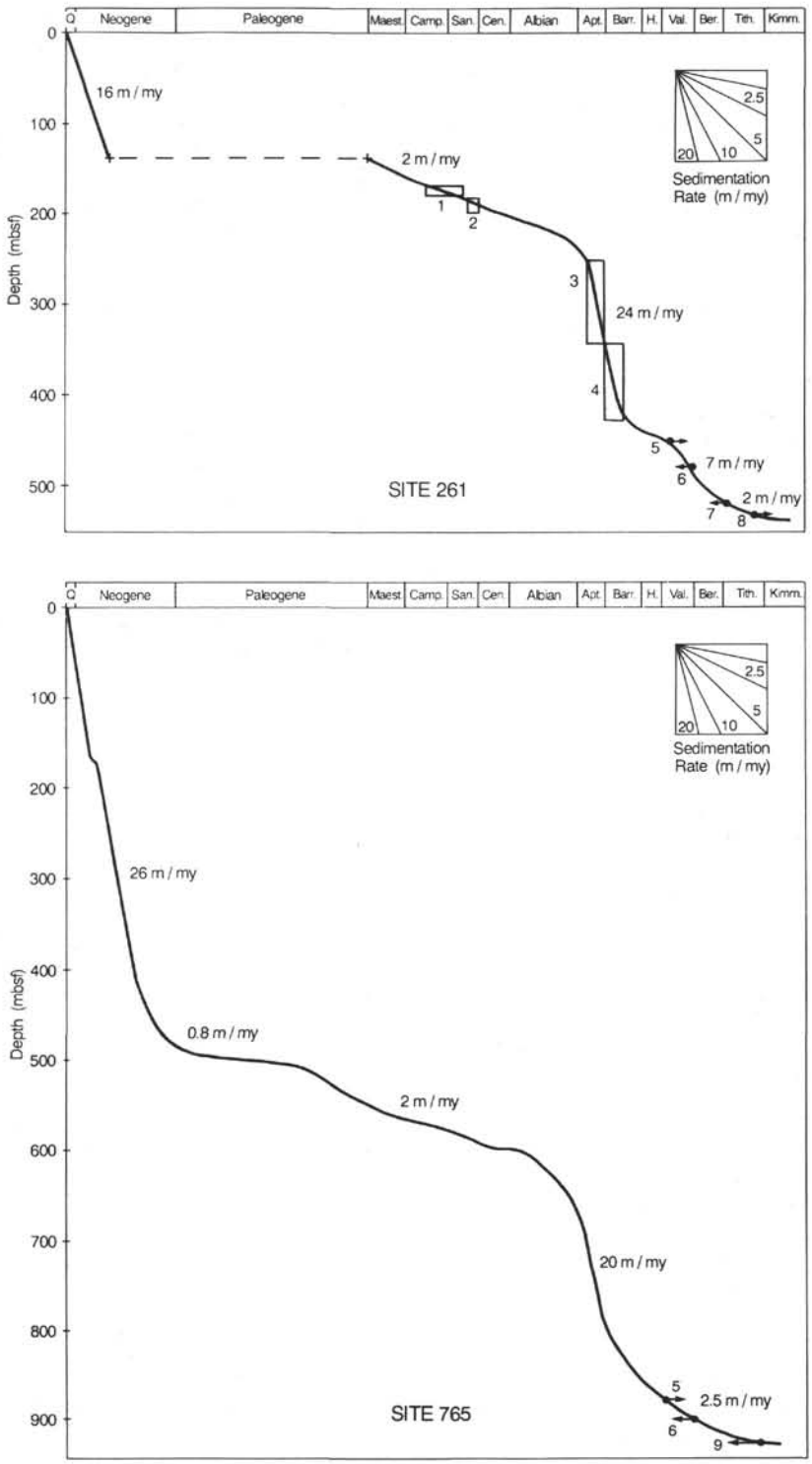

Figure 5. Sediment accumulation rate (age vs. depth) diagrams for Sites 765 and 261. Site 765 diagram is adapted from Ludden, Gradstein, et al. (1990) and modified in the lower part using nannofossil data presented here. Site 261 diagram is adapted from Veevers, Heirtzler, et al. (1974) and modified in the Mesozoic interval based on the following datums: (1) foraminifer data, Coniacian–early Campanian; (2) foraminifer data, Turonian; (3) dinoflagellate *O. operculata* Zone, Aptian; (4) dinoflagellate *M. australis* Zone, Barremian; (5) last occurrence *Tubodiscus verenae*, late Valanginian; (6) first occurrence *T. verenae*, early Valanginian; (7) first occurrence *Cruciellipsis cuvillieri*, latest Tithonian; (8) last occurrence *Stephanolithion bigotii*, early Tithonian; (9) abundance of *Watznaueria manivitae*, Tithonian. Sedimentation rates marked in the diagram provide an indication of variation through the sections.

ifers) and pelagic forms (nannofossils, calcispheres, thin-shelled bivalves, rare radiolarians and belemnites). Coarse detritus was winnowed and, perhaps, reworked by intermittent bottom currents. Turbidites, so important higher in the section at Site 765, are apparently rare or absent from this unit; if the calcisphere concentrations and/or (less likely) inoceramid prisms were introduced by gravity flows, they contain no structures indicative of such an origin. Sedimentation was slow and may have been discontinuous; manganese nodules formed throughout Unit L2.

Unit L3, Calcareous Sediment and Noncalcareous Claystone

Subunit L3A, Radiolarian Claystone (Tithonian[?]–Berriasian; Core 123-765C-61R-2, 150 cm, to -58R-2, 26 cm; 919.9–892.7 m sub-bottom)

Description

This interval consists of predominantly reddish-brown claystone locally rich in radiolarians; it is distinguished from directly underlying (L2) and overlying (L3B) units by the virtual absence of primary (nondiagenetic) carbonate. Volcanic lithic clasts, rare inoceramid prisms, and manganese nodules—all found in the underlying inoceramid sediment—occur in the lower part of the radiolarian claystone unit; a distinct ferromanganese crust is developed in Section 123-765C-61R-2. Layers of smectite claystone, interpreted as bentonites, occur above and below Subunit L3A, but are most numerous within this subunit. Thin beds of dark claystone, layers enriched in radiolarians, intervals containing diagenetic manganese carbonate, and redeposited sediments interpreted as turbidites are most notable in the upper part of Subunit L3A and occur in overlying units as well. Subunit L3A is essentially equivalent to Subunit VIIA of Ludden, Gradstein, et al. (1990); we have slightly shifted the upper boundary to exclude a 6-cm-interval of calcareous sediment that we reassigned to the overlying subunit (L3B).

The claystone that makes up most of the unit is homogeneous and has few sedimentary structures; rare millimeter-scale burrows (mostly *Chondrites*) were observed in core and thin-section. Thin layers and splotches of greenish-gray sediment occur locally and represent reduction halos around ash or microfossil concentrations. The claystone consists largely of smectitic I/S, illite, and microcrystalline quartz (Compton and Locker, this volume); carbonate content is negligible (0.3%–0.8%; Ludden, Gradstein, et al., 1990), except for a few intervals rich in authigenic carbonate (discussed below). Minor thin layers of dark claystone are slightly enriched in organic carbon (0.47%; Ludden, Gradstein, et al., 1990). Silt and sand, disseminated or in thin laminae, make up less than 15% (generally less than 5%) of the total sediment and consist mostly of angular quartz. A few corroded inoceramid prisms, some surrounded by patchy halos of replacement calcite, occur in Sections 123-765C-61R-1 and -61R-2. Distinct volcanic clasts (mafic lithic grains that have a jackstraw texture, altered glass) and manganese nodules also occur in these sections, but are rare higher in the unit.

An irregular ferromanganese crust 0.5 to 2.0 mm thick occurs in Section 123-765C-61R-2 at 95 cm (Fig. 6); manganese nodules

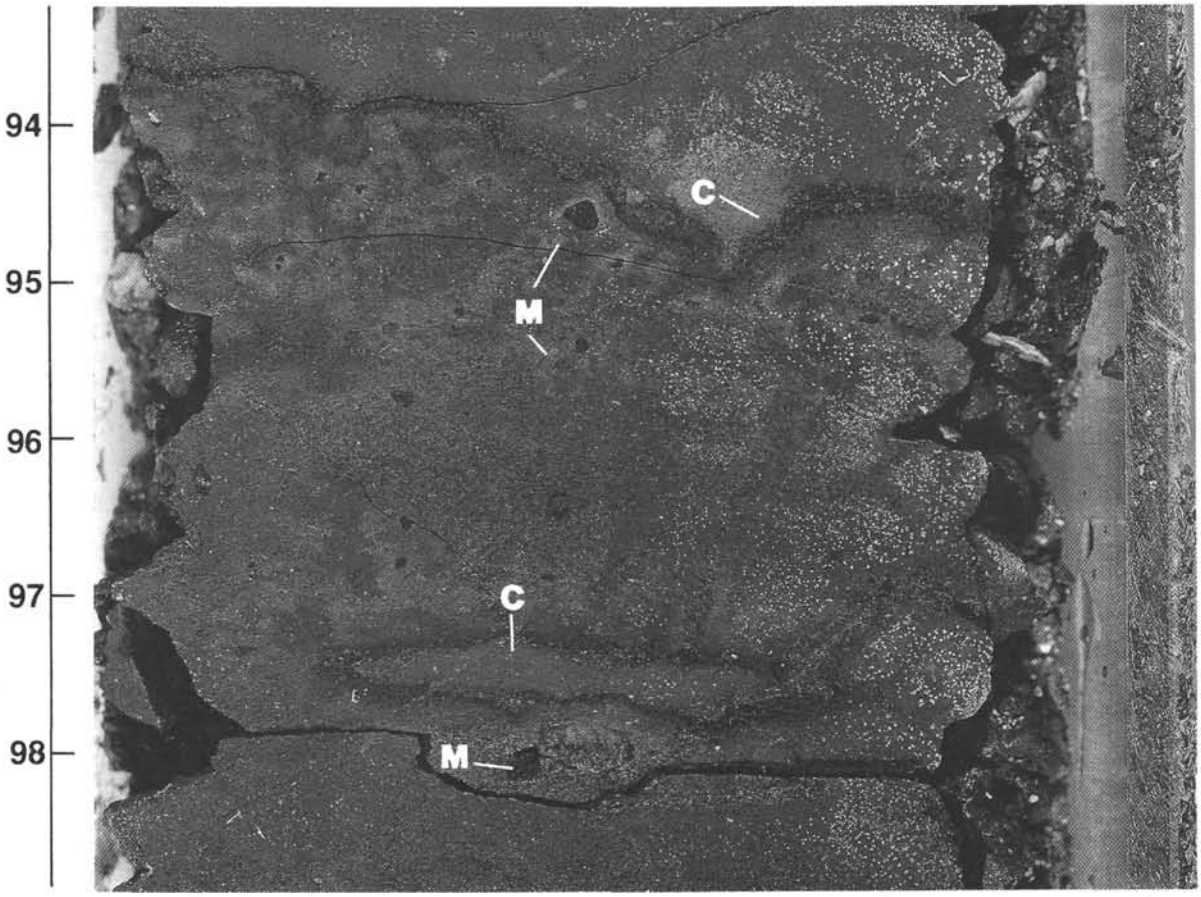

Figure 6. Irregular ferromanganese crusts (C) in radiolarian claystone; manganese nodules (M) are especially notable just below upper crust (interval 123-765C-61R-2, 93–99 cm).

(confirmed by microprobe) are especially notable (and as much as 2 mm in diameter) in a 3-cm-thick interval directly beneath the crust. Toward the base of this interval, a similar crust forms an ovoid 0.5 × 3.0 cm in size. The upper crust is developed on a closely packed, grain-supported sand layer 2.0 mm thick (Plate 4, Fig. 1); the sand contains calcitized radiolarians, lesser agglutinated foraminifers, and subordinate detrital material (mostly volcanic lithic clasts). No manganese nodules were observed above the upper crust.

The crust consists of a black basal layer 0.2 to 0.6 mm thick that locally has a well-developed colloform texture (Plate 4, Fig. 2), a middle layer 0.5 to 1.0 mm thick rich in microfossils and volcanic lithics like those seen directly below the crust, and a brownish-black thin (0.1 mm) upper layer. EDS and microprobe analyses of the upper and lower layers indicate that they consist largely of iron and manganese. Subordinate detrital grains and microfossils are embedded in the lower layer of the crust. The microfossils are mostly sessile arenaceous foraminifers similar to those illustrated by Wendt (1974) and include *Ammolagena clavata* (Plate 4, Fig. 3), a bathyal to abyssal form which requires a hard substrate (F. M. Gradstein, pers. comm., 1990) .

Layers 1 to 12 cm thick of waxy, white to pale gray to greenish-gray claystone occur throughout Unit L3A, but are especially notable in the lower part; eight such layers occur in the interval from Section 123-765C-60R-5 through -61-1. Shipboard XRD analysis indicates that these layers consist mostly of smectite (Ludden, Gradstein, et al., 1990); some samples contain grains of biotite and euhedral quartz. These layers are interpreted as bentonites; some are relatively pure, but others have been reworked and mixed with the background hemipelagic sediment by currents and bioturbation (Thurow and von Rad, this volume).

Agglutinated foraminifers like those in the underlying unit (L2) occur throughout the radiolarian claystone, but are less abundant and diverse upward; minor layers of fissile, relatively organic-rich, dark gray claystone in Core 123-765C-59R contain dinoflagellates (Ludden, Gradstein, et al., 1990).

Radiolarians are rare and typically have been replaced by carbonate below Core 123-765C-59R, but are increasingly abundant and generally recrystallized to microcrystalline quartz higher in the unit. They occur dispersed in the mud matrix, but also have been concentrated into lenses and layers a few millimeters to 6 cm thick; more than 40 radiolarian-rich intervals occur in Sections 123-765C-58R-2 through -59R-5.

Two major types of radiolarian concentration were observed (Fig. 7). The first stands out sharply in core and consists of silt- to sand-sized radiolarite in discrete, parallel- and cross-laminated layers one to several centimeters thick. These layers are white to greenish gray and have a green diagenetic halo that extends into the surrounding claystone. The second type of concentration contains more clayey matrix and is less distinctive in core; here, radiolarians form white wispy lenses 1 mm thick or less through several centimeters of reddish-brown claystone. Radiolarians in both types of concentration have been recrystallized to microcrystalline quartz, or less commonly, pyritized, and are generally filled with sheaves of length-fast chalcedony (Plate 4, Fig. 4).

Micronodules and rhombs of diagenetic carbonate occur locally, largely in the upper part of the unit. Micronodules are 30 to 90 μm (most, 40–60 μm) in diameter, spherical (less commonly ovoid or conical) and were found mainly just below and overlapping (Sections 123-765C-59R-3 to -6) the lowest occurrence of radiolarite. The nodules are concentrated into white layers, lenses, or ovoids a few millimeters thick, or less commonly, float in a claystone matrix. Size and shape of the micronodules, as well as mode and level of occurrence, indicate that they have replaced and grown around radiolarians, and perhaps calcispheres. The rhombs, 6 to 40 μm in diameter, make up a few percent (rarely,

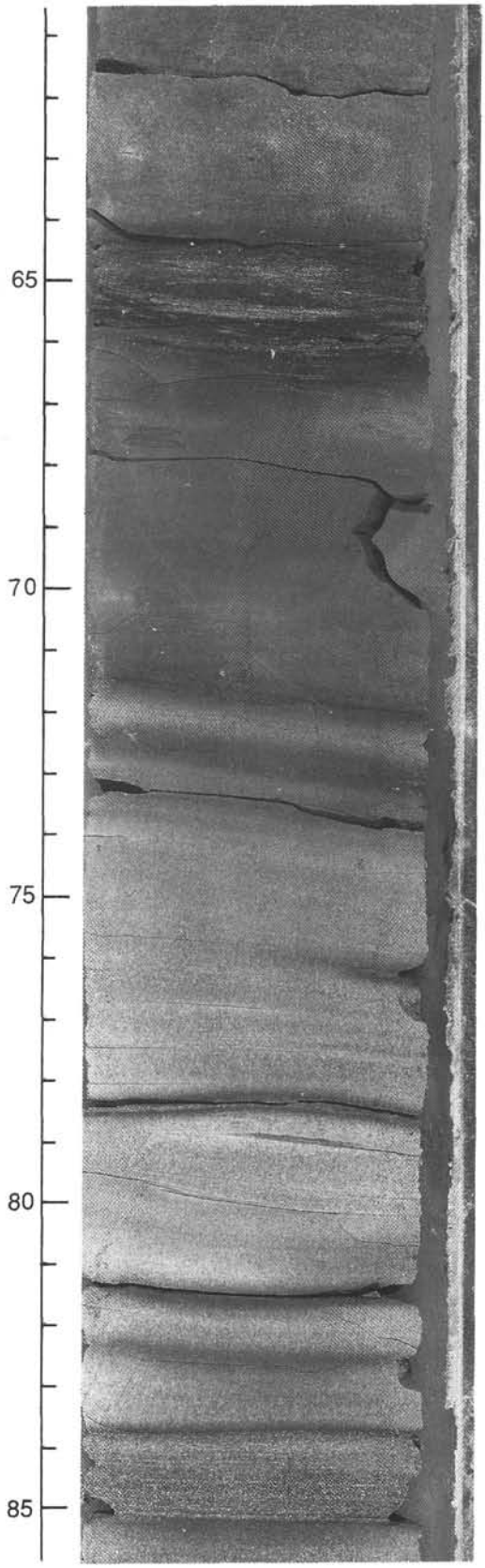

Figure 7. Radiolarian claystone in core. White radiolarite layer with well-developed parallel lamination and local small-scale cross lamination (72–85 cm) underlies interval of brown claystone containing white wispy lenses of radiolarians (64–66 cm) (interval 123-765C-58R-2, 60–85 cm).

30%–40%) of most claystone samples from Cores 123-765C-58R and -59R. All carbonate rhombs and micronodules analyzed from this unit consist of rhodochrosite (XRD analyses in Ludden, Gradstein, et al., 1990; EDS analyses of this study). Authigenic barite also occurs in this unit, chiefly as euhedral crystals within radiolarian tests.

Several of the claystone layers rich in carbonate rhombs have a distinctive pale red color like that characteristic of nannofossil-bearing claystone in the overlying unit. These layers have probably been redeposited; they contain *Chondrites* burrows (increasingly abundant toward the tops of the layers) and silty parallel laminae near the base. One layer (Section 123-765C-59R-4, 87–102 cm) is clearly graded; it has a sandy base a few centimeters thick composed of angular quartz, poorly preserved radiolarians, phosphatic debris, and opaques, plus minor carbonate grains (including inoceramid prisms) and glauconite.

Interpretation

Pelagic claystone makes up most of Unit L3A; the red-brown color and lack of primary carbonate material in these sediments indicate deposition in an oxidizing environment below the CCD. Distinct volcanic detritus (obvious volcanic clasts, bentonite layers) is most evident at the base of the unit, but the abundance of iron-rich smectite clays throughout the interval suggests continued volcanic input (Compton and Locker, this volume).

The radiolarian claystone accumulated slowly (Fig. 5), as did the underlying units. The upper ferromanganese crust in Section 123-765C-61R-2 developed on a shell lag, likely formed by winnowing bottom currents; the lower, ovoid-shaped crust may outline a burrow. The microtexture of the upper crust (colloform structures, embedded clastic debris) is identical to that of ferromanganese crusts in the southwest Pacific Ocean (Kang and Hein, 1988). Such crusts may form largely through hydrogenetic mechanisms, involving precipitation from seawater at ambient temperatures, and need not entail hydrothermal processes. The colloform texture (typical of growth into open space) and the presence of sessile benthic foraminifers within the crust denote formation on the seafloor, rather than below the sediment surface during diagenesis.

The abrupt appearance of abundant intervals of radiolarite in Core 123-765C-59R reflects changes in circulation in the Argo Basin as Gondwanaland split apart and consequent influx of cold, circum-Antarctic water that upwelled along the northwest Australian margin (Baumgartner, this volume). Both winnowing bottom currents and density (turbidity) currents were involved in reworking and deposition of the radiolarian claystone (Ludden, Gradstein, et al., 1990). Light-colored, graded radiolarites that have well-developed parallel- and cross-lamination were probably deposited by turbidity currents. Some exhibit partial Bouma sequences (BCDE, BDE), and most have greenish reduction halos; such halos commonly form during diagenesis of suddenly deposited organic-rich layers (e.g., Kelts and Arthur, 1981). In contrast, radiolarian-enriched intervals that are the same reddish-brown color as the background claystone and that have discontinuous wispy laminae and abundant clayey matrix more likely formed as pelagic accumulations that were then concentrated by bottom currents.

The reddish claystone intervals, burrowed in their upper parts and laminated and graded toward the base, also appear to be turbidites. They resemble nannofossil-bearing turbidites in the overlying unit (see below), but any calcareous component they may once have contained has been lost during diagenesis.

Subunit L3B, Calcareous Sediment and Noncalcareous Claystone (Valanginian–lower Barremian; Cores 123-765C-58R-2, 26 cm, to -53-1, 0 cm; 892.7–844.1 m sub-bottom)

Description

General features. This subunit corresponds to Unit VI and the lower part of Subunit VC of Ludden, Gradstein, et al., 1990; it consists of reddish-brown noncalcareous claystone, similar to that in the underlying units, intercalated with intervals of redeposited calcareous sediment. Both sediment types are present in roughly equal amounts and form layers a few millimeters to several meters thick. The calcareous intervals consist largely of nannofossil claystone, but some grade downward into siltstone or sandstone. Calcispheres and marl intraclasts as well as radiolarians, quartz, and clay clasts make up the coarser grained sediments. The subunit also includes subordinate interlayers of radiolarite and bentonite, and locally abundant rhombs and micronodules of manganese carbonate. Cores 123-765C-53R and -54R contain only minor amounts of primary calcareous material, but we have included them in this subunit because they contain relatively abundant and thick graded sequences similar to the underlying redeposited calcareous sediment layers but rich in clay clasts, radiolarians, quartz, and authigenic carbonate.

Calcareous sediment. Fifty-eight calcareous intervals occur in this subunit (see Dumoulin, this volume, for a more detailed description of the calcareous sediment). Most intervals (75%) are less than 10 cm thick, but four are thicker than 1.0 m, and one is almost 3 m thick. Color and sedimentary structures make most calcareous intervals distinctive in core. The calcareous sandstones and siltstones are white, gray, green, or pale brown; calcareous claystones are generally red or brown, but are lighter in color than the intercalated noncalcareous claystones. A few calcareous claystones, however, can only be distinguished megascopically by hydrochloric acid.

Almost all calcareous intervals have sharp (locally scoured) bases and gradational tops. Horizontal burrows (mainly *Chondrites*) occur in the upper 1 to 30 cm of most intervals, are filled with calcareous siltstone or noncalcareous claystone, and decrease markedly in abundance downward. Coarser grained calcareous intervals are clearly graded, contain well-developed parallel and cross lamination, and form base-cut-out (BCDE, BDE) Bouma sequences.

Carbonate content analyses (Table 1; Ludden, Gradstein, et al., 1990; Dumoulin, this volume) indicate both fine- and coarse-grained calcareous layers contain 8% to 33% $CaCO_3$. Clay- and fine silt-sized calcareous grains are mostly whole or broken nannofossils. Coarse calcareous silt is primarily calcispheres, which exhibit a wide variety of surface textures and wall structures (Fig. 8A). Sand-sized calcareous grains are predominantly intraclasts of nannofossil- and/or calcisphere-bearing marl or claystone (Fig. 8B), but also include inoceramid prisms and benthic foraminifers.

Noncalcareous material is thoroughly intermixed with calcareous components in all of the calcareous layers. Clay (chiefly smectitic I/S; Compton and Locker, this volume) makes up most of the finer grained layers, and claystone clasts occur abundantly in the sandstones. Radiolarians are dispersed in the finer grained sediment and dispersed or concentrated into discrete layers in coarser sediment. Other components include quartz, glauconite, and agglutinated foraminifers.

Noncalcareous claystone. Most intervals of noncalcareous claystone in this subunit are less than 20 cm thick, and a few are less than 1 cm; more than 3 m of continuously noncalcareous material occurs toward the base of Core 123-765C-57R. This

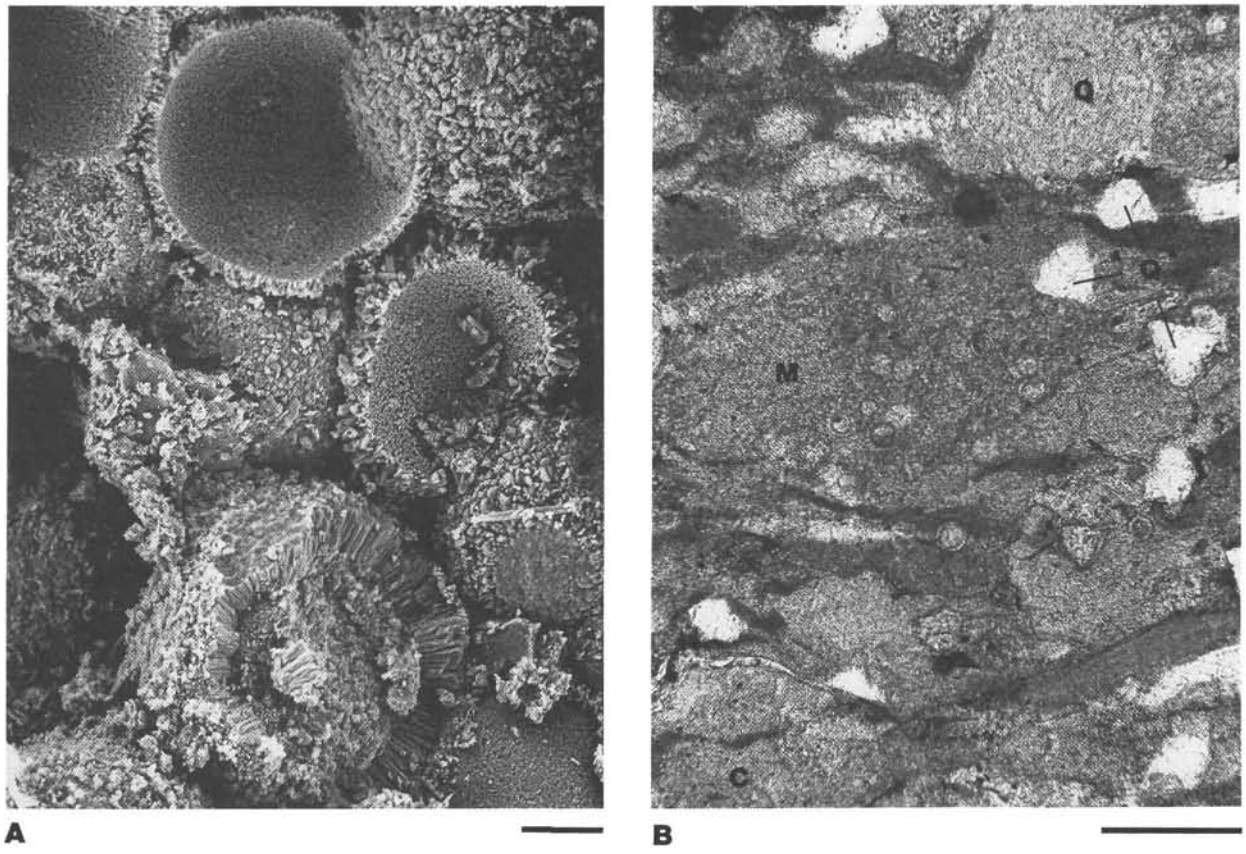

Figure 8. Microtextures of redeposited sediment (Valanginian–Barremian). **A.** SEM micrograph showing concentration of calcispheres in calcareous turbidite; note variety of test wall textures (Sample 123-765C-57R-4, 4–7 cm; scale bar is 10 μm). **B.** Photomicrograph of calcareous turbidite containing marlstone clast rich in calcispheres (M), claystone clasts (C), and angular quartz (Q) (Sample 56R-4, 148–150 cm; scale bar is 0.2 mm).

claystone is virtually identical to that in the upper part of the underlying subunit (L3A) and the lower part of the overlying unit (L4). The clay is largely smectitic I/S and lesser illite (Compton and Locker, this volume); minor (less than 5%) disseminated coarse detritus includes radiolarians, agglutinated foraminifers, and quartz. Sedimentary structures are few, mainly *Chondrites*-type burrows. Carbonate content is low (1.5%; Ludden, Gradstein et al., 1990) and consists mainly of small rhombs of manganese carbonate (rhodochrosite and kutnahorite) formed during diagenesis (Dumoulin, this volume).

Several layers of greenish gray to red waxy claystone occur in this subunit, mostly in Core 123-765C-57R, and appear to be bentonites, as described above. Layers rich in radiolarians occur throughout the unit and are a few millimeters to several centimeters thick. Both concentrated, laminated layers and more diffuse, wispy lenses of radiolarite were observed. Most radiolarians are recrystallized to microcrystalline quartz and are filled with chalcedony cement.

Interpretation

This subunit formed under oxidizing, sub-CCD conditions like those inferred for the underlying unit, but it contains allochthonous calcareous sediments not found in the underlying section. The noncalcareous claystone layers are slowly deposited pelagic sediments; the calcareous sediments are turbidites derived from the adjacent continental margin. Sedimentary structures characteristic of the Bouma sequence occur in most of the coarser grained calcareous intervals and indicate deposition by turbidity currents; fine-grained calcareous intervals lack such structures, but their sharp bases and burrowed, gradational tops support a turbidite origin (Dumoulin, this volume).

The calcareous material in these turbidites is well-preserved, particularly in comparison to that in the underlying inoceramid sediment unit (L2). Nannofossil assemblages are more diverse and much less etched; some inoceramid prisms are pitted (bored and etched), but many are not. Thus, this material was originally deposited above the CCD, most likely above the lysocline. However, no grains diagnostic of a shallow-water (photic zone) origin were found; the benthic foraminifers are characteristic of bathyal or abyssal depths (Ludden, Gradstein, et al., 1990; Kaminski, Gradstein, et al., this volume). All the calcareous components—nannofossils, calcispheres, foraminifers, and inoceramid prisms—were found in the underlying inoceramid sediment unit; the marl that makes up the sand-sized clasts is identical to the material forming the fine-grained turbidites. The calcareous grains were probably derived from a source close to Site 765 but above the CCD—most likely higher parts of the adjacent continental slope or rise.

The noncalcareous component of these turbidites is also largely indicative of a deep-water, fairly local origin. Radiolarians are abundant. The radiolarian assemblages found in sand layers at Site 765 are more diverse than those disseminated in the background claystone; the sand assemblages are thought to have been penecontemporaneously displaced by density flows or bottom currents from an area of upwelling circum-Antarctic water near the continental slope (Baumgartner, this volume). Clay clasts resemble the intercalated noncalcareous claystone layers and may have been derived from nearby deposits on the lower continental

slope or rise. Angular quartz and glauconite, notable but subordinate components of these sediments, are the only grains suggestive of a shelf or truly continental provenance.

Obvious volcanic detritus is scarce throughout this subunit. Rare volcanic lithic grains occur in the turbidites, and only a few possible bentonite layers were found in the intercalated claystones. However, smectite is the dominant clay mineral in both "background" claystone and in clay and clay clasts in the turbidites; the high Mg and Fe content of this smectite indicates a volcanogenic origin (Compton and Locker, this volume). Triassic–Lower Jurassic volcanic rocks make up much of the northern margin of the Exmouth Plateau south of Site 765 (von Rad and Exon, 1983; N. Exon, pers. comm., 1989) and may have been the ultimate source of these smectitic clays.

The turbidites in this subunit show no striking changes in thickness or composition with time, although most of the thickest, coarsest grained calcareous intervals occur in the lower (Valanginian) half of the unit. Sedimentation rates throughout Unit L3B are relatively low (about 5 m/m.y.; Fig. 5). Turbidites are similar in composition, but coarser grained than those in the correlative Unit L3 at Site 261 and appear largely derived from the Exmouth-Wombat Plateau continental margin to the south. The influx of pelagic calcareous turbidites to Site 765 at this time is probably a result of Early Cretaceous eustatic lowstands of sea level (Dumoulin, this volume).

Unit L4, Radiolarian Claystone (Barremian–Aptian; Cores 123-765C-52R through -34R; 844.1–664.4 m sub-bottom)

Description

Claystone with subordinate layers rich in radiolarians and/or manganese carbonate makes up this interval (upper part of Subunit VC, Subunits VB, VA, IVD, and IVC of Ludden, Gradstein, et al., 1990); redeposited calcareous sediment occurs in Cores 123-765C-40R through -34R. The claystone is varicolored in the lower cores (123-765C-52R through 42R), mainly shades of reddish brown, gray, and green that alternate in centimeter- to decimeter-thick layers, but is dominantly greenish gray in the upper cores. Dark gray to black claystone layers a few centimeters thick are scattered throughout this unit; a layer in Section 123-765C-45R-3 contains 5% organic carbon (Ludden, Gradstein, et al., 1990). The claystone in Unit L4, like that in the underlying units, consists mainly of smectitic I/S, illite, and microcrystalline quartz (Compton and Locker, this volume); XRF analyses indicate a consistently high SiO_2 content (68%–86%; Ludden, Gradstein, et al., 1990).

Unit L4 sediment is massive and contains few sedimentary structures, except for dark lenses and wispy layers a few millimeters to several centimeters long and a few millimeters thick; these structures generally parallel bedding and are particularly notable in Cores 123-765C-52R through -47R. Lenses examined in thin section contain abundant opaque material (pyrite and/or organic grains). The streaky texture suggests flattened burrows and/or compositional layering disrupted by bioturbation.

Microfossils in these sediments include palynomorphs, benthic foraminifers, and radiolarians. Diverse and abundant palynomorphs occur throughout Unit L4; the ratio of spores and pollen to dinoflagellates is high, particularly in the upper (Aptian) cores (Ludden, Gradstein, et al., 1990). Agglutinated foraminifers occur in Cores 123-765C-52R through -47R; assemblages are increasingly diverse with depth (Kaminski, Gradstein, et al., this volume). Radiolarians occur throughout the unit and are sparsely dispersed in claystone or concentrated into grain-supported lenses and layers a few millimeters to 4 cm thick. Both the winnowed and redeposited types of concentration described in Unit L3 occur in this unit; some layers appear to have been disrupted by bioturbation after deposition. Test preservation is variable and changes with depth. In the lowest cores (123-765C-42R and below), most radiolarians have been completely replaced by carbonate or occur as ghosts (sometimes pyritized) within carbonate micronodules (Plate 4, Fig. 5). Other tests have been dissolved, leaving detailed molds in the claystone matrix, and rare tests are filled with glauconite. In the higher cores, most tests have been replaced by opal-CT (Dumoulin, this volume).

Diagenetic carbonate is common throughout this unit and occurs as rhombs and spherical micronodules (Fig. 9A). Rhombs, 4 to 50 μm in diameter, were found mainly in the lower cores, sparsely dispersed in claystone or radiolarite. Micronodules are concentrated into larger nodules, layers, or lenses, a few millimeters to several centimeters thick, or float in a claystone matrix. Some have filled burrows or replaced fecal pellets (Fig. 9B). Layers consist exclusively of closely packed micronodules or contain minor amounts of detrital material, radiolarian tests recrystallized to microcrystalline quartz, clay matrix, or poikilitic carbonate cement. Layers of micronodules may exhibit parallel lamination, normal or reverse grading, and sharp or diffuse boundaries; their megascopic form, internal textures, and sedimentary structures commonly resemble those of the radiolarian-rich layers described above. Individual micronodules are 30 to 800 μm in diameter (mostly 100–400 μm), and many contain one or several obvious radiolarians (Plate 4, Fig. 5).

Shipboard XRD analyses suggested that the carbonate-rich layers in Unit L4 contain rhodochrosite, dolomite, and/or mixed Mg- and Mn-carbonates (Ludden, Gradstein, et al., 1990). However, EDS analyses of numerous carbonate rhombs and micronodules from Unit L4 sediments indicate the presence of abundant Mn, generally minor Ca, and no Mg (this study; J. Thurow, pers. comm., 1989). Thus, manganese carbonate (mostly rhodochrosite, lesser kutnahorite) appears to be the dominant authigenic carbonate mineral in this unit. Authigenic barite also occurs sparsely but persistently throughout Unit L4, generally as large poikilotopic euhedra (Plate 4, Fig. 5).

In addition to the radiolarite layers described above, which may show normal or reverse grading, another type of graded layer, similar to those in Unit L3, also occurs in the radiolarian claystone. These layers have sharp bases and diffuse tops; most are base-cut-out (BCDE) Bouma sequences with well-developed parallel- and cross-lamination. In the lower cores (123-765C-41R and below), such layers are rare (less than 2% of the section), relatively thin (5–25 cm), and include little or no primary calcareous material. They contain abundant radiolarians (generally replaced by carbonate; some filled with glauconite), but also numerous clay clasts and quartz. Inoceramid prisms and calcareous foraminifers occur sparsely; nannofossils were found in only one sample (Sample 123-765C-47R-1, 56–58 cm), which appears to be a caving from higher in the section. Some layers contain abundant micronodules and/or rhombs of manganese carbonate that obscure the primary texture. Graded layers in the upper cores (123-765C-40R through -34R) are abundant (more than 50% of section), thick (to 3.5 m), and rich in nannofossils, calcareous foraminifers, and other primary calcareous components (Dumoulin, this volume). Carbonate makes up 10% to 55% of most layers (Dumoulin, this volume); other constituents include clay, clay clasts, quartz, radiolarians, and glauconite.

Interpretation

This interval consists mainly of claystone rich in radiolarians and deposited below the CCD. Red-brown sediment in the lower cores gives way to green-gray sediment above; this shift coincides with a sharply increased overall sedimentation rate (20 m/m.y.; Fig. 5), and with increased terrestrial input, as indicated by the greater abundance of spores and pollen relative to dinoflagellates

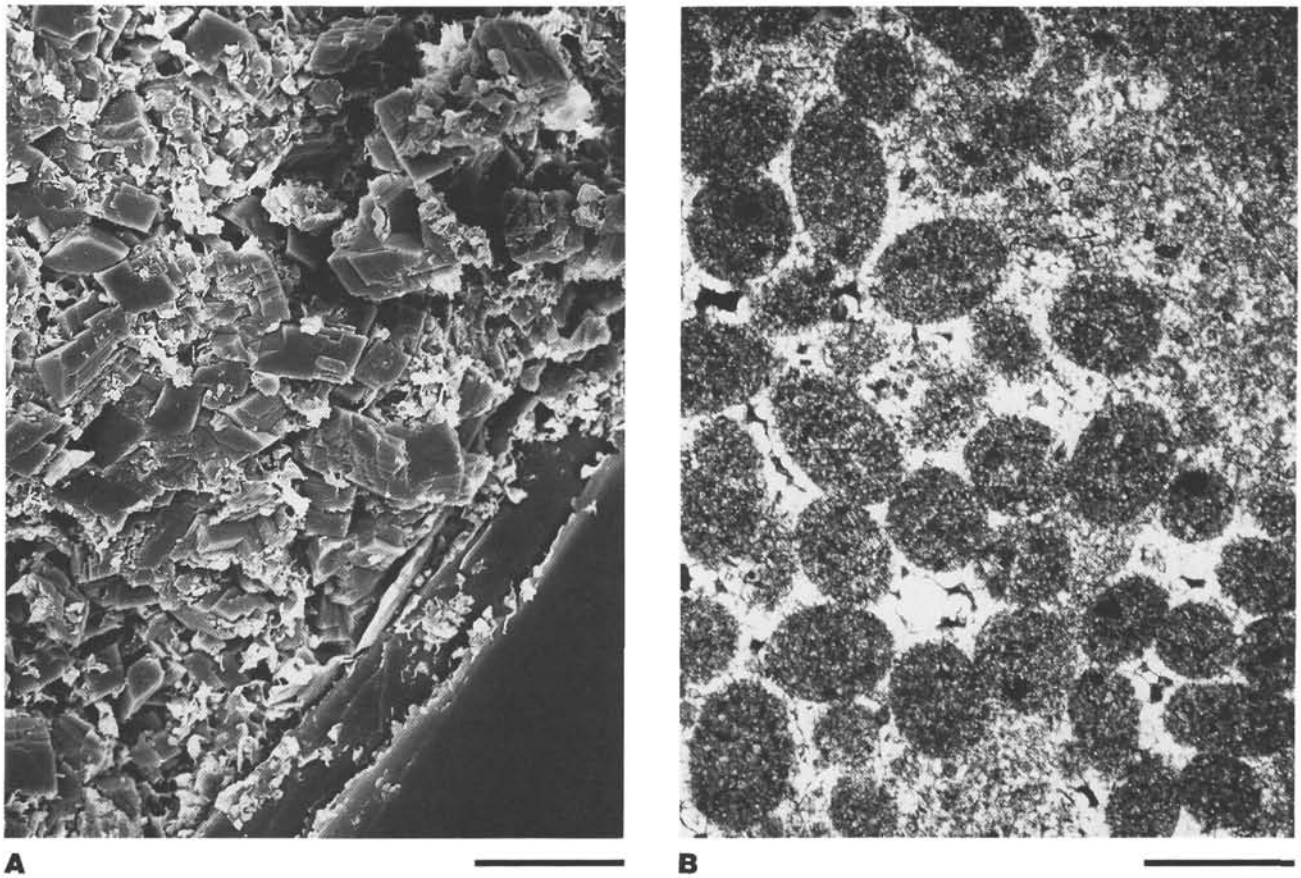

Figure 9. Microtextures of radiolarian claystone (Barremian–Aptian). **A.** High-magnification SEM photograph of rhombs of manganese carbonate concentrated into micronodule (Sample 123-765C-47R-1, 56–59 cm; scale bar is 10 mm. **B.** Photomicrograph of probable fecal pellets containing pyritized radiolarian tests; pellets composed mainly of manganese carbonate (Sample 123-765C-52R-1, 114–116 cm; scale bar is 0.6 mm).

in Aptian palynomorph assemblages (Ludden, Gradstein, et al., 1990).

Although Unit L4 is predominantly fine-grained, processes other than pelagic settling have been involved in its accumulation. As in underlying units, radiolarians have been concentrated by winnowing bottom currents and redeposited by turbidity currents. Obviously redeposited sediment other than radiolarite is rare through most of this unit, but becomes abundant in the upper Aptian section. Any primary calcareous component in most of the older turbidites was lost during diagenesis, but upper Aptian graded sequences are moderately calcareous and similar to those in Subunit L3B. Calcareous fossils in Unit L4 turbidites indicate a source above the CCD, but at bathyal or greater depths (Ludden, Gradstein, et al., 1990), such as the adjacent continental slope or rise (Dumoulin, this volume).

Biostratigraphic data (Ludden, Gradstein, et al., 1990) indicates that the sharp increase in sedimentation rate at Site 765 occurred about the level of Core 123-765C-45R, somewhat prior to the influx of calcareous turbidites. Thus, it is likely that at least some of the Unit L4 claystone at Site 765 constitutes fine-grained turbidites. Structures diagnostic of turbidites, such as obvious graded bedding and Bouma sequences, were not observed in the claystone, but such features are generally not seen in fine-grained "mud turbidites." Stow and Piper (1984), for example, recognized mud turbidites on the basis of subtle attributes, including fine parallel lamination and small-scale (mm to cm) changes in sediment color and amount of bioturbation. Such features occur throughout Unit L4 claystone and are consistent with the inference that fine-grained turbidites form an important part of this unit. The lack of calcareous material and the finer grain size in these turbidites, in contrast to the coarser, more calcareous sediment redeposited in the higher cores, probably reflects global shifts in sea level and concomitant changes in the CCD (see further discussion below).

Authigenic barite and manganese carbonate, found sparsely in the underlying sediments of Unit L3, occur throughout Unit L4 ; presence of these minerals reflects both initial sediment composition and later diagenesis. Barite can be derived from biogenic material and is commonly associated with clay-rich biosiliceous sediments deposited below regions of high surface productivity (Compton et al., this volume). Manganese carbonate minerals also occur in such sediments; their formation and concentration appears largely controlled by the position of oxidation-reduction boundaries within the sediment column (Hein and Koski, 1987). Isotopic data from manganese carbonates at Site 765 suggest that they formed early within the sulfate reduction zone, but were later recrystallized at deeper burial depths (Compton, this volume).

Upper Sequence (Cores 123-765C-33R through -1R and 123-765B-41X through -1H)

Unit U1, Zeolitic Claystone and Calcareous Sediment (Albian–lower Miocene; Cores 123-765C-33R through -14R; 664.5–474.1 m sub-bottom)

Description

This interval (Subunits IVB, IVA, and Unit III of Ludden, Gradstein, et al., 1990) consists of locally zeolitic, varicolored,

noncalcareous claystone and redeposited calcareous sediment. Claystones are primarily brown, red, and yellow, in contrast to the greenish-gray claystones found above and below. Zeolite (clinoptilolite) occurs through most of the unit, but is particularly abundant in the lower (Albian-Cenomanian) cores. I/S with variable amounts of interstratified illite is the dominant clay mineral throughout this unit, but palygorskite is abundant in Cores 123-765C-30R through -24R and kaolinite is notable in the higher cores (Core 123-765C-18R through -14R) (Compton and Locker, this volume). Manganese oxide forms a distinct horizon 1.5 cm thick within claystone in Core 123-765C-24R and occurs as micronodules, crusts, and bundles of diffuse laminae elsewhere in the unit. The claystone contains locally common agglutinated foraminifers and rare radiolarians, some of which have been replaced by clinoptilolite.

The redeposited calcareous layers are mostly less than 50 cm (rarely, as much as 5 m) thick and consist largely of clayey nannofossil chalk that grades downward into sand-sized calcareous fragment and/or foraminifer chalk; subordinate layers of matrix-supported conglomerate occur in Cores 123-765C-23R and -19R and contain clasts to 8 cm in diameter. Both fine- and coarse-grained calcareous layers contain considerable amounts of noncalcareous material, including clay, quartz, and claystone and volcanic lithic clasts. Calcareous layers have sharp, commonly scoured, bases and gradational, bioturbated tops; trace fossils include *Chondrites, Planolites,* and rare *Zoophycos.* Sand- and silt-sized chalk intervals typically show well-developed parallel- and cross-lamination, and local climbing ripples. Sandy chalks are noticeably coarser grained in Unit U1 than in the underlying units and may contain clay pebbles to several centimeters in diameter. They also include reworked biogenic components that are considerably older than the sediments containing them; Hauterivian-Barremian radiolarians, for example, were found in Cenomanian and Campanian chalks (p. 127, Ludden, Gradstein, et al., 1990).

Calcareous layers generally are more abundant, thicker, and purer in the upper part of Unit U1. Calcareous sediment makes up only about 10% of Cores 123-765C-33R through -28R, but is more than 65% of Cores 123-765C-18R through -16R. Calcareous layers in the lower cores are generally less than 50 cm thick, but may reach 2 to 5 m thick above Core 123-765C-19R. Shipboard analyses found a sharp increase in the carbonate content of individual layers at the base of Core 123-765C-25R (Turonian). Below this level, maximum values are about 35%; above it, they are 60% to 80%.

Interpretation

This unit consists of pelagic claystone that accumulated slowly in an oxic environment below the CCD, interlayered with allochthonous calcareous sediment originally deposited above the CCD. Sedimentation rates of 0.8 to 2.0 m/m.y. (Fig. 5) are the lowest calculated for Site 765. Presence of palygorskite and of manganese micronodules and crusts in the pelagic claystones supports the inference of slow sedimentation based on biostratigraphic constraints. Kaolinite, virtually absent from all underlying units, is increasingly abundant upward within Unit U1. Kaolinite generally indicates low-latitude source areas, and its presence in these sediments reflects the rapid northward movement of the Australian plate during the Cenozoic (Compton and Locker, this volume). In contrast to underlying Units L3 and L4, Unit U1 contains relatively few radiolarians in both background and redeposited sediments. This suggests cessation of the high productivity (upwelling?) conditions thought to have existed along the northwest Australian coast throughout the mid-Cretaceous (P. O. Baumgartner, pers. comm., 1990). The presence of zeolite in this unit probably reflects the scarcity of radiolarian tests and consequent low silica concentration during diagenesis.

The occurrence of Bouma sequence sedimentary structures in many of the calcareous layers in Unit U1 indicates that most were deposited by turbidity currents. Biotic components of these turbidites denote a relatively deep-water provenance (continental rise, slope, or outer shelf) like that inferred for redeposited sediments in underlying units. The higher carbonate content of turbidites in the upper (Turonian and younger) part of Unit U1 probably reflects the establishment of "mature" circulation and more calcareous sedimentation throughout the Indian Ocean at this time (e.g., Veevers and Johnstone, 1974), as will be further discussed below. The presence in Unit 1 of considerably older reworked material, coarse-grained turbidites, and local debris flows indicates that more vigorous erosional and redepositional processes, such as active incisement of submarine canyons, were operating along the Australian margin at this time; evidence of such processes is even more pronounced in the overlying units.

Unit U2, Calcareous Sediment (lower Miocene–Pliocene; Cores 123-765C-13R through -1R and 123-765B-41X through -10H; 474.1–86.4 m sub-bottom)

Description

Redeposited calcareous sediments dominate this interval (Subunits IIC–IC, lower half of Subunit IB of Ludden, Gradstein, et al., 1990). It is interlayered with subordinate, thin layers of noncalcareous clay; the clay is greenish gray, not brown or red like Unit U1 clay, and contains little or no siliceous biogenic material, unlike Unit U3 clay. Sediments are increasingly lithified lower in the interval; oozes and clays give way to chalks and claystones at about Core 123-765B-32X.

Redeposited calcareous sediments are of two main types: (1) graded sequences of clay to silt or sand size, or (2) more complex, thicker sequences that include clast- or matrix-supported conglomerate. The simple graded sequences consist largely of nannofossils and lesser clay; whole and broken foraminifers and lesser quartz make up most of the coarse fraction. Most layers have gradational, bioturbated tops, and sharp, commonly scoured bases. Recognizable burrows are mainly *Chondrites* or *Planolites,* but *Zoophycos* is particularly notable in middle Miocene sediments. Sedimentary structures are best-developed in the more lithified Miocene cores, and include parallel-, cross-, and convolute-lamination.

Composition and distribution of the graded calcareous layers also changes throughout Unit U2. Middle Miocene layers are mostly less than 50 cm thick (average, 10–25 cm) and contain 40% to 99% carbonate. Layers in the upper Miocene sequence rarely exceed 100 cm (average 15-40 cm) and contain 73% to 95% carbonate. Layers are thickest (up to 350 cm) and contain more siliciclastic material (carbonate content mostly 57%–73%) in the Pliocene cores.

Most of the biogenic grains in Unit U2 calcareous sand layers appear to have been redeposited soon after their initial accumulation, but considerably older reworked material also is present. The oldest reworked components were found in the youngest strata: Miocene sediments contain Upper Cretaceous, Oligocene, and Eocene for-aminifers; upper Miocene-Pliocene sediments contain Jurassic spores, pollen, and dinoflagellates; and upper Pliocene sediments contain Permian and Triassic pollen.

Conglomerate occurs mostly in lower Miocene and Pliocene cores. Lower Miocene sediment includes more than 3 m of matrix-supported conglomerate with rounded pebbles to 8 cm in diameter. Conglomerate and pebbly sandstone are absent from the middle Miocene section and occur only rarely in upper Miocene sediment. The Pliocene cores contain complex sequences of clast-

and/or matrix-supported conglomerate 6 to 42 m thick. These sequences include blocks up to 175 cm in diameter and are grossly graded; most clasts are 1 to 40 cm in diameter.

Clasts and matrix in the conglomerates are mainly clayey nannofossil ooze (chalk) that were apparently locally and contemporaneously derived. However, clasts of exotic and/or older lithologies occur throughout this unit. Clasts of basalt, Upper Cretaceous (Turonian) brown claystone, and Middle Jurassic (upper Bathonian–Callovian) black silty claystone were identified in the middle Miocene sediments; older Jurassic (lower Bajocian, Aalenian–Bajocian) black claystone clasts occur in the uppermost Miocene and Pliocene sediments. Ages of these clasts are based on nannofossil assemblages (p. 125, Ludden, Gradstein, et al., 1990).

Composition and distribution of the noncalcareous clay layers changes through the unit (Compton and Locker, this volume). Palygorskite, kaolinite, and randomly interstratified illite/smectite/chlorite are the major lower and middle Miocene clay minerals, whereas upper Miocene clay is mostly sepiolite and kaolinite, with lesser I/S and palygorskite. Kaolinite, I/S, and illite are the main Pliocene clay minerals. Clay layers are 1 to 30 cm thick and make up a few percent to 15% of cores throughout this unit. Layers are thin, but are relatively abundant in the lower and middle Miocene cores (7% clay layers, mostly 1-6 cm thick), rare and thin in the upper Miocene cores (1%–4% clay layers, mostly 1–3 cm thick), and thickest and relatively abundant in the Pliocene cores (about 10% clay layers, up to 30 cm thick). Abundant (to 30%) small rhombs of authigenic dolomite occur in the Miocene claystones.

Interpretation

This interval, like the underlying Upper Cretaceous-Paleogene section, consists of interlayered pelagic clay and redeposited calcareous sediment. The noncalcareous composition of the clay indicates that deposition took place below the CCD; the clay's greenish-gray color suggests relatively reducing conditions during deposition and/or diagenesis, which in turn probably reflect the rapid accumulation of this unit (26 m/m.y.; Fig. 5). Total volume and relative abundance of redeposited material in Unit U2, as well as overall sedimentation rate, are greater than those in any other unit at Site 765.

Most clay- to sand-sized calcareous layers in Unit U2, like those in the underlying units, have Bouma sequence sedimentary structures that indicate deposition by turbidity currents. Thick, coarser grained (conglomeratic) layers were most likely emplaced by debris flows and may have formed during periods of catastrophic failure along the continental margin. Redeposited calcareous material in Unit U2, like that found throughout the Site 765 sedimentary section, had a relatively deep-water (slope or deep shelf) provenance. Benthic for-aminifer assemblages are dominantly bathyal; forms typical of the photic zone are absent.

The influx of calcareous and lesser siliciclastic detritus to Site 765 during the late Paleogene-early Neogene reflects increased erosion along the northwest Australian margin and accentuated canyon incisement at the shelf edge; this influx coincides with a significant eustatic lowstand (see below). The abundance of reworked, considerably older fossils and clasts in Unit U2 demonstrates that mass flows contributing to these sediments were significantly erosive and downcut into progressively older strata; by Pliocene time, material of Middle Jurassic, Triassic, and Permian age was being redeposited. This suggests that submarine canyons along the Exmouth Plateau, such as Swan Canyon due south of Site 765, were no longer mainly passive conduits for redistribution of contemporaneous material, as they appear to have been during the Cretaceous (Dumoulin, this volume), but were being actively incised at this time.

Unit U3, Siliceous Ooze and Calcareous Sediment (Quaternary; Cores 123-765B-9H through -1H; 86.4–0 m sub-bottom)

Description

Unit U3 (upper half of Subunit IB, all of Subunit IA of Ludden, Gradstein, et al., 1990) consists of diverse fine- to coarse-grained calcareous sediments intercalated with subordinate layers of olive to dark greenish-gray noncalcareous clayey siliceous ooze. The noncalcareous layers are 5 to 120 cm thick; they are distinguished from those in Unit U2 by their abundance of siliceous biogenic material (30%-80% of most samples). Radiolarians are particularly diverse and well-preserved, but sponge spicules, diatoms, silicoflagellates, and ebridians also occur. Minor coarse detritus in the clay includes quartz and up to several percent volcanic glass. Kaolinite, I/S, and lesser illite are the major clay species (Compton and Locker, this volume).

Calcareous layers make up more than 85% of Unit U3; most contain 45% to 80% carbonate. Cores 123-765B-9H through -5H contain complex sequences of matrix- and clast-supported conglomerate like those in the underlying Pliocene section. Clasts in these conglomerates are largely intraformational—calcareous ooze and clay—but include exotic lithologies, such as Campanian chalk, Middle Jurassic claystone, and basalt. These cores also contain calcareous layers 10 to 200 cm thick that consist mostly of clayey nannofossil ooze; some oozes grade downward into silt- or sand-sized foraminifer ooze with subordinate quartz and siliceous microfossils. The upper four cores of Unit U3 contain similar layers of nannofossil and foraminifer ooze, but none of the complex conglomeratic sequences.

Interpretation

The noncalcareous layers, like those in the underlying unit, are pelagic deposits that accumulated rapidly under reducing conditions and beneath the CCD; intercalated calcareous layers are turbidites and debris flows derived from a deep shelf or slope source. Relative abundance, thickness, and calcareous content of these layers are similar to those of the carbonate layers in the underlying unit, and overall sedimentation rate is high (Fig. 5). The abundance of siliceous biogenic material in the Quaternary section is a result of Australia's northward movement into the zone of equatorial high productivity (Cook, 1977); volcanic glass is probably derived from the nearby Indonesian volcanic arc.

SITE 261 SEDIMENTS

Sedimentary Sequence

The general sedimentary succession at Site 261 is summarized here and in Figure 10 and is described in detail below. A 579.5-m-thick section was drilled (including 47.5 m of igneous basement) and overall recovery was 23%. Our study concentrates on the lower sequence, 323 m of sediments (Cores 27-261-34 through -10; Units 4 and 3B of Veevers, Heirtzler, et al., 1974), which we subdivided into four lithologic units, L1 through L4 (one unit has been split further into two subunits), on the basis of composition, color, and microstructures. The lowest unit comprises two intervals of limestone intercalated within the upper few meters of basalt and 25 cm of red nannofossil marl directly overlying the uppermost basalt. The second unit, 4.6 m of brown nannofossil claystone, gradationally overlies the first and includes a distinctive 30-cm-thick interval of calcite needle-rich marl. The third unit, redeposited calcareous sediment and intercalated noncalcareous claystone, may be as much as 100 m thick. (Because Leg 27 was not continuously cored, the exact boundaries of this unit are uncertain and have been arbitrarily placed at the top of the recovered portion of Core 27-261-32 and the base of

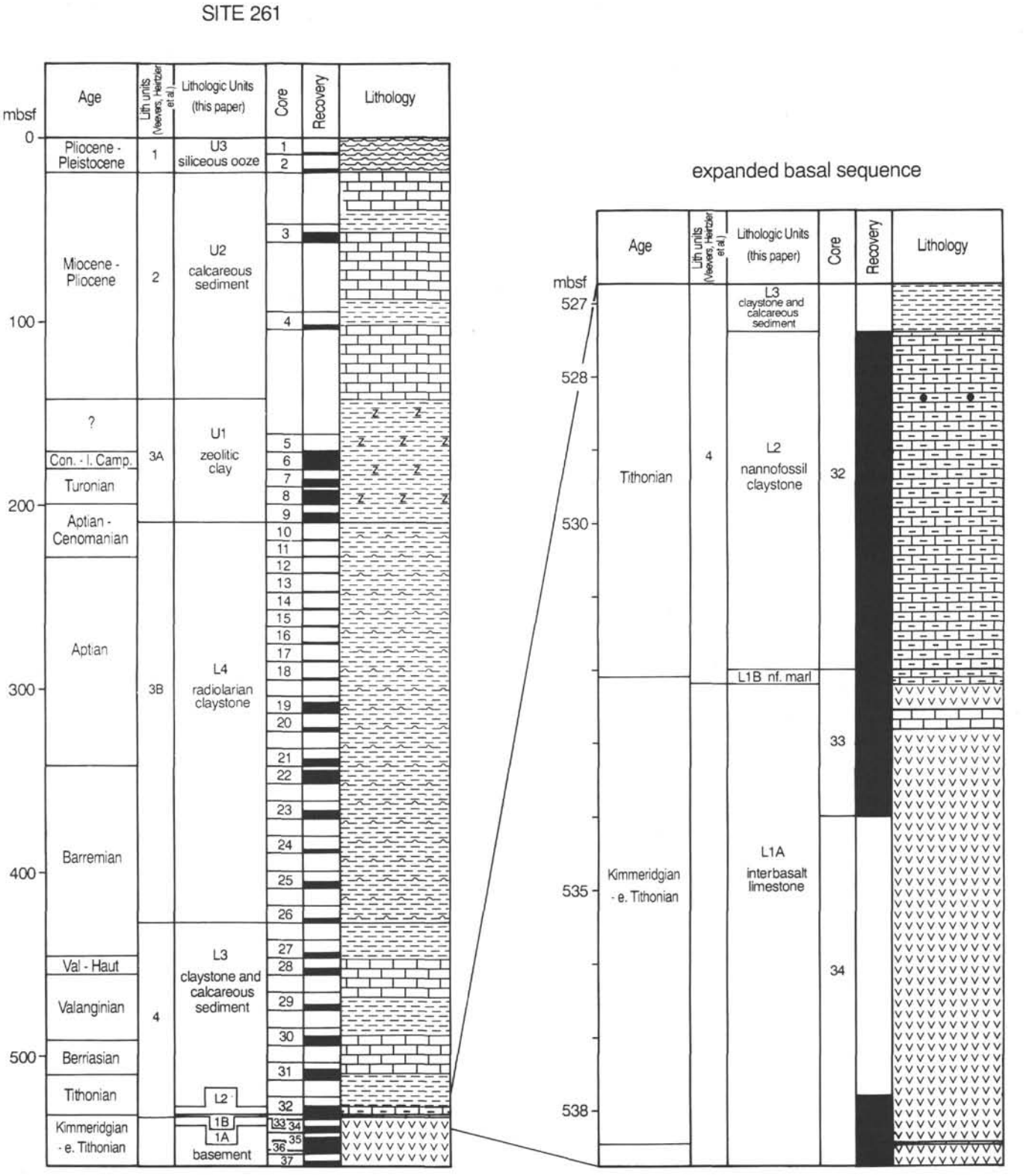

Figure 10. Stratigraphic section at DSDP Site 261; depths are in meters below the seafloor. Age determination is based on new nannofossil data presented here and reinterpreted microfossil data from Veevers, Heirtzler, et al. (1974). Lithologic symbols as for Figure 2.

Core 27-261-26.) The fourth unit, gray radiolarian claystone, makes up the bulk of the lower cores and is more than 200 m thick.

The upper sequence at Site 261 (Cores 27-261-9 through -1) has been studied, and is described, in less detail. Three units (U1–U3) are recognized and consist of brown zeolitic clay, greenish-gray calcareous sediment, and greenish-gray siliceous ooze (Units 3A, 2, and 1, respectively, of Veevers, Heirtzler, et al., 1974).

Lower Sequence (Cores 27-261-34 through -10)

Unit L1, Limestone and Marl

Subunit L1A, Interbasalt Limestone ([?]Kimmeridgian–lower Tithonian; Samples 27-261-34-1, 68–67 cm, and -33-1, 82–54 cm; 538.4–532.5 m sub-bottom)

Description

The deepest *in-situ* sediments recovered at Site 261 consist of recrystallized, fine-grained, pale pinkish gray limestone intercalated with basalt; a 1-cm-thick layer occurs in Core 27-261-34 and a 30-cm-layer in Core 27-261-33 (Fig. 11). These sediments were not noted in the Site 261 visual core descriptions nor described elsewhere in the Leg 27 *Initial Reports* volume (Veevers, Heirtzler, et al., 1974). Upper and lower contacts of both layers are sharp and marked by several millimeters of fine-grained green celadonite. The limestone layer in Core 27-261-34 has a thin, even, basal fringe of bladed sparry calcite, and a thicker, more irregular, upper margin of coarser grained, more equant calcite (Fig. 12).

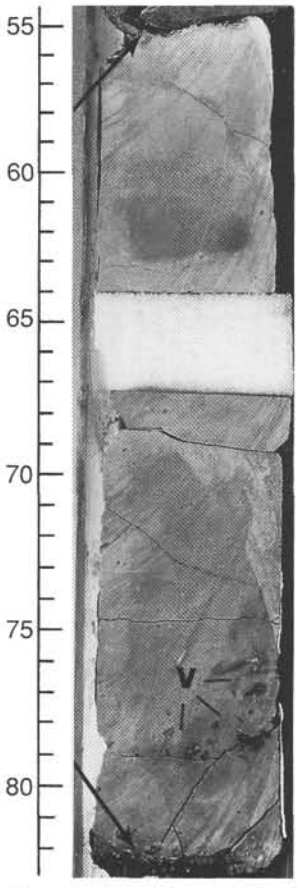

Figure 11. Thick limestone layer intercalated with basalt; note angular volcanic lithic clasts (V) toward base. Arrows indicate limestone/basalt contacts (interval 27-261-33-1, 55–82 cm).

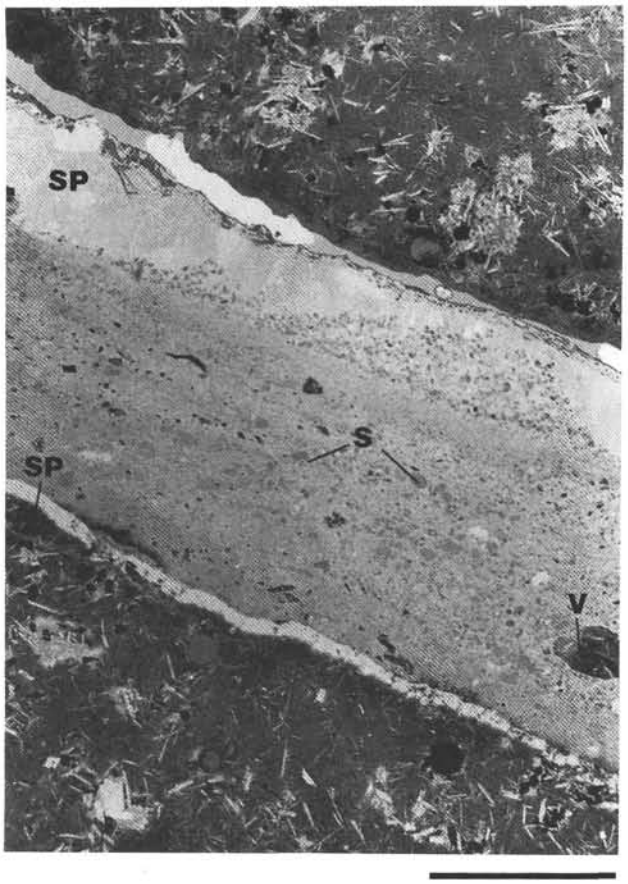

Figure 12. Photograph of entire thin section showing geopetal fabric in thin limestone layer intercalated with basalt. Sedimentary (S) and volcanic (V) lithic clasts float in a matrix of fine crystalline calcite; bladed sparry calcite (SP) occurs along the basalt/limestone contacts and is thicker along the upper contact (Sample 27-261-34-1, 66–70 cm; scale bar is 5 mm).

The bulk of both interbasalt limestone layers consists of relatively equant to slightly elongate calcite crystals 20 to 100 μm in size. Scattered throughout this matrix are calcispheres, inoceramid prisms (some of which contain pits and tubes that are probable microborings, as described above from Unit L2 at Site 765), calcareous foraminifers, and coccoliths (Figs. 13, 14). Also distributed throughout the matrix (but especially common toward the base of the limestone layers) are sedimentary and volcanic lithic clasts (Figs. 11, 12, 13A, 14A). The sedimentary clasts are mostly rounded to irregular in form, 40 μm to 1 cm in size, and made up of red to dark brown claystone and marl that contain calcispheres, coccoliths, and/or radiolarian ghosts. The volcanic clasts consist of basalt and altered glass that are texturally and compositionally identical to the igneous rocks intercalated with the limestone. The volcanic clasts are angular and are 0.1 to 7.0 mm in diameter. Total carbonate content of this facies is about 90% (Table 2).

Interpretation

The limestone layers within the igneous section at Site 261 formed as detrital sediment filling fissures within basalt flows; deposition could have been contemporaneous with, or at some time subsequent to, volcanism. Sediment is dominantly fine-grained calcareous pelagic material (coccoliths) and a subordinate amount of coarse silt- and sand-sized debris, such as calcispheres, inoceramid prisms, and lithic clasts. The rounded to irregular shapes of some sedimentary clasts indicate that they were soft

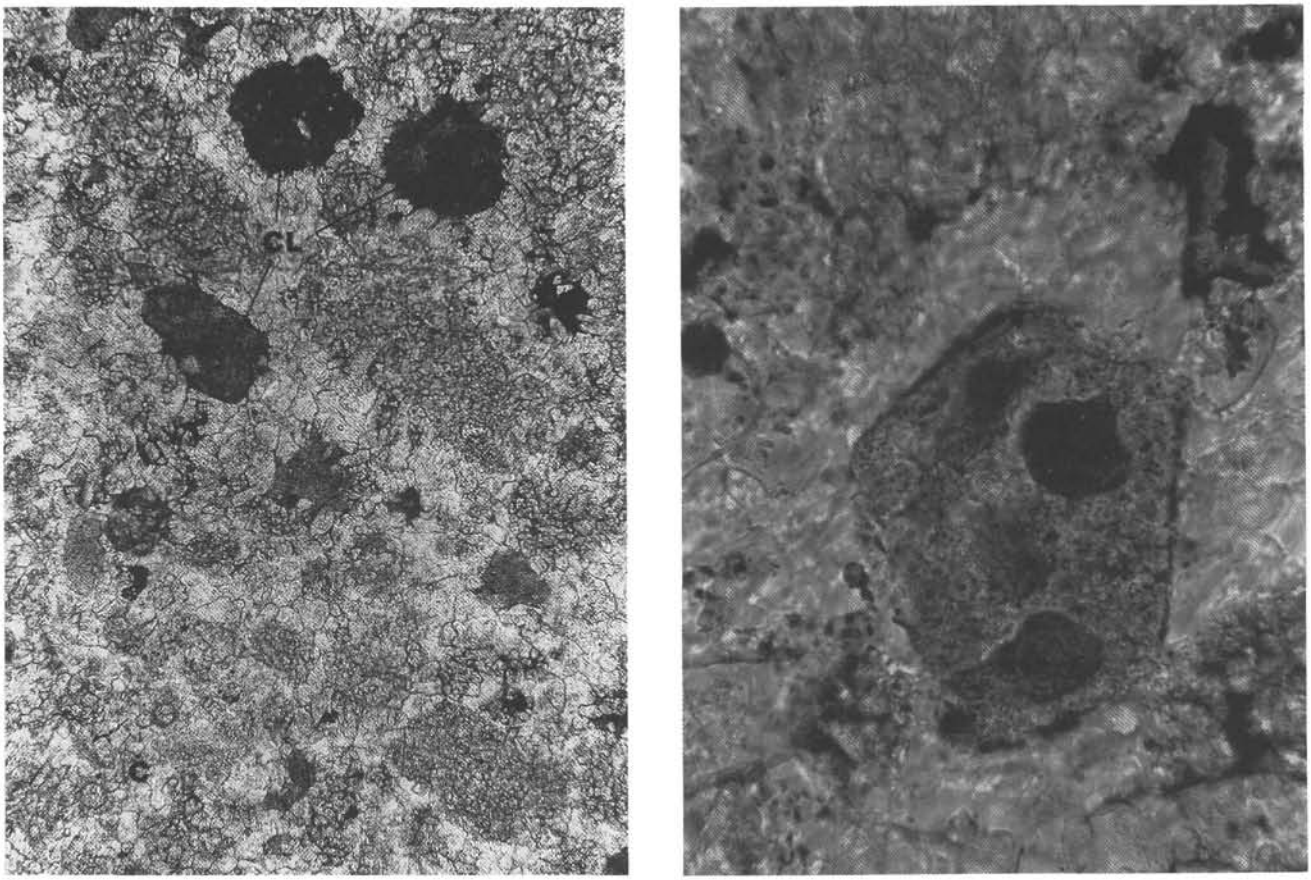

Figure 13. Photomicrographs of limestone layers within basalt; Sample 27-261-34-1, 66–70 cm. **A.** Calcispheres (C) and claystone clasts (CL) in recrystallized calcite matrix; scale bar = 0.2 mm. **B.** Inoceramid prism with large, clay-filled pits (probable microborings); scale bar = 30 µm.

when deposited, and their textural and compositional similarity to the red nannofossil marl directly overlying the basalt suggests that they represent intraclasts that have not been transported far. The volcanic fragments also appear locally derived.

The basal sparry rim of the lower limestone layer formed through nucleation and growth of calcite cement along the base of the basalt fissure shortly after it formed and before any sediment was deposited. Coarse-grained spar eventually filled the void that remained above the sediment accumulation. Thicker rim cements along the roofs of former voids and thinner rim cements on the floors are typical geopetal fabrics (see Bernoulli et al., 1978).

The interbasalt limestones are harder, more lithified, and less porous than all other sediments recovered at Sites 261 and 765. Their induration reflects both depositional and diagenetic processes. Sediments that accumulate in a protected environment such as a fissure are more porous than sediment that accumulates on the seafloor because the roof of the fissure protects them from compaction by overlying sediment. Thus, such protected sediments retain more intergranular space that can later be filled by cement. Much of the equant crystalline calcite noted in thin-section and SEM observations of the interbasalt limestones appears to be intergranular cement. For example, some inoceramid prisms are rimmed by calcite spar in optical continuity with the host grains, and coccoliths are surrounded and locally overgrown by blocky calcite crystals (Fig. 14B).

Recrystallization of originally finer grained calcareous material (such as coccoliths and coccolith debris) is the other important process that has indurated these limestones. Partially recrystallized coccoliths are noted in SEM observations, and the best-preserved nannofossils in these limestones occur within clay-rich clasts. Recrystallization of carbonate sediment can result from thermal effects of igneous intrusions; however, low-temperature alteration of basaltic glass can also induce calcite precipitation and recrystallization (Garrison et al., 1973). Low- temperature processes seem more likely to have affected the Site 261 limestones because recrystallization is not pervasive and textural relationships suggest that the sediment filled fissures in already cooled basalts.

Thus, the interbasalt limestone consists of pelagic sediments that have been indurated by cementation and recrystallization. Their original composition appears to have been equivalent to that of the overlying red nannofossil marl.

Subunit L1B, Nannofossil Marl (Kimmeridgian–lower Tithonian; Section 27-261-33-1, 25–0 cm; 532.2–532.0 m sub-bottom)

Description

Directly overlying the uppermost basalt interval in Core 27-261-33 is 25 cm of firm red nannofossil-bearing marl (Fig. 15A). The sediment is homogeneous and shows few sedimentary structures in core or thin-section. It consists largely of clay-sized to fine silt-sized material: about 35% nannofossils, 10% fine-grained (5 to 25 µm) rounded to equant to elongate carbonate grains, 50% clay, and 5% opaque grains. Total carbonate content of this facies is about 45% (Table 2). Some of the fine carbonate grains are needles several micrometers long. SEM observations

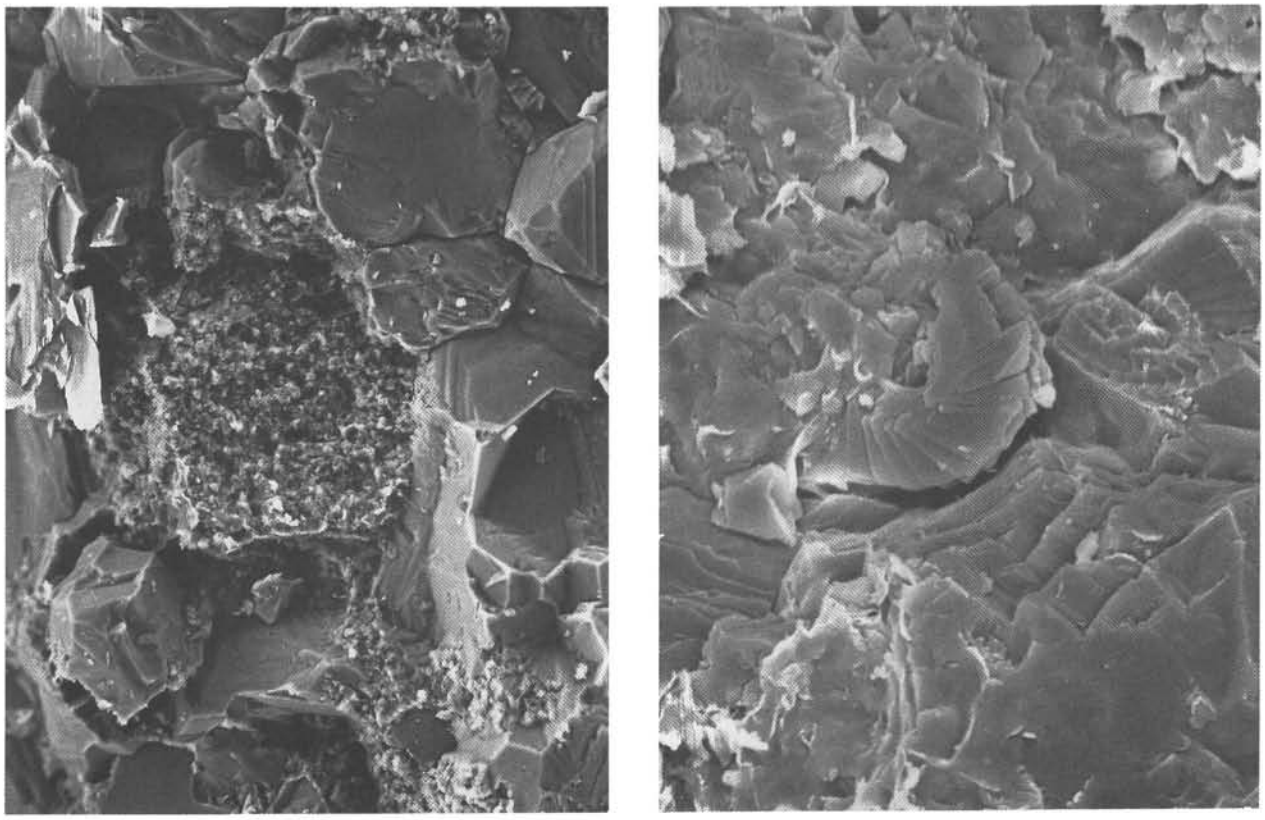

Figure 14. High-magnification SEM photographs of limestone layers within basalt. **A.** Claystone clast in coarsely recrystallized calcite matrix (Sample 27-261-34-1, 66–70 cm; scale bar = 35 mm). **B.** Coccoliths (*Watznaueria* sp.) surrounded by coarsely crystalline calcite matrix (Sample 27-261-33-1, 55–58 cm; scale bar is 4 μm).

Table 2. Carbonate content of selected samples from lower sequence at Site 261.

Core, section, interval (cm)	Unit	Lithology	$CaCO_3$ (%)
27-261-28-1, 83	L3	Calcareous sediment	[a]28
28-3, 24	L3	Claystone	[a]1
29-2, 112	L3	Calcareous sediment	13
29-3, 24	L3	Claystone	[a]3
30-2, 24	L3	Calcareous sediment	[a]21
30-3, 24	L3	Calcareous sediment	[a]34
31-2, 115	L3	Calcareous sediment	42
31-2, 140	L3	Calcareous sediment	34
31-2, 143	L3	Bioturbated boundary between calcareous sediment and claystone	13
31-5, 24	L3	Claystone	[a]0
32-2, 24	L2	Nannofossil claystone	[a]6
32-2, 49	L2	Calcisphere concentration	58
32-3, 24	L2	Nannofossil claystone	[a]10
32-3, 82	L2	Nannofossil claystone	10
32-4, 114	L2	Nannofossil claystone	17
33-1, 0	L1B	Nannofossil marl	44
33-1, 19	L1B	Nannofossil marl	47
33-1, 65	L1A	Interbasalt limestone	90

[a] From Bode (1974a).

indicate that nannofossils are randomly oriented in the clay-rich matrix.

Dispersed throughout the matrix, and locally concentrated into sub-millimeter thick layers and lenses, is subordinate (5%) coarse silt- and sand-sized material. Calcispheres dominate the coarse fraction; minor constituents include inoceramid prisms, ostracodes (Oertli, 1974), calcareous and agglutinated foraminifers, calcareous and phosphatic biotic debris, and mud intraclasts. The calcispheres, like those in the interbasalt limestone and unlike those higher in the section, are almost all filled with sparry calcite, and some have been coarsely recrystallized (Fig. 15B). Some of the inoceramid prisms contain irregular elongate to spherical pits (probable microborings) that have been filled with red mud.

Interpretation

The red nannofossil marl represents pelagic accumulation on the seafloor; deposition occurred above the lysocline, as indicated by the diversity and relatively good preservation of the nannofossils (see below). Rare, thin lenses rich in coarser grained material (calcispheres) are probably current lag deposits. Needles noted in the fine fraction were derived from the breakdown of calcisphere tests; more equant fine-grained calcite is nannofossil debris and intergranular cement. This unit is compositionally similar to, but much less recrystallized and indurated than, the interbasalt limestone.

Unit L2, Nannofossil Claystone (Tithonian; Core 27-261-32; 532–527.4 m sub-bottom)

Description

General features. Gradationally overlying the red nannofossil marl is 4.6 m of firm nannofossil claystone; the interval is distinguished by evidence of slow sedimentation (winnowed microtextures, manganese nodules) and by a distinctive 30-cm-thick layer rich in calcisphere debris (calcite needles) toward the top. The

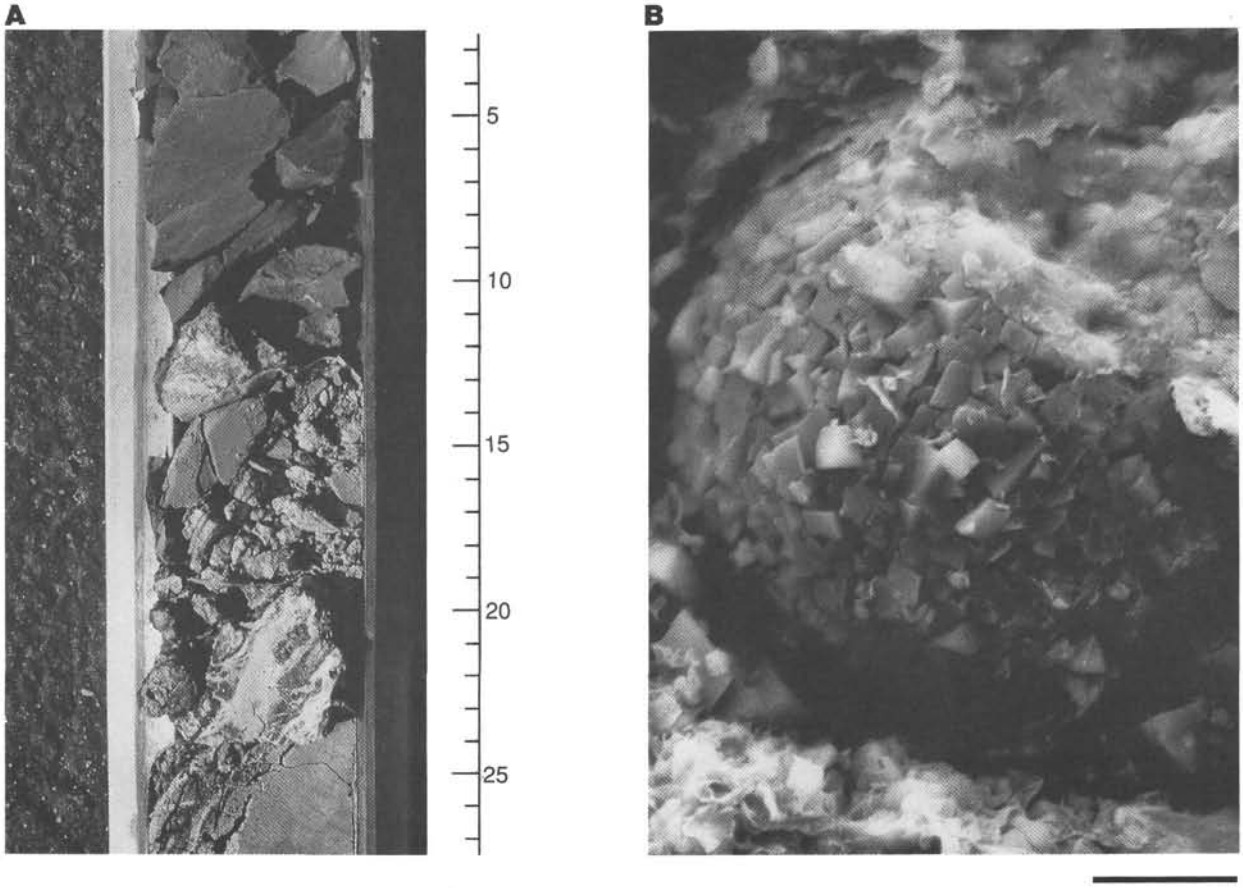

Figure 15. **A.** Nannofossil-bearing marl overlying volcanic basement; interval 27-261-33-1, 2–28 cm. **B.** SEM micrograph of calcisphere with coarsely recrystallized surface texture (Sample 27-261-33-1, 0–2 cm; scale bar is 5 μm).

claystone is dominantly brown, with lesser thin zones of redder or grayer hue. Nannofossils constitute most of the calcium carbonate in this sediment and consist mostly of large specimens (15–20 μm) of the robust coccolith, *Watznaueria manivitae* (Plate 5, Figs. 1, 2).

Carbonate content (nannofossil abundance) fluctuates throughout this facies, but in general decreases upsection. LECO analyses of claystone samples (Bode, 1974a; this study) determined 17% $CaCO_3$ toward the base of the unit and 6% near the top (Table 2). Our examination of smear slides, thin sections, and SEM samples confirmed the general upsection decrease in carbonate, but found local millimeter-scale concentrations of calcareous material (mostly in the lower half of the unit), as well as intervals devoid of carbonate (all in the uppermost third of the unit, and particularly above and below the needle-rich marl). Carbonate content of the needle-rich marl (58%) is notably high.

Unit L2 is dominantly fine-grained, but contains 2% to 10% coarse silt- and sand-sized material; some is disseminated but most is concentrated into millimeter-thick lenses. Carbonate grains within these lenses have interpenetrative and sutured contacts that are typical of dissolution-enhanced overly close packing. The noncarbonate fraction of the nannofossil claystone consists largely of smectite and micro-crystalline quartz (Veevers, Heirtzler, et al., 1974).

Megascopic sedimentary structures in this unit are rare; faint millimeter-scale laminae occur locally and a burrow 1 cm in diameter is found toward the base of Section 27-261-32-4. Microlenses and laminae rich in nannofossils are notable in thin-section and SEM examination (Plate 5, Fig. 3) and are described below.

Calcareous nannofossils. Nannofossils in these claystones are diverse, numerous, and less well-preserved than those in the underlying red marl. Abundances (as estimated from smear slide and thin section) vary from 3% to 30% through most of the unit, but reach 40% to 60% locally, and 80% to 100% in the most concentrated lenses. The nannofossils exhibit a high degree of etching, and floras appear to be impoverished as a result of selective dissolution.

In thin section and SEM samples, striking millimeter- and micrometer-thick layers of concentrated coccoliths (dominantly the large and robust form, *Watznaueria manivitae*) alternate with zones less rich in coccoliths but richer in clay. In the most carbonate-rich lenses, the coccoliths are stacked one on top of another, with essentially no interstitial material (Plate 5, Fig. 3). Even where less concentrated, the nannofossils are typically well-aligned parallel to the overall fabric (Plate 5, Fig. 4), a textural feature not noted in other sediments from either Argo Abyssal Plain site. Compared to the red marl unit, the nannofossil claystone contains little calcite cement and has a more porous microtexture.

Calcisphere concentrations. Calcispheres, and calcite needles derived from the breakdown of calcisphere tests, occur sparsely throughout the nannofossil claystone, but are extremely abundant in an interval of marl in the upper part of the unit (Section 27-261-32-2, 40–74 cm) (Fig. 16). Contact between the marl and the underlying brown claystone is sharp and appears to have been disturbed by drilling; the claystone in this part of the unit contains little carbonate. Much of the marl interval is layered on a scale of one to several millimeters; layers are alternately pinkish brown with abundant white clasts, and darker brown with clasts rare to

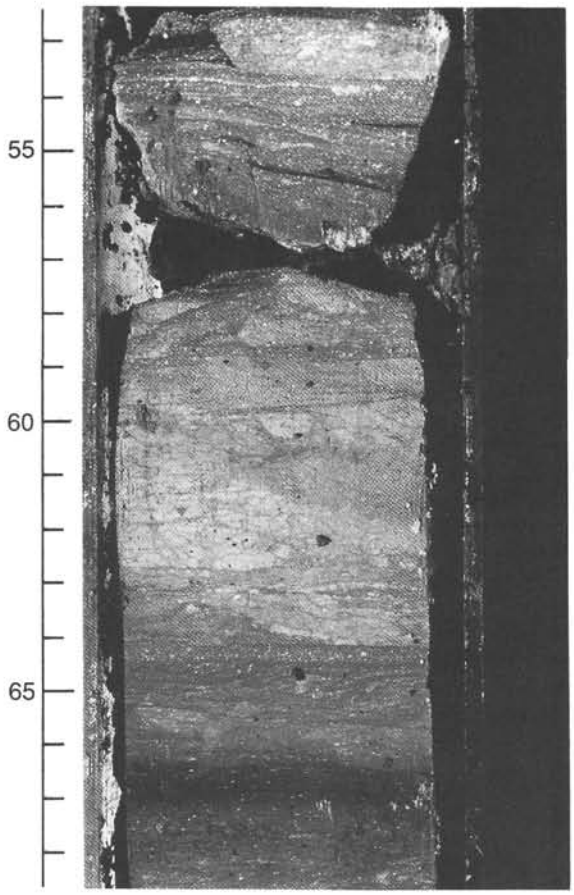

Figure 16. Calcite needle-rich marl within brown nannofossil claystone. Light-colored layers and laminae contain abundant needle-shaped calcite crystals derived from the breakdown of calcisphere tests; dark layers contain little carbonate. Irregular mottles due to bioturbation (interval 27-261-32-2, 52–69 cm).

absent. Locally, layering has been partly or entirely disrupted by bioturbation, and discrete *Chondrites*-type burrows are noted. In one instance, a subvertical burrow is filled with clasts.

The clasts consist chiefly of calcite needles; the needles, clasts, and overall textures in this interval are identical to those in the calcite needle-rich interval at Site 765 (Section 123-765C-61R-5, 54–62 cm) (Plate 2). The reddish matrix also contains needles, as well as subordinate clay. Rare to abundant nannofossils and very rare calcareous benthic foraminifers are found in both matrix and clasts.

Other fossils. Coarse (sand-sized) grains in the nannofossil claystone are largely inoceramid prisms, almost all of which are riddled with mud-filled pits and tubes (probable microborings). Other biotic constituents of this facies include agglutinated and rarer calcareous benthic foraminifers, ostracodes, and calcareous and phosphatic debris (Plate 5, Figs. 3, 5). Scarce dinoflagellates also have been reported (Veevers, Heirtzler, et al., 1974).

Noncalcareous component. Clay, largely smectitic I/S (Compton et al., this volume), is the dominant constituent of Unit L2. Disseminated noncalcareous coarse silt and sand occurs in trace amounts and consists of quartz, volcanic lithics (lathwork clasts and altered glass), reddish brown claystone intraclasts, and plagioclase.

Small black nodules are scattered but persistent throughout the unit; they are especially abundant in Section 27-261-32-3, which also contains the most concentrated and abundant lenses of nannofossils. EDS analyses of several nodules indicate that they consist mostly of manganese and lesser iron. Nodules range from a few tens of micrometers to 6 × 2 mm in size. The larger nodules exhibit concentrations of calcareous material (largely nannofossils) at the nodule margins and a halo of tiny (micrometer-size) micronodules in the sediment surrounding the main nodule body. Similar micronodules coat inoceramid prisms and other coarse detritus throughout the unit.

Interpretation

The brown nannofossil claystone is pelagic sediment, most of which accumulated above the CCD, but below the lysocline; parts of the upper interval that are devoid of carbonate may have been deposited below the CCD. The gradational contact with the underlying red marl, and the upward decrease in carbonate content throughout the unit, reflect normal sedimentation patterns on young oceanic crust (e.g., Jenkyns, 1986). As igneous basement cools and sinks, the zone of sediment accumulation above this basement deepens and approaches the CCD. Intervals particularly rich in carbonate within the brown claystone could indicate minor fluctuations in the position of the lysocline, but could also occur as a result of mechanical (current) concentration of coarser carbonate debris. The latter explanation is favored here; the locally extreme concentration and alignment of *Watznaueria* suggest winnowed lag deposits from which all the finer clay fraction has been removed by currents. Texturally, the *Watznaueria*-rich lenses are analogous to, though finer grained than, the inoceramid-rich lenses at Site 765.

Winnowed textures in these sediments suggest low rates of sedimentation, an interpretation further supported by sedimentation rate estimates (Fig. 5), the red-brown color of the sediment (indicating deposition under oxidizing conditions), and the presence of manganese nodules. The nodules show textures characteristic of *in situ* occurrence and no indication of reworking (for example, the nodules have halos of micronodules and lack concentric crusts).

The distinctive needle-rich marl formed during a period dominated by deposition of clays near or just below the CCD, but punctuated by sporadic influxes of allochthonous calcareous sediment. We interpret the dark brown, weakly to noncalcareous claystone layers as autochthonous "background" sediment, and the pink and white calcareous clasts as allochthonous material. The clasts consist largely of calcisphere debris; as previously discussed, calcispheres are most commonly found in deep shelf settings, and their occurrence in floods may indicate environmental stress (Masters and Scott, 1979; Thierstein, 1981). The calcisphere concentrations in the marl have likely been reworked and redeposited, by bottom or turbidity currents, from the adjacent continental slope or shelf. Disaggregation of calcisphere tests into individual needles, as at Site 765, was probably facilitated by a corrosive (sub-CCD) environment.

The nannofossil claystone unit thus accumulated slowly (perhaps episodically) near the level of the CCD and was bioturbated and winnowed by bottom currents. The layer of calcareous needle-rich marl toward the top of the unit consists of calcisphere debris probably derived from the continental margin and redeposited by currents on the abyssal plain.

Unit L3, Calcareous Sediment and Noncalcareous Claystone (Tithonian–Barremian; Cores 27-261-31 through -27; 527.4–427.5 m sub-bottom)

Description

General features. This unit consists of roughly equal amounts of intercalated calcareous sediment (mostly marl and calcareous claystone) and noncalcareous claystone; the calcareous sediment

appears to have been redeposited by turbidity currents, and its presence is the distinguishing feature of the unit (Fig. 17). Both sediment types form layers a few meters to several millimeters thick. Noncalcareous zones were recognized by testing the cores with hydrochloric acid and were confirmed through smear slide, thin section, carbonate content (Bode, 1974a; this study), and/or XRD (Veevers, Heirtzler, et al., 1974; Cook et al., 1974)) analyses. Shades of red and brown predominate throughout the unit. Most—but not all—noncalcareous intervals are darker in color than the intercalated calcareous sediment. Both sediment types contain subordinate thin layers and irregular blebs and mottles of green and greenish gray; these color bands do not seem to mark any sharp difference in sediment composition, but are most common in relatively radiolarian-rich noncalcareous claystones. Transitions from calcareous sediment to noncalcareous claystone are locally sharp, but more often are gradational or obscured by bioturbation.

Bioturbation is most evident in the calcareous sediment and in thin, noncalcareous intervals; it is particularly notable in Sections 27-261-27-1, -28-1, -30-3, and -31-2. Burrows within claystone contain mostly lighter colored (white to pink) calcareous material, whereas those in calcareous sediment are filled with brown claystone or white concentrations of calcareous silt (mostly calcispheres). Horizontal and subhorizontal ichnofossils predominate, and burrows are larger and more diverse in form lower in the unit. *Chondrites* and *Planolites* (generally smeared and deformed) are most common, but a well-developed *Zoophycus* occurs in Section 27-261-30-3 (Fig. 4 in Veevers, Heirtzler, et al., 1974). The most diverse ichnofossil assemblage occurs in Section 27-261-31-2, 108–150 cm (Fig. 17B) within 2- to 10-cm-thick interlayers of dark brown, slightly calcareous claystone and white to pink marl. Burrows are most abundant in the brown claystones and at least two generations can be discerned. Thick intervals of noncalcareous claystone, found toward the base of Core 27-261-31, show no evidence of bioturbation.

Other than trace fossils, megascopic structures are uncommon in this unit. However, some intervals of calcareous sediment contain structures typical of turbidite deposits and form partial Bouma sequences, as described below.

Diagenetic minerals developed in both calcareous sediment and intercalated claystone include trace amounts of barite and up to several percent carbonate. The carbonate occurs mostly as small, disseminated rhombs, 5 to 32 µm in diameter (Fig. 18A) and is most abundant in claystone intervals. Less common larger carbonate masses (to 200 µm) have replaced and/or grown around radiolarians and generally retain some trace of skeletal structure. These masses are packed into lenses (as much as 3 mm long and 0.6 mm thick) in which they comprise 30% to 80% of the sediment; it would appear that pods of relatively concentrated radiolarians were particularly susceptible to carbonate replacement.

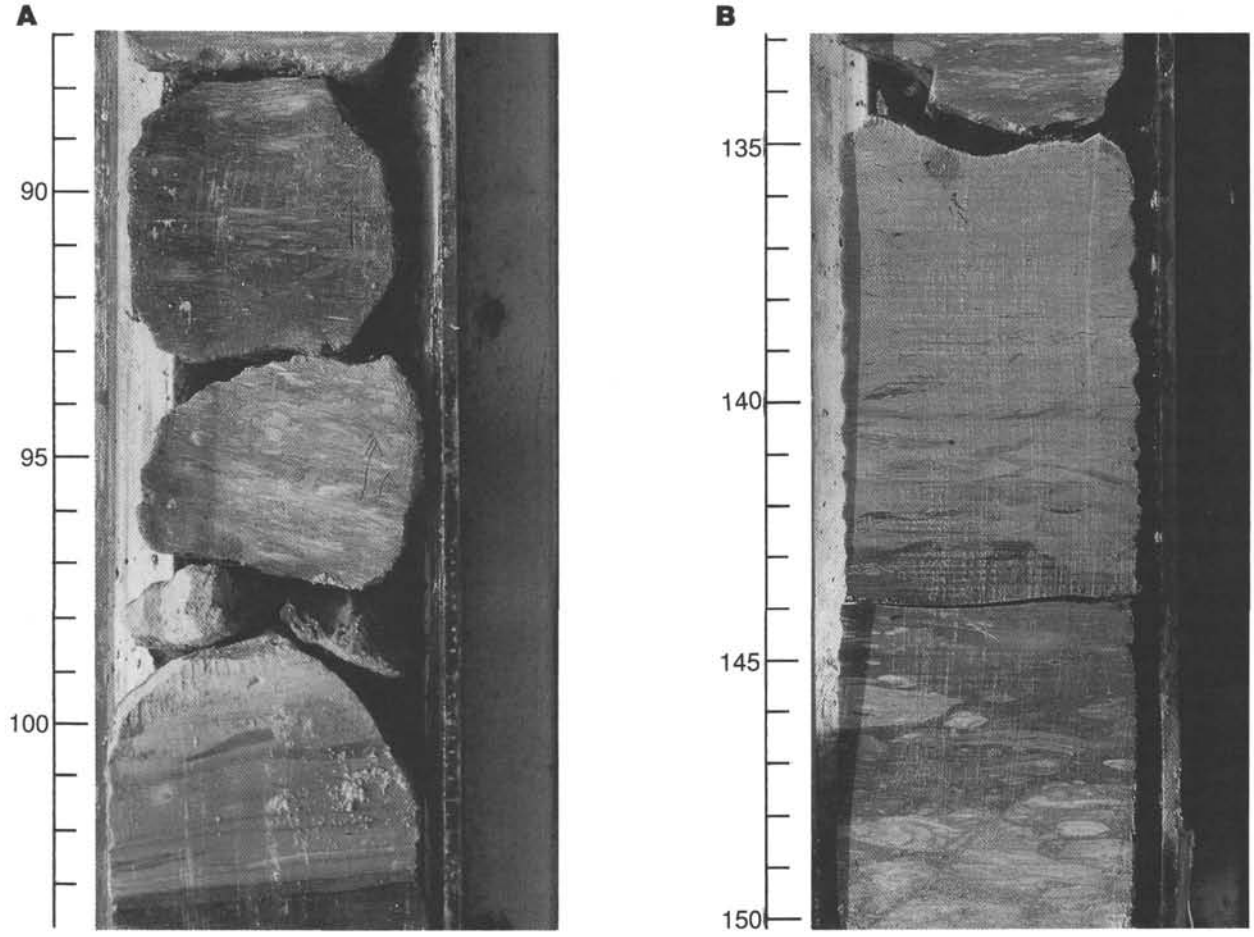

Figure 17. Tithonian–Barremian calcareous turbidites. **A.** Lighter colored turbidite intercalated with darker background claystone; both lithologies are burrowed. Parallel- and cross-laminae in turbidite concentrate silt and fine sand grains (calcispheres and lesser volcanic and sedimentary lithic clasts; interval 27-261-28-1, 87–103 cm). **B.** Alternation of lighter colored calcareous turbidites and dark, less calcareous background claystone; lithologies partially homogenized by pervasive bioturbation. Burrows chiefly *Chondrites* and *Planolites* (interval 27-261-31-2, 133–150 cm).

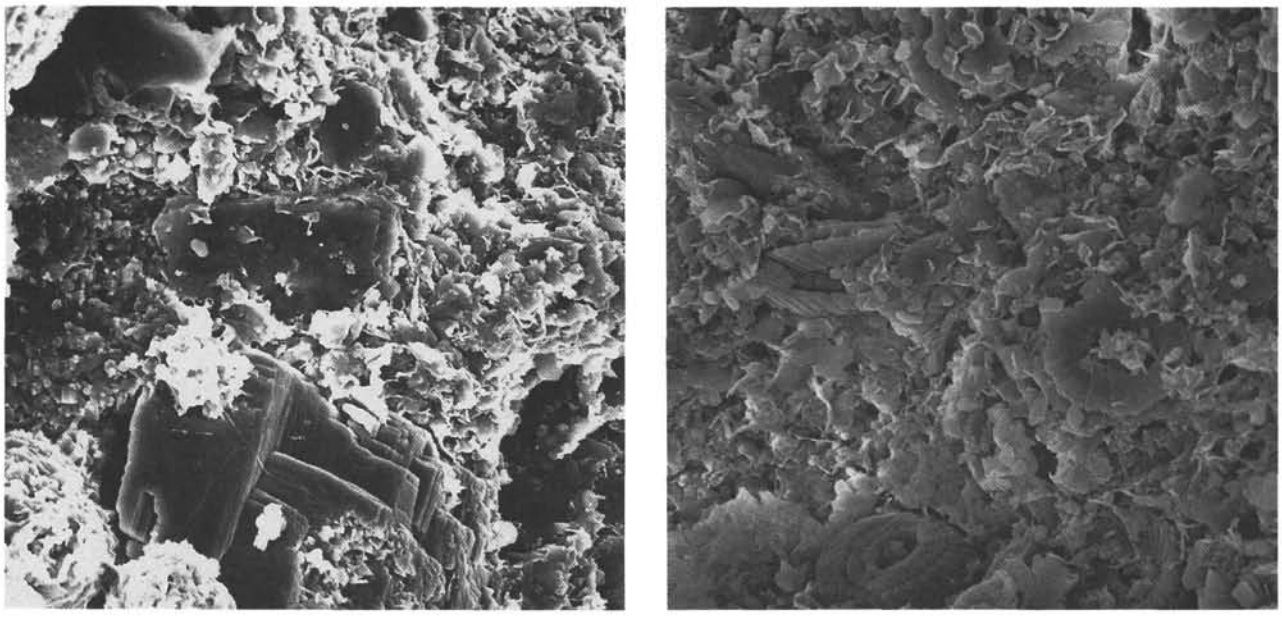

Figure 18. High-magnification SEM photographs of calcareous turbidite and background claystone shown in Figure 17 (Sample 27-261-31-2, 140–143 cm; scale bar equals 5 μm). **A.** Authigenic carbonate rhombs (rhodochrosite) in claystone. **B.** Typical turbidite fabric: randomly ordered nannofossils (*Watznaueria* sp.) in clayey matrix. View perpendicular to bedding.

EDS analyses of small carbonate rhombs and the larger carbonate masses that replace radiolarians indicate that both are rhodochrosite, with only minor Ca substitution for Mn.

Calcareous sediment. At least 26 discrete calcareous intervals, separated by virtually noncalcareous zones, occur in the cores recovered. The longest of these (Core 27-261-30, Section 3-4) is 290 cm thick, but most are less than 50 cm, and many are less than 10 cm. The thickest calcareous intervals are generally bioturbated throughout and contain zones that are alternately richer and poorer in carbonate. These thick intervals thus appear to represent a series of thin calcareous and noncalcareous layers that have been homogenized and amalgamated by bioturbation.

Smear slide, thin section, and SEM observations indicate that the amount of calcium carbonate in these sediments varies both between intervals and vertically within a single interval. LECO analyses of samples from seven calcareous layers found a range of 13% to 42% calcite (Bode, 1974a; this study) (Table 2). Lower values occur in layers from the upper half of the unit and in samples taken near the top or bottom of a layer, where bioturbation has mixed calcareous and noncalcareous sediment; highest values come from samples taken toward the middle of layers in Cores 27-261-30 and -31. Quartz and smectite are the other major constituents of the calcareous sediment, and minor components include mica, potassium feldspar, and hematite (shipboard XRD analyses, Veevers, Heirtzler, et al., 1974).

Most of the calcareous sediment is clay-sized or fine silt-sized and relatively homogeneous in megascopic appearance (Fig. 18B). However, coarser sediment occurs locally and exhibits graded bedding and Bouma sequence structures. For example, a 5-cm interval in Section 27-261-31-3 (37–42 cm) grades upward from silt-sized calcisphere packstone to clay-sized nannofossil marl, and Section 27-261-28-1 (99–103 cm; Fig. 17A) contains a base-cut-out (BCDE) Bouma sequence in which millimeter-scale parallel and cross-laminae concentrate calcispheres, lithic grains, and radiolarians.

Samples from fine-grained calcareous intervals show a complex microfabric in thin section. Most consist of an intimate mixture (on a millimeter scale) of two kinds of material: (1) light brown to pinkish brown to white nannofossil-rich sediment with lesser clay, and (2) less abundant dark brown clay with few if any nannofossils. This fabric, characterized by blebs and patches of one material in a "matrix" of the other, represents mixing of two originally discrete sediment types by bioturbation. Sand-sized grains make up a few to 30% of most calcareous sediment samples; most of this coarser material floats in the finer grained matrix (Fig. 19A). Locally, coarse detritus is concentrated into thin layers or lenses, or fills burrows.

The nannofossils in the calcareous sediment are randomly oriented (Fig. 18B), in contrast to the stacked, aligned nannofossils in the underlying nannofossil claystone unit (Plate 5). Local concentrations of pure nannofossils may be fecal pellets (Fig. 19B). In general, nannofossils in this unit are poorly preserved, and assemblages show low diversity due to selective dissolution (see "Calcareous Nannofossil Biostratigraphy" section below). The best preserved and most diverse assemblages occur in thicker calcareous intervals, mostly in Cores 27-261-30 and -31, that have good Bouma sequence structures. Some of these diverse assemblages contain forms restricted to nearshore environments, a point discussed further below.

Composition of sand-sized and coarse silt-sized detritus within the calcareous intervals changes upsection: calcareous material is more abundant in the lower cores, whereas radiolarians dominate the coarse fraction in the higher cores (particularly Core 27-261-29 and above). Calcareous benthic foraminifers are rare, and inoceramid prisms were not found, above Core 27-261-31. Calcispheres are most abundant in the lower cores, where they may constitute 50% to 90% of millimeter to centimeter thick layers and lenses. Radiolarians range from poorly to moderately well preserved. Some have been completely dissolved, leaving behind finely detailed molds (Fig. 20); others have been replaced by

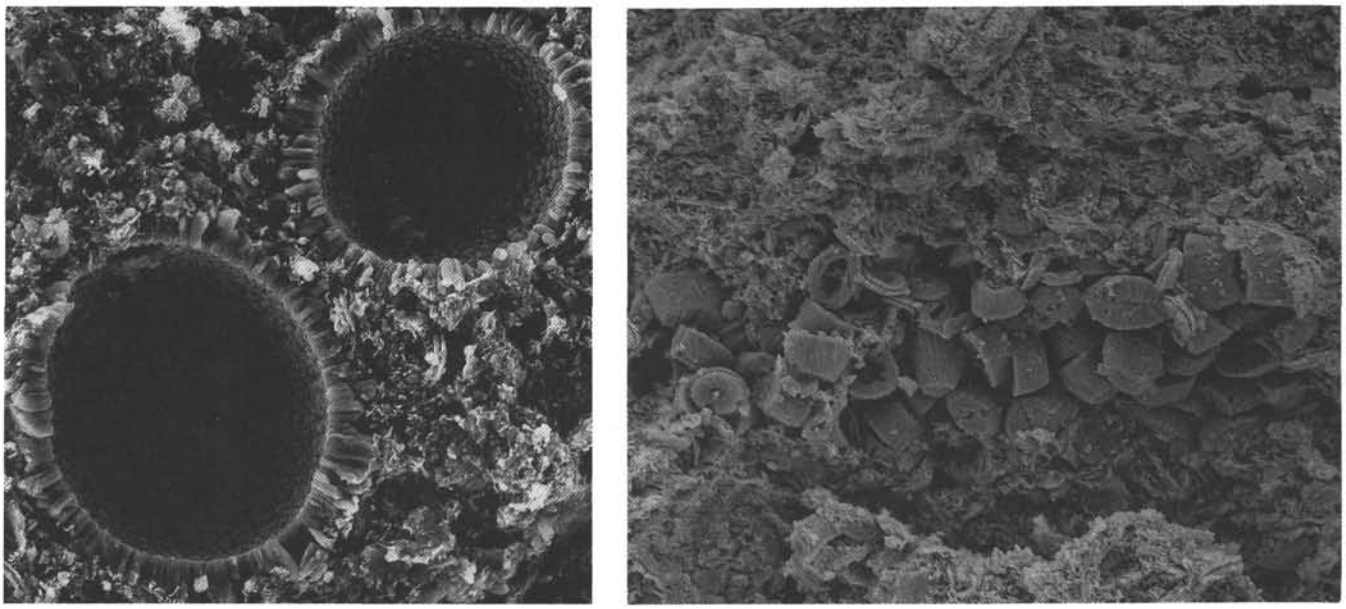

Figure 19. High-magnification SEM photographs of calcareous turbidite shown in Figure 17 (Sample 27-261-31-2, 140–143 cm; scale bar is 10 µm). **A.** Calcispheres in turbidite. **B.** Nannofossils in turbidite; cluster of *Zeugrhabdotus cooperi*, possibly a collapsed coccosphere in a fecal pellet, with *Watznaueria* sp.

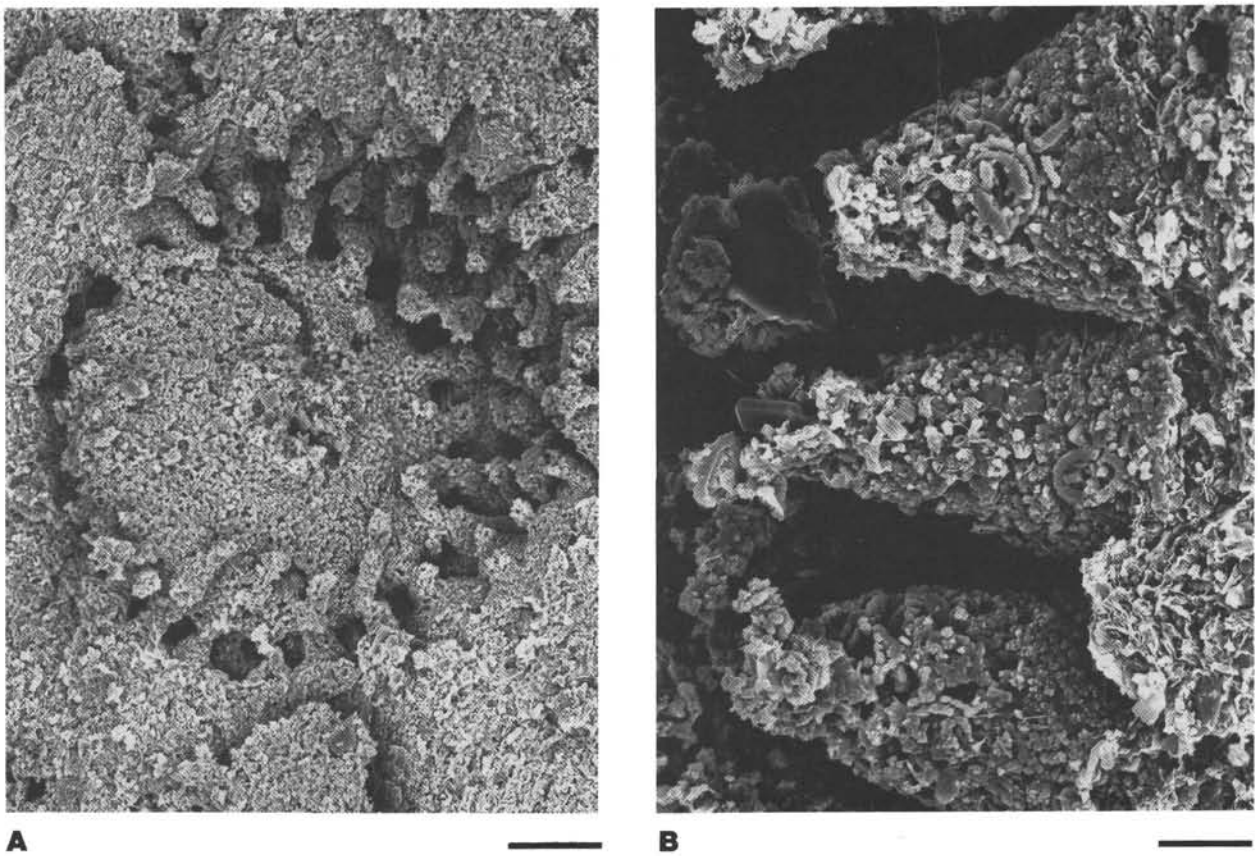

Figure 20. **A.** SEM micrograph of radiolarian mold in redeposited calcareous sediment (Sample 27-261-29-2, 23–26 cm; scale bar is 20 µm). **B.** Detail of **A**; nannofossils strongly etched. Scale bar = 6 µm.

fine-crystalline quartz or chalcedony. Carbonate and/or pyrite replacement is particularly notable in zones with green or gray coloration.

The coarse fraction in the calcareous sediment also includes trace amounts of agglutinated foraminifers, phosphatic and opaque grains, angular quartz, and lithic clasts. Lithic clasts include volcanic grains with lathwork textures and orange-brown clayey clasts that could be mud intraclasts and/or altered volcanic lithics. Lithic clasts are particularly notable in samples from intervals with well-developed parallel and cross-laminae, such as 27-261-28-1, 96–100 cm.

Noncalcareous claystone. Noncalcareous claystone forms three thick (1–2 m) intervals at the base of the unit (Sections 27-261-31-2 through -5) and thinner (2–65 cm) layers through the rest of the section. Shipboard and shore-based XRD analyses (Veevers, Heirtzler, et al., 1974; Cook et al., 1974) indicate that most of the claystone is siliceous (80%–86% microcrystalline quartz), with lesser clay (8%–13%) and minor mica, hematite, and potassium feldspar; the clay fraction is dominated by I/S that contains less than 10% illite (Compton et al., this volume). LECO analyses (Bode, 1974a; Table 2) confirm that carbonate content of this lithology is negligible (0%-3%).

Thin sections of siliceous claystone contain 3% to 20% disseminated sand- and coarse silt-sized components, largely radiolarians (present as molds, or replaced by finely crystalline quartz or carbonate). Radiolarians also occur concentrated into discrete lenses or laminae, at most a few millimeters thick. The remainder of the coarse fraction (1%–2%) consists of agglutinated foraminifers, phosphatic debris, rare lithic clasts, and detrital quartz (largely silt-sized and angular). Heavy mineral samples from this lithology consist largely of opaque grains, with minor garnet and zircon (McKnight, 1974).

Two intervals of relatively pure (93%–99%) smectite claystone were detected by shipboard XRD analyses in sections 27-261-28-2 (92–95 cm) and 27-261-31-4 (53–54 cm) (Veevers, Heirtzler, et al., 1974). Both intervals are a distinctive pale brown color with a waxy sheen and soapy feel. A similar brown layer occurs higher in Section 27-261-28-2 but was not analyzed.

Interpretation

We interpret this unit as calcareous turbidites intercalated with noncalcareous "background" sediment. The unit accumulated below the CCD, but the calcareous sediment was originally deposited above the CCD along the continental margin and then redeposited by gravity flows. The presence of local graded bedding and partial Bouma sequences indicate that turbidity currents were the main mechanism of redeposition.

Veevers, Heirtzler, et al. (1974) suggested that both sediment types in this unit formed as pelagic accumulations in the abyssal plain environment and inferred that their different calcareous contents reflected fluctuation in the position of the CCD/lysocline through time. Cyclic fluctuation in the level of the lysocline in the Quaternary Indian Ocean was proposed by Peterson and Prell (1985) to explain variations in carbonate preservation detected in piston cores. Their study suggests that the lysocline may have shifted almost 1000 m in less than 50,000 yr.

We favor interpretation of the calcareous sediment as turbidites because of (1) the generally large difference in carbonate content between the two types of sediment (essentially noncalcareous vs. more than 40% calcium carbonate), (2) sharp contacts between calcareous and noncalcareous sediment observed in core and in thin section, (3) occurrence of sedimentary structures characteristic of gravity flows (parallel and cross-lamination, graded bedding), and (4) microfossil evidence. CCD/lysocline fluctuations, such as those described by Peterson and Prell (1985), produce gradual changes in the amount of carbonate and degree of preservation of calcareous faunas within a sedimentary sequence, not radical shifts from noncalcareous to richly calcareous sediment over a distance of a few millimeters. Where contacts between calcareous and noncalcareous sediment at Site 261 are gradational or obscure, homogenization of two initially distinct sediment types by bioturbation appears responsible; discrete burrow structures and other trace fossils are abundant throughout the unit. The relative scarcity of sedimentary structures in the calcareous sediment is attributable to its fine grain size; it consists mostly of nannofossils and smectite. Where coarse silt- and sand-sized material is abundant, normal grading and Bouma sequence structures were observed. Microfossil assemblages in the calcareous sediment provide additional support for the idea that this sediment was redeposited. For example, nannofossil assemblages (see below) include species characteristic of nearshore environments and suggest redeposition of material that originally accumulated on the continental shelf. A radiolarian assemblage like those found in the "sand faunas" at Site 765, and thought to have been derived from the Australian margin, also occurs in at least one interval of calcareous sediment (Baumgartner, this volume).

Possible sources for the redeposited calcareous sediment at Site 261 lie to the east and south. The biotic components of the calcareous sediment are mostly pelagic microfossils and indicate derivation from a source above the CCD but below the photic zone; shallow-water biotics are not in evidence. The clay fraction is largely smectite and denotes volcanogenic input. Both the Scott Plateau region to the east and the Exmouth Plateau area to the south might have provided sediment of this description. Nannofossil ooze most likely accumulated all along the Australian continental margin during the Early Cretaceous, as it does today (Davies and Kidd, 1977). Both the Scott Plateau and northern Exmouth Plateau contain volcanic sediments of Mesozoic age and are cut by large submarine canyons that may have been active in the Early Cretaceous (von Rad and Exon, 1983; Hinz et al., 1978). The location of Site 261 almost 150 km from the eastern continental margin, and more than 350 km from the southern margin, resulted in accumulation of dominantly thin, fine-grained (distal) turbidites that were subject to bioturbation and dissolution once deposited.

The two mechanisms discussed above for deposition of the calcareous sediment—turbidity current deposits and fluctuating position of the CCD/lysocline—are not mutually exclusive. It is possible that long intervals that contain little calcareous material (such as much of Core 27-261-31) were deposited when the CCD was higher relative to Site 261's position on the Argo Abyssal Plain than it was when largely calcareous intervals (such as Core 27-261-30, Sections 2 and 3) were deposited. A relatively low CCD throughout the Indian Ocean at certain times would increase the area wherein calcareous oozes could accumulate, and thus more allochthonous calcareous material would be available for introduction onto the abyssal plain. Depression of the CCD during the early Cretaceous has been suggested for the Atlantic Ocean (Jansa et al., 1979).

The smectite-rich claystone intervals in this unit are similar in color and composition to layers encountered at Site 765 and are interpreted as bentonites—altered volcanic ash, probably reworked and mixed with pelagic clays (Thurow and von Rad, this volume). Thin, radiolarian-rich layers in the background claystone were probably concentrated by bottom currents; none contain sedimentary structures indicative of a turbidite origin (cf. Lower Cretaceous radiolarites at Site 765 discussed above).

Unit L3 is the oldest unit at Site 261 to contain abundant redeposited sediment (calcareous turbidites), but sedimentation rates are still low (7 m/m.y.; Fig. 5). Turbidites have a mixed composition of clay and calcareous and siliceous biotics, are "distal" in character (thin and fine-grained), and appear to have

derived from slope or outer shelf sources along the eastern and southern continental margins. Smectite clays dominate both background and redeposited sediment in this unit and indicate significant volcanogenic input. Bentonites and radiolarites are minor components of this unit.

Unit L4, Radiolarian Claystone (Barremian–Aptian/Cenomanian; Cores 27-261-26 through -10; 427.5–209.0 m sub-bottom)

Description

Siliceous claystone, locally rich in radiolarians and lacking any primary calcareous component, makes up this unit (3B of Veevers, Heirtzler, et al., 1974). Shades of gray and greenish gray predominate, except in the lower cores (particularly Cores 27-261-20 through -23), which are characterized by the alternation of red and green tints on a scale of 5 to 10 cm.

Horizontal to subhorizontal layers, lenses, and wispy parallel laminae occur throughout much of the unit. Most are darker in color than the surrounding claystone; lenses examined in thin section contain concentrations of opaque granules (pyrite and/or organic material). The overall streaky texture probably reflects a combination of burrow forms (locally flattened) and partial disruption of original sedimentary layering by bioturbation. Discrete burrows are mostly small (1 mm or less in diameter—*Chondrites* and *Trichichnus*), but larger *Planolites* burrows occur locally. Elongate horizontal traces with preserved spreite are found in Section 27-261-19-3.

Shipboard bulk XRD analyses indicate that claystone of Unit L4 consists largely of microcrystalline quartz (56%–91%) and lesser clay; minor components include mica, potassium feldspar, and barite (Veevers, Heirtzler, et al., 1974). Shore-based XRD analyses (Compton et al., this volume) detected opal-CT in addition to quartz in the upper part of the unit (Cores 27-261-18 and above), and determined that most of the clay is I/S containing less than 10% illite layers. The unit contains no primary calcareous components, such as nannofossils or calcispheres; LECO analyses of 21 samples detected at most trace amounts of carbonate (Bode, 1974a).

Sediments of this unit are largely fine-grained—claystone and lesser silty claystone (Bode, 1974b; Thayer et al., 1974). Sand-sized grains (predominantly radiolarians and carbonate micronodules) are concentrated into layers and lenses 0.5 mm to 3 cm thick or, more commonly, disseminated in abundances of 1% to 20%. Minor detrital components include quartz and feldspar; McKnight (1974) recognized grains of clinopyroxene and orthopyroxene in a heavy mineral separate from Section 27-261-22-5. Rare arenaceous foraminifers occur throughout the unit; palynomorphs (dinoflagellates and minor pollen) were found in Cores 27-261-14 through -16 and 27-261-21 through -26 (Veevers, Heirtzler, et al., 1974).

Radiolarians occur in every core. They form rare grain-supported, wispy lenses, 0.5 to 2 mm thick, or more commonly, are diffusely distributed (in abundances of up to 40%) through intervals a few to tens of centimeters thick. In Sample 27-261-11-1, 148–150 cm, radiolarite fills horizontal burrows 0.5 cm in diameter (Fig. 21). Test preservation is moderate to poor. Some tests consist partly or entirely of opal-CT; others have been recrystallized to microcrystalline quartz, filled with sheaves of length-fast chalcedony, or replaced by pyrite or carbonate. Dissolution of radiolarian tests, and reprecipation as disseminated cryptocrystalline and microcrystalline opal-CT and quartz, appears to be the major factor responsible for the lithification of the radiolarian claystone (Robinson et al., 1974).

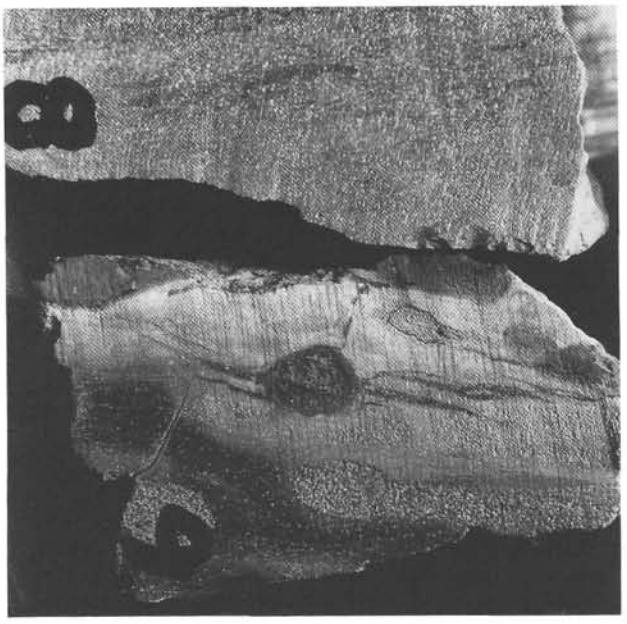

Figure 21. Radiolarite fills horizontal burrows in gray claystone; radiolarians mostly recrystallized to microcrystalline quartz (Sample 27-261-11-1, 145–150 cm; scale bar = 1 cm).

Authigenic carbonate micronodules, observed in Cores 27-261-15, -19, -21 through -23, and -26, range from 15 to 200 μm in diameter (average 30–80 μm). They occur most commonly in grain-supported ovoid concentrations a few millimeters to 4 cm long, or in wispy to relatively continuous layers up to 3 cm thick. In Sample 27-261-19-4, 58–60 cm, lenses filled with micronodules resemble flattened burrows (Fig. 22). EDS analysis of nodules from Cores 27-261-19, -22 and -26 indicates that they consist of rhodochrosite with only minor Ca substitution for Mn.

The relationship between carbonate micronodules and radiolarian tests is clear in Sample 27-261-21-2, 76–77 cm. In this sample, almost every carbonate nodule includes distinct dark traces of a radiolarian form; the original siliceous tests have completely dissolved and left behind detailed opaque (pyritic?) outlines of the skeletal structure . Other nodules examined from Site 261 do not contain skeletal outlines, but the spherical habit, size range, and distribution of the nodules suggest that they also have replaced and/or grown around radiolarian tests (Fig. 23).

Most sandy intervals in Unit L4 consist exclusively of radiolarians or carbonate micronodules, although individual layers containing both grain types occur in Cores 27-261-15 and -22, and most cores contain both layers of radiolarians and layers of nodules. If most carbonate micronodules do represent replaced radiolarians, no obvious features (i.e., depth of burial or matrix composition) were discerned that control this alteration. However, denser concentrations of radiolarians were more susceptible to such replacement, because diffuse occurrences of carbonate micronodules were not observed. The greater porosity and permeability of the sand-sized radiolarite layers (relative to the surrounding claystones) most likely enhanced fluid movement and subsequent alteration, as has been suggested for similar occurrences of manganese carbonate minerals in black shales of the western Alps (Tassé and Hesse, 1984) .

Authigenic carbonate also occurs in the radiolarian claystones as sparsely disseminated small rhombs (5–40 μm, most 5–20 μm);

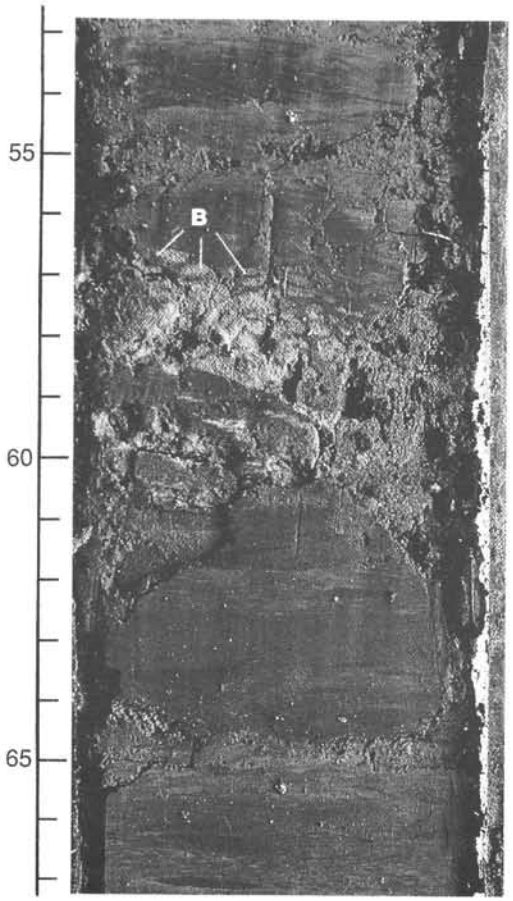

Figure 22. Authigenic carbonate in gray claystone. Rhombs of manganese carbonate (lighter colored material) fill ovoid lenses that are probably flattened burrows (B) (interval 27-261-19-4, 53–67 cm).

rhombs were noted in thin sections or smear slides from Cores 27-261-12, -14, -15, -18 through -23, -25, and -26. EDS analyses of several samples found that the rhombs also consist of rhodochrosite.

Several intervals of black claystone a few centimeters to decimeters thick occur in Cores 27-261-14 and -15. A layer near the top of Core 27-261-15 contains 1.3% organic carbon (Bode, 1974a), the highest value obtained in any sample analyzed from this site.

Interpretation

The gray radiolarian claystones were deposited below the CCD, as indicated by the absence of primary carbonate. They are similar to the noncalcareous intervals of underlying Unit L3, but differ in their predominant color (grays and greens vs. reds and browns), in their greater abundance of radiolarians, and in the lack of intercalated calcareous sediment.

Unit L4 claystones have many features typical of pelagic sediments, including overall fine grain size and abundant siliceous microfossils, but sedimentation rates determined for this unit (24 m/m.y.; Fig. 5) are an order of magnitude higher than those characteristic of pelagic claystones (e.g., Jenkyns, 1986). This suggests that material redeposited from the continental margin may constitute an important part of this unit, as postulated above for Unit L4 at Site 765. Features characteristic of mud turbidites, such as fine parallel lamination and small-scale changes in sediment color and degree of bioturbation (Stow and Piper, 1984), occur throughout Unit L4. Thus, fine-grained turbidites similar to those in the underlying subunit (L3B), but without the calcareous component that made those sediments so distinctive, probably form an important part of the L4 sedimentary succession. Green and gray sediment colors, suggesting accumulation and/or diagenesis under reducing conditions, are in accord with the interpretation that the radiolarian claystones were deposited rapidly.

Abundant radiolarians appear in mid-Cretaceous sediments across the northwest Australian shelf and adjacent marginal and abyssal basins (e.g., Aptian Windalia Radiolarite of the Carnarvon Basin; Veevers and Johnstone, 1974) and reflect large-scale paleoceanographic shifts in response to the break-up of Gondwanaland; such shifts resulted in intermittent influx of circum-Antarctic cold water and concomitant upwelling along the northwest Australian margin (Baumgartner, this volume). Varying abundance of radiolarians throughout Unit L4 at Site 261 reflects both sedimentologic and oceanographic factors. Millimeter- to centimeter-thick lenses and layers of concentrated radiolarians (and of carbonate micronodules presumed to have formed after radiolarians) are best explained as the result of winnowing and/or redeposition by bottom currents. Low-density turbidity currents may also have concentrated some radiolarians, but this mechanism appears to have been relatively unimportant at Site 261; thick radiolarites with well-developed sedimentary structures, such as grading and parallel- and cross-lamination, are abundant at Site 765, but were not found at Site 261. Most radiolarians at Site 261 occur as floating grains in a clayey matrix, not in grain-supported sands with sedimentary structures that indicate current action. Alternations of radiolarian-rich and radiolarian-poor claystone throughout Unit L4 may reflect changes in surface-water productivity, and/or differential diagenesis (P. O. Baumgartner, pers. comm., 1990).

Upper Sequence (Cores 27-261-9 through -1)

Unit U1, Zeolitic Clay (Aptian–Upper Cretaceous; Cores 27-261-9 through -5; 209.0–142.0 m sub-bottom)

Description

This unit (3A of Veevers, Heirtzler, et al., 1974) consists of stiff brown to grayish-brown noncalcareous clay and is distinguished by the presence of palygorskite and zeolite. The unit preserves no obvious sedimentary structures, but is characterized by irregular mottles and swirls of yellowish brown or blackish brown, probably formed through drilling disturbance of clays with slight differences in original composition and/or diagenesis. Unit U1 is uniformly fine-grained; it is mostly clay and has rare intervals of silty clay, but contains essentially no sand (Bode, 1974b; Thayer et al., 1974).

Much of the clay fraction in this unit consists of relatively illite-rich I/S (Compton et al., this volume), but palygorskite occurs in all samples and is locally the dominant clay mineral (Veevers, Heirtzler, et al., 1974; Cook et al., 1974). Zeolite (determined as clinoptilolite by shipboard XRD analysis) occurs throughout the unit and reaches abundances of 15% in Cores 27-261-8 and -9. Our smear slide studies, supported by shipboard and shore-based XRD and carbonate content analyses (Cook et al., 1974; Bode, 1974a), indicate that Unit U1 is virtually devoid of primary and authigenic carbonate. Phosphate content of this unit is the highest recorded at Site 261 (Cook, 1974).

Microfossils are rare; Cores 27-261-8 through -5 contain only arenaceous benthic foraminifers and fish debris. Phosphatic debris is particularly abundant in the upper part of the unit and accounts for the phosphate maximum in this interval. Radiolarians

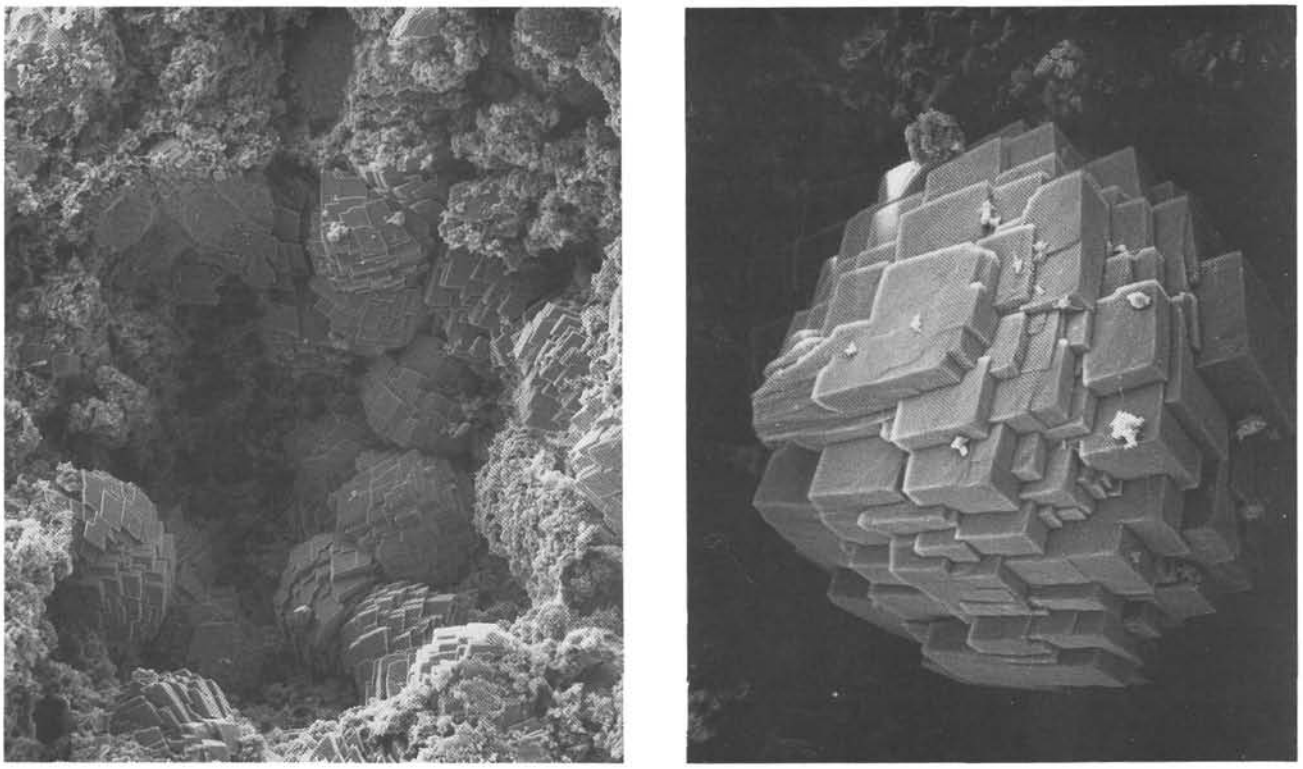

Figure 23. High-magnification SEM photographs of authigenic carbonate in gray claystone. **A.** Rhodochrosite rhombs growing in mold left by dissolution of radiolarian test (Sample 27-261-19-4, 59–60 cm; scale bar = 30 μm). **B.** Detail of rhomb shown in **A**; scale bar = 10 μm.

occur in Core 27-261-9, but are poorly preserved; some have been replaced by clinoptilolite or by chalcedony (Robinson et al., 1974).

Interpretation

Pelagic clay slowly deposited below the CCD makes up this unit; turbidites or other redeposited sediments were not identified in the cores recovered. Sedimentation rates (2 m/m.y.; Fig. 5) are an order of magnitude less than those of the underlying radiolarian claystone, and distinctive features of the zeolitic clay facies appear largely attributable to its slow accumulation. Palygorskite is commonly found in slowly deposited sediments; the magnesium needed to form this mineral can be supplied by diffusion from overlying seawater when sediment accumulation rates are low (Ludden, Gradstein, et al., 1990). The predominantly brown color of Unit U1 sediments, indicating deposition in an oxidizing environment, and the abundance of phosphatic (fish) debris in this interval also reflect slow sedimentation.

Sedimentation rates influenced other characteristics of the zeolitic clay as well. Slow sedimentation results in increased dissolution (and thus decreased preservation) of siliceous microfossils (e.g., Kennett, 1982). Thus, the scarcity of radiolarians in Unit U1, in contrast to their relative abundance in Unit L4, is at least in part a function of sedimentation rates, although changing oceanographic conditions (cessation of upwelling along the northwest Australian margin) also played a role (P. O. Baumgartner, pers. comm., 1990). The presence of zeolite in Unit U1 is in turn linked to radiolarian scarcity. Clinoptilolite forms during diagenesis of sediments that contain low concentrations of silica (Ludden, Gradstein, et al., 1990), a condition that prevailed in these radiolarian-poor clays.

Unit U2, Calcareous Sediment (Miocene–Pliocene; Cores 27-261-4 and -3; 142.0–19.0 m sub-bottom)

Description

Redeposited calcareous sediment dominates this unit (Unit 2 of Veevers, Heirtzler, et al., 1974) and is intercalated with noncalcareous clay; both lithologies are greenish gray. Calcareous intervals consist of stiff nannofossil ooze and lesser foraminiferal ooze and make up 82% of the sediment recovered (80% of Core 27-261-3 and 90% of Core 27-261-4). Nine distinct calcareous layers occur; the thickest is more than 180 cm, but most are 20 to 80 cm. Clay layers are typically much thinner (about 2 cm), but an interval 53 cm thick occurs in Core 27-261-3.

All the calcareous intervals have gradational tops and sharp bottoms; the bases of three layers are scoured. The upper 5 to 10 cm of most layers are bioturbated; burrows (largely *Planolites* and *Chondrites*) are filled with noncalcareous clay and decrease in abundance (and in some cases, in average diameter) downward within a given interval. Other features of these layers include graded bedding and parallel lamination. Most layers are distinctly coarser grained and lighter in color toward the base. The thickest interval (Section 27-261-4-2, 100 cm, to -1, 0 cm) grades upward from fine-grained sand to silty clay to clay through a distance of 90 cm; the sand contains parallel laminae made of alternating concentrations of coarser and finer grained foraminiferal tests (thin section observations, this study, and grain-size analyses of Bode, 1974b, Thayer et al., 1974). Base-cut-out Bouma sequences (BCDE, BDE) occur in the coarser grained, graded intervals. Some calcareous intervals are not obviously graded, but consist of homogeneous, poorly sorted (Thayer et al., 1974) silty clay with distinct millimeter- to centimeter-thick basal lags of fine-grained (foraminiferal) sand.

Calcareous layers consist chiefly or entirely of nannofossil ooze, locally clayey; carbonate content ranges from 48% to 73% (Bode, 1974a). Noncarbonate material (mostly clay) is generally more abundant upwards within a given layer. Coarse silt and sand grains in these oozes consist chiefly of small whole foraminifers and foraminifer fragments. Both benthonic and planktonic foraminifers occur; assemblages are heterogenous and size-sorted (Veevers, Heirtzler, et al., 1974; this study). Foraminifer chambers may be empty, or filled with pyrite or nannofossil ooze. Noncarbonate detrital grains are a subordinate (Tr-5%) part of the coarse fraction and consist largely of quartz, but a diverse heavy mineral suite (including clino- and orthopyroxene, hornblende, epidote, garnet, tourmaline, and zircon) (McKnight, 1974) occurs near the base of the thick, graded interval in Section 27-261-4-2.

A dominantly clast-supported intraformational conglomerate, somewhat disturbed by drilling, makes up the top 20 cm of Core 27-261-4. Clasts range from a few millimeters to 4 cm in maximum diameter and are rounded to elongate. Most clasts are gray nannofossil ooze, but some consist of foraminiferal sand or noncalcareous clay. The matrix is light gray nannofossil ooze.

The intercalated clay layers in Unit U2 appear homogeneous and structureless; they are olive gray to green, locally vaguely mottled. The clay mineral assemblage includes abundant kaolinite, which is virtually absent from all underlying units, as well as variably smectitic-rich I/S , lesser illite, and mica (Veevers, Heirtzler, et al., 1974; Compton et al., this volume). Smear slide analyses (Veevers, Heirtzler, et al., 1974; this study) indicate these clays contain little carbonate and only minor detrital silt or siliceous microfossils.

Interpretation

This unit consists of pelagic clay and intercalated biogenic ooze; the clay layers are *in-situ* deposits formed below the CCD, whereas the ooze originally accumulated above the CCD but has been reworked and redeposited on the abyssal plain. Sedimentary features, such as graded bedding, scoured bed bottoms, and Bouma sequences, indicate that the oozes were redeposited by turbidity currents; structures are relatively rare, because most of the redeposited material is fine-grained. The intraformational conglomerate at the top of Core 27-261-4 is a debris flow or the basal part of an unusually coarse-grained turbidite. Sedimentation rates are relatively rapid, about 16 m/m.y. (Fig. 5).

The nine calcareous intervals recovered in Unit U2 represent at least 16 discrete depositional events. About half the intervals seem to have been formed by a single flow; these intervals are homogeneous and massive, or smoothly graded, with burrowed tops and sharp bases. Other intervals represent amalgamated deposits of two or more events, as indicated by the presence of a scoured horizon, sand lag, and/or burrowed zone toward the center of the interval.

Unit U2 resembles Unit L3 in containing calcareous turbidites, but derivation and abundance of turbidites in the two units differ. The composition of the calcareous sediment is similar in both units: biotic grains are largely pelagic and include no shallow-water indicators. A continental slope or outer shelf provenance is inferred, and material derived from the Australian continent itself is minor. The specific source for the calcareous sediment in Unit U2, however, appears more restricted than that proposed for Unit L3. Seismic profiles across the Argo Abyssal Plain, discussed below, indicate Unit U2 turbidites were derived chiefly from the southern (Exmouth Plateau) continental margin; there is no evidence of input from the eastern (Scott Plateau) margin. In spite of this more limited provenance, turbidites are relatively more abundant in Unit U2 than in Unit L3; redeposited sediments make up more than 80% of the younger unit, but only 50% of Unit L3.

Unit U3, Siliceous Ooze (Pliocene–Quaternary; Cores 27-261-2 and -1; 19.0–0 m sub-bottom)

Description

Greenish-gray siliceous ooze, locally clayey, makes up this unit (Unit 1 of Veevers, Heirtzler, et al., 1974). No sedimentary structures are visible, but vague color lamination and mottling occur locally. A variety of whole and fragmentary siliceous fossils comprise the ooze, including abundant and diverse radiolarians (Renz, 1974), as well as diatoms, silicoflagellates, and sponge spicules. Clay minerals consist of I/S having 30% to 40% illite layers and lesser illite and kaolinite (Compton et al., this volume). Volcanic glass forms up to 15% of some smear slide samples (Veevers, Heirtzler, et al., 1974). Smear slide observations indicate most of the unit contains little carbonate, but a sample from a thin layer of greenish sandy clay in Sample 27-261-2-1, 118–119 cm, contains several percent nannofossils and calcareous foraminifers in addition to abundant whole radiolarians.

Interpretation

This unit consists of pelagic siliceous ooze deposited below the CCD and containing notable volcanic glass. Rare calcareous microfossils have been redeposited, probably by turbidites, as proposed for the underlying unit. However, allochthonous calcareous material in Unit U3 is much less abundant than in Unit U2 and is nowhere plentiful enough to form discrete dominantly calcareous intervals. Reduction in the amount of redeposited sediment reaching Site 261 during the Quaternary is most likely a result of higher global sea levels and subsequent decrease in turbidite generation. The presence of abundant siliceous biogenic material in these sediments reflects the rapid northward movement of the Australian plate during the Cenozoic; by Quaternary time, Site 261 was situated beneath the equatorial zone of high productivity (Cook, 1977). Volcanic glass was most likely derived from the active Indonesian volcanic arc to the north.

CALCAREOUS NANNOFOSSIL BIOSTRATIGRAPHY: ODP SITE 765 AND DSDP SITE 261

Introduction

The geographic position of Sites 765 and 261 (Argo Abyssal Plain) is far removed from the areas in which existing Mesozoic nannofossil zonal schemes have been established. Most of the nannofossil research in the Upper Jurassic/Lower Cretaceous interval has taken place in the European, Mediterranean, and North Atlantic areas. The nannofloras from these areas define two discrete paleobiogeographic realms, comparable to those observed in other fossil groups at this time (e.g., ammonites). Northern Europe and the Russian Platform comprise the northern Boreal Realm, and the Mediterranean-Tethys and proto-Atlantic are included in the Tethyan Realm. The nannofloral provinces are recognized by the presence of endemic species, distinct assemblage compositions, and differing stratigraphic ranges. These regional variations have necessitated the development of separate biostrati-graphic schemes, e.g., Bown et al. (1988) and Crux (1989) (Boreal); Roth et al. (1983) and Bralower et al. (1989) (Tethyan). Our knowledge of nannofossil distribution away from the areas stated above is at present limited. The existence of a third, Austral, biogeographic subdivision to the south of the tropical/subtropical Tethyan Realm has been recognized in mid to Late Cretaceous nannofloras (Wise, 1988), but has yet to be fully documented for the earlier Mesozoic.

The nannofloras from Sites 765 and 261 exhibit features that are found in both the Boreal and Tethyan realms, along with

additional attributes not observed elsewhere. For these reasons, none of the existing biostratigraphic zonal schemes are directly applicable to these sections, and thus selected bioevents were utilized for sediment dating. Wherever possible well-established and distinctive bioevents have been selected from the following sources: Bown et al. (1988); Bralower (1987); Bralower et al. (1989); Cooper (1985); Crux (1989); Jakubowski (1987); and Roth et al. (1983). Clearly, this region requires further research before a separate zonal scheme can be established.

In addition, preservation of nannofossils at the two sites is variable, and a number of barren intervals are present. This has resulted in lowered diversities, and the probability that some biostratigraphically useful species are missing, or are present rarely and with truncated ranges. Despite these problems of provincialism and preservation, we are confident that a reasonably good degree of biostratigraphic control has been achieved.

These two sites are also of interest for providing continuous marine sedimentary sequences across the Jurassic/Cretaceous boundary in facies different from those present in Europe, i.e., regressive/nonmarine facies in the Boreal area and massive carbonate facies in the Mediterranean-Tethys area. Both of these facies types yield poor nannofossil records, and only at the North Atlantic DSDP Sites 534 and 391 have well-preserved and diverse nannofloras been recovered (Roth, 1983; Bralower et al., 1989). Site 534 in particular provides an excellent sequence of Tithonian-Berriasian nannofloras revealing the importance of this interval in the evolutionary history of the group (Bown et al., in press). The Jurassic/Cretaceous boundary interval at Site 261 yielded a poorly preserved but interesting nannofossil record, which is distinct from that seen in the Tethyan area. The equivalent interval at Site 765 was barren of nannofossils.

The age determinations presented below differ from those originally presented in Ludden, Gradstein, et al. (1990), and Proto Decima (1974). Taxonomic discussion and selected illustrations of the nanno-floras are given in Bown (this volume).

ODP Site 765

Introduction

This section describes the nannofossil biostratigraphy of the lower cores (Cores 123-765C-62R through -55R) of ODP Site 765. The Lower Cretaceous nannofossil biostratigraphy is also discussed in Mutterlose (this volume).

The sediments lying directly on basalt basement are red claystones, which are virtually devoid of nannofossils in the lower 3.18 m. There follows an interval of 8.65 m, in which nannofossils are present, but the assemblages are of extremely low diversity and highly corroded (Table 3). A second interval barren of nannofossils ranges from Samples 123-765C-61R-3, 3 cm, to -58R-2, 10 cm. Above this, nannofossil-bearing claystones are present between Samples 123-765C-58R-2, 10 cm, and -55R-1, 5 cm, yielding assemblages of moderate to good preservation and high diversity (Table 4). Above this interval, up to Core 123-765C-40R, primary calcareous components are extremely rare and nannofossils are absent.

The lowermost nannofossil bearing interval in Cores 123-765C-61R and -62R contains highly etched assemblages that were deposited *in situ*, at or near the level of the CCD. All younger nannofossil bearing strata are redeposited sediments (carbonate turbidites).

Biostratigraphy

The lowest productive interval for calcareous nannofossils is dated as Tithonian (Unit L2). The nannofossil claystones of Unit L3B are dated as Valanginian to Hauterivian, based on the occurrence of *Tubodiscus verenae* and *Cruciellipsis cuvillieri*. The

Table 3. Stratigraphic distribution of calcareous nannofossils from Site 765 (Cores 123-765C-62R to -61R).

Age	Sample	Preservation	*Watznaueria barnesae*	*Watznaueria manivitae*	*Watznaueria britannica*	Calcispheres (fragments)	Coccolith indet. (*Watz.*)	*Watznaueria fossacincta*	*Cyclagelosphaera margerelii*	Retecapsid indet.
	61-2, 145		.	.	.	.	.	.	.	.
	61-3, 3	P	.	.	.	.	F	.	.	.
	61-3, 15.5	P	.	.	.	A	.	.	.	.
	61-3, 16	P	.	.	.	A	.	.	.	.
	61-3, 18.5	P	.	C	.	C	.	.	.	.
	61-3, 19.5	P	.	.	.	C	.	.	.	.
	61-3, 25	P	.	.	.	C	.	.	.	.
	61-3, 48	P	.	C	.	.	.	.	.	.
	61-4, 16	P	.	C	.	.	.	.	.	.
	61-4, 25	P	F	C	F	C	.	?	R	F
	61-4, 66	P	.	F	.	.	.	.	.	.
	61-4, 67	P	F	C	F	.	.	.	.	.
	61-4, 82	P	.	C	.	.	.	.	.	.
	61-4, 92	P	.	C	.	.	.	.	.	.
	61-4, 97	P	F	C	.	.	.	.	.	.
	61-4, 99	VP	.	C	.	.	.	.	.	.
	61-4, 101	P	.	C	.	.	.	.	.	.
	61-4, 104	VP	.	F	.	.	.	.	.	.
	61-4, 108	VP	.	C	.	.	.	.	.	.
	61-4, 108.5	VP	.	F	.	C	.	F	.	.
	61-5, 14	P	?	F	.	.	?	.	.	.
	61-5, 37	P	.	C	.	.	F	.	.	.
	61-5, 56.5	P	F	C	F	C	.	.	.	.
	61-5, 57	P	.	.	.	C	.	.	.	.
	61-5, 58	P	F	C	.	C	.	.	.	.
Tithonian	61-5, 125		.	.	.	.	.	.	.	.
	61-5, 141		.	.	.	.	.	.	.	.
	62-1, 9	VP	.	F	.	.	.	.	.	.
	62-1, 12	P	.	F	.	.	.	.	.	.
	62-1, 35	P	.	F	.	.	.	.	.	.
	62-1, 45	P	.	C	.	.	.	.	.	.
	62-1, 54	VP	.	C	.	.	.	.	.	.
	62-1, 56	P	.	C	.	.	.	.	.	.
	62-1, 57	P	.	C	.	.	.	.	.	.
	62-1, 58	P	.	C	.	.	.	.	.	.
	62-1, 59	VP	.	C	.	.	.	.	.	.
	62-1, 60	VP	.	C	.	.	.	.	.	.
	62-1, 61	VP	.	F	.	.	.	.	.	.
	62-1, 62	VP	.	F	.	.	.	.	.	.
	62-1, 74	P	.	F	.	.	.	.	.	.
	62-1, 85	P	.	C	.	.	.	.	.	.
	62-1, 104	P	F	C	R	.	.	.	.	.
	62-1, 110	P	.	C	.	.	.	.	.	.
	62-1, 123	VP	.	C	F	.	.	.	.	.
	62-1, 128	VP	.	C	.	.	.	.	.	.
	62-1, 134	P	.	C	.	.	.	.	.	.
	62-1, 135	P	.	F	.	.	.	.	.	.
	62-1, 137	P	.	F	.	.	.	.	.	.
	62-1, 145	VP	.	F	.	.	.	.	.	.
	62-2, 5	P	.	C	.	.	.	.	.	.
	62-2, 13	P	F	C	.	.	.	.	.	.
	62-2, 61		.	.	.	.	.	.	.	.

Note: Abbreviations used in calcareous nannofossil range charts (Tables 3 through 5) are (1) for abundance, R, rare (1–2 specimens); F, few (3–10 specimens); C, common (11–100 specimens); A, abundant (greater than 100 specimens); counting was performed using the light microscope over 20 fields of view; (2) for preservation, VP, very poor (extreme etching); P, poor (etching and overgrowth; obscured, damaged, or destroyed central area structures); M, moderate (moderate etching or overgrowth); G, good (little or no etching or overgrowth).

Table 4. Stratigraphic distribution of calcareous nannofossils from Site 765 (Cores 123-765C-58R to -55R).

Age	Sample	Preservation	*Assipetra infracretacea*	*Crucibiscutum salebrosum*	*Cruciellipsis cuvillieri*	*Cyclagelosphaera argoensis*	*Cyclagelosphaera margerelii*	*Diazomatolithus lehmanii*	*Haquis circumradiatus*	*Lithraphidites carniolensis*	*Manivitella pemmatoidea*	*Microstaurus chiastius*	*Pickelhaube furtiva*	*Rhagodiscus asper*	*Rotelapillus laffittei*	*Tegumentum striatum*	*Watznaueria barnesae*	*Watznaueria fossacincta*	*Watznaueria manivitae*	*Zeugrhabdotus cooperi*	*Zeugrhabdotus embergeri*	Calcisphere sp. indet.	*Retecapsa crenulata*	*Eihmorhabdus hauterivianus*	*Haquis ellipticus*	*Retecapsa surirella*	*Speetonia colligata*
late Valanginian–Hauterivian	55-1, 05	M	.	.	.	.	.	.	F	.	F	R	.	.	.	.	C	C	.	.	C	.	.	.	.	.	.
	55-1, 41	M	.	.	R	F	.	.	F	.	F	F	.	.	.	.	C	C	R	.	C	.	.	.	.	.	.
	55-1, 139	M	.	F	.	.	C	.	F	C	F	F	.	R	R	?	C	C	.	.	C	F	.	.	.	.	.
	55-2, 110	G	.	C	F	R	C	.	F	C	C	F	.	R	.	R	C	A	.	.	C	F	F	R	.	.	.
	55-3, 98	M	.	F	.	.	F	.	F	C	.	C	.	R	F	R	C	C	.	.	C	.	.	.	.	.	.
	55-3, 119	G	.	C	.	.	C	.	R	C	C	F	.	R	.	F	A	A	R	.	C	F	.	R	.	F	.
	55-CC	M	.	.	F	.	C	.	F	.	C	.	.	.	.	.	A	A	R	.	C	.	.	.	.	.	.
	56-1, 12	M	.	.	.	F	C	.	F	C	C	.	.	.	.	.	C	A	F	.	C	F	.	.	.	.	.
	56-2, 65	G	.	C	.	.	C	.	.	C	C	.	.	.	.	.	C	A	F	.	C	.	.	.	.	.	.
	56-2, 67	G	.	C	F	F	C	F	F	C	C	F	R	R	F	F	C	A	.	.	C	.	.	.	.	R	.
Valanginian	56-3, 142	G	F	C	F	C	F	R	F	C	F	F	.	R	R	F	A	A	F	.	C	.	R	.	.	R	R
	56-4, 19	M	.	C	F	.	C	F	.	C	.	.	.	R	F	R	C	A	.	.	C	.	.	.	.	.	.
	56-CC	G	.	C	F	F	C	.	.	C	C	F	.	R	.	F	C	C	.	.	C	R	.	.	.	R	R
	57-1, 08	M	.	C	.	.	C	.	F	F	F	.	.	R	.	F	C	C	.	.	C	.	.	.	.	R	.
	57-1, 29	M	?	.	.	.	C	.	.	C	.	.	.	.	.	.	A	A	.	.	C	.	.	.	.	.	.
	57-1, 116	M	?	C	F	F	.	.	F	C	C	F	.	.	.	.	C	C	.	.	C	.	F	.	.	.	.
	57-2, 39	G	?	C	F	F	C	.	F	C	C	C	.	R	R	F	A	A	.	.	C	F	.	.	.	.	.
	57-2, 145	G	.	C	.	F	F	.	C	C	C	F	.	F	F	F	A	A	.	.	C	F	.	.	.	R	.
	57-3, 115	G	.	F	F	F	F	R	F	C	C	.	.	F	.	F	A	A	.	R	C	R	.	.	.	R	.
	57-4, 83	M	.	.	F	F	F	.	F	C	C	.	.	.	.	.	C	C	.	.	C	.	.	.	.	.	.
	57-6, 107	P	.	.	.	.	.	.	.	.	.	.	.	.	.	.	.	C	.	.	C	F	.	.	.	.	.
	58-1, 56	G	?	C	F	F	C	R	F	C	C	F	.	R	F	F	A	A	F	F	C	F	.	R	R	F	R
	58-1, 85	G	?	C	F	F	C	.	C	C	C	F	.	R	F	F	A	A	.	F	C	.	.	?	R	R	R
	58-1, 131	M	?	R	R	R	F	.	F	C	C	F	.	.	.	F	C	C	.	.	C	.	F	.	.	.	.
	58-2, 10	M	F	F	R	F	C	F	F	F	C	C	R	R	F	?	C	A	R	F	C	C	.	.	.	.	.

Valanginian-Hauterivian assemblages correlate well with those from Site 261, but are generally better preserved and of higher diversity.

Tithonian (Sections 123-765C-62R-2, 13 cm, to -61R-3, 3 cm)

Nannofossil assemblages occur consistently throughout this interval but are extremely impoverished and poorly preserved. The assemblages are characterized by high abundances of large (20 µm) *Watznaueria manivitae* (= *C. deflandrei*) coccoliths, which are highly corroded. Also present are poorly preserved specimens of *Watznaueria barnesae, W. britannica,* and *W. fossacincta,* along with etched retecapsid coccolith rims. The abundance of *W. manivitae* correlates with similar assemblages from Site 261 (27-261-32-4, 140 cm to -32-3, 10 cm) that have been dated as Tithonian.

Clearly, these assemblages have been altered by selective etching of all but the most dissolution-resistant species. Despite this, the assemblages are still considered to reflect originally high abundances of *W. manivitae* (see also Site 261). Such high abundances of *W. manivitae* have not been recorded from the Boreal or Tethyan areas, and this may be a feature unique to this region or to the Austral nannofloral province, and of widespread biostratigraphic value.

Valanginian (Sections 123-765C-58R-2, 10 cm, to -56R-3, 142 cm)

This interval is characterized by relatively well-preserved and diverse nannofossil assemblages containing *Tubodiscus verenae,* which has a restricted range in the Valanginian (Bralower, 1987; Bralower et al., 1989). The lowest two samples come from a single turbidite that also includes Sample 123-765C-58R-1, 85 cm, in which the lowest occurrence of *Tubodiscus verenae* is observed, and are thus dated as Valanginian.

The *C. salebrosum* specimens from this interval exhibit variable morphology that ranges from the typical *Biscutum*-type forms (narrow rim and central area) to those having a *Sollasites*-type appearance (broad rim and more open central area). These specimens are identical to those from the Berriasian-lowermost Valanginian of Site 261 suggesting an early Valanginian age. The lowest occurrence of *Eiffellithus windii* in Sample 123-765C-58R-1, 56 cm, is also indicative of the early Valanginian (Bralower et al., 1989). The occurrence of *Vagalapilla matalosa* and *Repagulum parvidentatum* in Valanginian sediments is unique to this region; the former has been previously reported from the late Barremian in the European area (Crux, 1989), the latter from the early Barremian (Jakubowski, 1987; Crux, 1989).

Upper Valanginian–Hauterivian (Sections 123-765C-56R-2, 67 cm, to -55R-1, 5 cm)

The base of this interval is marked by the highest occurrence of *Tubodiscus verenae,* indicating a late Valanginian age (Roth, 1978; Perch-Nielsen, 1985; Bralower, 1987). Applegate et al. (1989) record a Hauterivian last occurrence for *T. verenae,* but further work will be needed to substantiate this claim. The continued presence of *Cruciellipsis cuvillieri* infers an age no younger than Hauterivian (Bralower, 1987).

The assemblages from this interval are identical in composition to those from Core 27-261-28-2, 121 cm, to -27-2, 57 cm, at Site 261.

Table 4 (continued).

Age	Sample	Preservation	*Tubodiscus verenae*	*Vagalapilla matalosa*	*Vagalapilla stradneri*	*Watznaueria britannica*	*Zeugrhabdotus erectus*	*Axopodorhabdus dietzmannii*	*Biscutum ellipticum*	*Eiffellithus windii*	*Grantarhabdus coronadventis*	*Sollasites* sp. indet.	*Watznaueria biporta*	*Cretarhabdus conicus*	*Discorhabdus ignotus*	*Micrantholithus hoschultzi*	*Micrantholithus obtusus*	*Retecapsa angustiforata*	*Grantarhabdus meddii*	*Repagulum parvidentatum*	Podorhabdid indet.	*Chiastozygus* sp.	Retecapsid indet.
late Valanginian–Hauterivian	55-1, 05	M	.	F	.	.	.	.	.	.	.	.	.	.	.	.	.	.	.	.	.	.	F
	55-1, 41	M	.	.	.	.	.	.	.	.	.	.	.	.	.	.	.	.	.	.	.	.	C
	55-1, 139	M	.	F	.	.	.	.	R	.	.	R	.	F	R	.	.	F	.	.	.	.	.
	55-2, 110	G	.	C	.	F	.	.	F	.	.	.	R	F	.	F	.	.	.	.	.	.	.
	55-3, 98	M	.	.	.	.	.	.	.	.	.	.	.	F	.	.	.	.	.	F	C	R	.
	55-3, 119	G	.	C	F	.	F	F	.	.	F	.	F	F	.	F	.	R	.	F	.	R	.
	55-CC	M	.	C	.	.	.	.	.	.	.	.	.	.	.	.	.	.	.	.	.	.	F
	56-1, 12	M	.	C	.	F	.	.	.	.	.	.	.	.	.	.	.	.	.	.	.	.	.
	56-2, 65	G	.	C	.	.	.	.	.	.	.	.	.	.	.	.	.	.	.	.	.	.	.
	56-2, 67	G	.	C	.	.	.	.	R	.	R	.	F	F	.	.	.	F	.	.	.	.	.
Valanginian	56-3, 142	G	F	C	F	F	.	F	F	.	R	R	.	F	.	F	R	F	.	.	.	R	.
	56-4, 19	M	.	C	R	.	.	.	F	.	.	.	.	F	.	F	F	.	R	F	C	.	.
	56-CC	G	R	C	F	F	F	.	.	R	F	.	.	F	.	F	R	F	.	.	.	.	.
	57-1, 08	M	.	C	.	.	.	.	F	.	F	.	.	F	.	.	.	.	.	.	.	.	.
	57-1, 29	M	.	C	.	.	.	.	.	.	.	.	.	.	.	.	.	.	.	.	.	.	.
	57-1, 116	M	.	C	.	F	.	.	.	.	.	R	.	.	.	.	.	.	.	.	.	.	.
	57-2, 39	G	.	C	.	.	.	.	.	.	.	.	.	F	.	.	.	.	.	.	.	.	.
	57-2, 145	G	.	C	.	.	.	.	F	.	R	.	.	F	.	.	.	.	.	.	.	.	.
	57-3, 115	G	.	C	F	.	.	.	F	R	.	F	.	F	R	.	.	.	.	.	.	.	.
	57-4, 83	M	.	.	.	.	.	.	.	.	.	.	.	.	.	.	.	.	.	.	.	.	.
	57-6, 107	P	.	.	.	.	.	.	.	.	.	.	.	.	.	.	.	.	.	.	.	.	.
	58-1, 56	G	F	.	F	F	F	R	F	R	F	R	F	.	.	.	.	.	.	.	.	.	.
	58-1, 85	G	F	C	F	F	F	.	.	.	.	.	.	.	.	.	.	.	.	.	.	.	.
	58-1, 131	M	.	.	.	.	.	.	.	.	.	.	.	.	.	.	.	.	.	.	.	.	.
	58-2, 10	M	.	.	.	.	.	.	.	.	.	.	.	.	.	.	.	.	.	.	.	.	.

DSDP Site 261

Introduction

A total of 80 samples were analyzed for calcareous nannofossils from the lower cores of DSDP Site 261 (Cores 33 through 27). Twenty of the samples are barren of nannofossils, while the remainder yield assemblages of variable diversity and preservation. The dominant preservational state is poor, with nannofossils slightly to severely etched and also overgrown. Low assemblage diversities reflect selective dissolution of delicate, solution-prone species. Such poor preservation is thought to indicate a depositional environment near or below the CCD, compounded by further post-depositional redistribution of calcite during diagenesis. Assemblages severely affected by dissolution are of low diversity and are dominated by solution-resistant species, particularly members of the Family Watznaueriaceae, and the genus *Zeugrhabdotus*. Preservation is best in the lowest core (Core 27-261-33), reflecting probable deposition above the CCD; and in Sections 27-261-31-2, -30-3, -30-2, and -28-2, which represent transported shelf/slope, carbonate-rich sediments deposited below the CCD. The Mesozoic cores above Core 27-261-27 (Cores 26 through 5) are noncalcareous and devoid of nannofossils.

Biostratigraphy

The lower cores of Site 261 were dated as Late Jurassic to Early Cretaceous, based on well-known and well-constrained nannofossil datums. The exact position of stage boundaries and the Jurassic/Cretaceous boundary is somewhat problematic, but the interval ranges from Kimmeridgian to Hauterivian with the system boundary falling within Core 27-261-31 (Table 5).

Kimmeridgian/Lower Tithonian (Sections 27-261-34-1, 68 cm, to -33-1, 10 cm)

The top of this interval is marked by the highest occurrence of *Stephanolithion bigotii*, a well-established and distinctive marker species that has never been reported above the lower Tithonian (Bown et al., 1988; Bralower et al., 1989). The abundance of *Watznaueria britannica* and *W. barnesae* confirms the Jurassic nature of these assemblages as both these species decline markedly toward the top of the Tithonian (Cooper, 1985). The presence of coccoliths transitional in morphology between *Zeugrhabdotus erectus* and *Z. embergeri* (e.g., *Zeugrhabdotus* sp. 1 and *Z. cooperi*) indicates a Kimmeridgian to Tithonian age (Roth, 1983). The occurrence of *Ethmorhabdus gallicus* and *Axopodorhabdus cylindratus* and the absence of *Lotharingius crucicentralis, Podorhabdus grassei, Crepidolithus perforata,* and *Hexapodorhabdus cuvillieri* suggest an age no older than Kimmeridgian and no younger than early Tithonian (Bown et al., 1988). The lowest occurrence of small and rare specimens of *Conusphaera mexicana minor* in the top sample of this interval (27-261-33-1, 10 cm) indicates a latest Kimmeridgian (*sensu gallico*) age (Bralower et al., 1989).

Preservation in Core 27-261-33 is good throughout, and the assemblages are entirely compatible stratigraphically. There is no evidence of reworking and the calcareous nannofossils indicate a Kimmeridgian/early Tithonian age. These assemblages are comparable to those seen in the Boreal and Tethyan areas at this time, and Tethyan affinities are indicated by the presence of *Conusphaera mexicana minor* and *Watznaueria manivitae* (Cooper, 1989). Samples from the interbasalt limestone intervals yield rare and poorly preserved assemblages that are not age diagnostic.

Table 5. Stratigraphic distribution of calcareous nannofossils from Site 261 (Cores 27-261-34 to -27).

Age	Sample	Preservation	*Watznaueria* sp. indet.	*Biscutum dubium*	*Biscutum erismatum*	*Vagalapilla stradneri*	*Watznaueria barnesae*	*Watznaueria britannica*	*Watznaueria fossacincta*	*Watznaueria manivitae*	*Zeugrhabdotus* sp. 1	Podorhabdid indet.	Retecapsid indet.	*Cretarhabdus conicus*	*Cyclagelosphaera margerelii*	*Zeugrhabdotus erectus*	*Axopodorhabdus cylindratus*	*Biscutum ellipticum*	*Ethmorhabdus gallicus*	*Stephanolithion bigotii*	*Conusphaera mexicana minor*	*Zeugrhabdotus cooperi*	*Pickelhaube furtiva*	*Zeugrhabdotus embergeri*	*Cyclagelosphaera argoensis*	*Lithraphidites carniolensis*	*Microstaurus chiastius*
	27-1, 140		.	.	.	.	.	.	.	.	.	.	.	.	.	.	.	.	.	.	.	.	.	.	.	.	.
	27-2, 57	VP	F	.	.	.	.	.	.	.	.	.	.	.	.	.	.	.	.	.	.	.	.	.	.	.	.
	27-2, 71		.	.	.	.	.	.	.	.	.	.	.	.	.	.	.	.	.	.	.	.	.	.	.	.	.
	27-2, 109		.	.	.	.	.	.	.	.	.	.	.	.	.	.	.	.	.	.	.	.	.	.	.	.	.
	27-2, 142	P	F	.	.	.	R	.	F	.	.	.	.	.	.	.	.	.	.	.	.	.	.	R	.	.	.
late	28-1, 70	P	.	.	.	.	R	R	A	.	.	.	F	.	R	.	.	.	.	.	.	.	.	F	.	.	.
Valanginian–	28-1, 71	P	.	.	.	.	R	R	C	.	.	.	R	.	R	.	.	.	.	.	.	.	.	R	.	.	.
Hauterivian	28-1, 99	M	.	.	.	.	R	R	C	.	.	.	.	.	R	R	.	.	.	.	.	.	.	R	.	R	.
	28-1, 145	P	C	.	.	.	.	.	.	.	.	.	R	.	R	.	.	.	.	.	.	.	.	.	.	.	.
	28-2, 07		.	.	.	.	.	.	.	.	.	.	.	.	.	.	.	.	.	.	.	.	.	.	.	.	.
	28-2, 59		.	.	.	.	.	.	.	.	.	.	.	.	.	.	.	.	.	.	.	.	.	.	.	.	.
	28-2, 112	P	.	.	.	.	A	.	A	.	.	.	C	.	F	.	.	.	.	.	.	.	R	C	.	.	.
	28-2, 121		.	.	.	.	.	.	.	.	.	.	.	.	.	.	.	.	.	.	.	.	.	.	.	.	.
	28-2, 128	G	.	.	.	.	C	R	A	.	.	.	.	R	C	F	.	R	.	.	.	.	R	C	.	C	F
	28-3, 48		.	.	.	.	.	.	.	.	.	.	.	.	.	.	.	.	.	.	.	.	.	.	.	.	.
	28-3, 103		.	.	.	.	.	.	.	.	.	.	.	.	.	.	.	.	.	.	.	.	.	.	.	.	.
	28-3, 110	P	.	.	.	.	R	R	C	.	.	R	.	.	.	.	.	.	.	.	.	.	.	R	.	.	.
	28-4, 10		.	.	.	.	.	.	.	.	.	.	.	.	.	.	.	.	.	.	.	.	.	.	.	.	.
	29-1, 134	P	.	.	.	.	.	.	A	.	.	.	F	.	.	.	.	.	.	.	.	.	R	R	.	.	.
	29-1, 140	VP	C	.	.	.	.	.	.	.	.	.	F	.	.	.	.	.	.	.	.	.	.	.	.	.	.
Valanginian	29-2, 38	P	C	.	.	.	.	.	.	.	.	.	F	.	R	.	.	.	.	.	.	.	R	.	.	.	.
	29-2, 80	P	.	.	.	.	.	.	A	.	.	.	F	.	R	.	.	.	.	.	.	.	.	R	R	.	.
	29-3, 30		.	.	.	.	.	.	.	.	.	.	.	.	.	.	.	.	.	.	.	.	.	.	.	.	.
	29-3, 130	P	.	.	.	.	R	R	A	.	.	.	C	.	R	.	.	.	.	.	.	.	.	R	.	.	R
	29-3, 138	M	.	.	.	.	R	R	A	.	.	R	C	.	C	.	.	.	.	.	.	.	.	R	.	.	.
	30-1, 104		.	.	.	.	.	.	.	.	.	.	.	.	.	.	.	.	.	.	.	.	.	.	.	.	.
	30-2, 17	P	.	.	.	.	R	R	A	.	.	.	C	.	F	.	.	.	.	.	.	.	R	F	.	.	.
	30-2, 60	M	.	.	.	.	F	F	A	.	.	.	C	R	F	.	.	F	.	.	.	F	R	F	F	R	R
	30-2, 130	M	.	.	.	.	.	F	A	.	.	.	C	.	F	.	.	R	.	.	.	.	R	F	F	.	R
	30-3, 90	VP	.	.	.	.	.	.	C	.	.	.	R	.	.	.	.	.	.	.	.	R	.	R	.	.	.
	30-3, 140	G	.	.	.	.	R	R	A	.	.	.	C	.	R	R	.	F	.	.	.	R	R	R	R	.	R
	30-4, 20	P	.	.	.	.	.	R	A	.	.	.	F	.	R	.	.	.	.	.	.	.	.	F	C	.	.
	30-4, 140	VP	.	.	.	.	.	.	F	.	.	.	.	.	.	.	.	.	.	.	.	.	.	.	R	.	.
Berriasian	31-2, 40		.	.	.	.	.	.	.	.	.	.	.	.	.	.	.	.	.	.	.	.	.	.	.	.	.
	31-2, 80		.	.	.	.	.	.	.	.	.	.	.	.	.	.	.	.	.	.	.	.	.	.	.	.	.
	31-2, 122	M	.	.	.	.	C	F	A	.	.	.	F	.	C	.	.	R	.	.	.	A	.	.	F	.	R
	31-2, 129	G	.	.	.	.	R	R	A	.	.	.	R	.	R	R	.	.	.	.	.	A	.	R	R	.	R
	31-3, 10	P	.	.	.	.	.	F	A	.	.	.	F	.	F	.	.	.	.	.	.	C	.	.	R	.	.
	31-3, 40	P	.	.	.	.	R	R	A	.	.	.	F	.	R	.	.	.	.	.	.	F	.	.	R	.	.
	31-3, 41	P	.	.	.	.	R	R	A	.	.	.	R	.	R	.	.	R	.	.	.	R	.	R	R	.	.
	31-3, 80		.	.	.	.	.	.	.	.	.	.	.	.	.	.	.	.	.	.	.	.	.	.	.	.	.
	31-3, 140		.	.	.	.	.	.	.	.	.	.	.	.	.	.	.	.	.	.	.	.	.	.	.	.	.
	31-4, 40		.	.	.	.	.	.	.	.	.	.	.	.	.	.	.	.	.	.	.	.	.	.	.	.	.
	31-4, 60	P	.	.	.	.	R	R	C	R	.	.	R	.	R	.	.	.	.	.	.	F	.	R	R	.	.
	31-4, 80	P	.	.	.	.	R	R	C	R	.	.	.	.	R	.	.	.	.	.	.	R	.	.	F	.	.
	31-4, 120		.	.	.	.	.	.	.	.	.	.	.	.	.	.	.	.	.	.	.	.	.	.	.	.	.
	31-5, 10		.	.	.	.	.	.	.	.	.	.	.	.	.	.	.	.	.	.	.	.	.	.	.	.	.
	31-5, 50		.	.	.	.	.	.	.	.	.	.	.	.	.	.	.	.	.	.	.	.	.	.	.	.	.
	31-5, 80		.	.	.	.	.	.	.	.	.	.	.	.	.	.	.	.	.	.	.	.	.	.	.	.	.
	31-5, 135		.	.	.	.	.	.	.	.	.	.	.	.	.	.	.	.	.	.	.	.	.	.	.	.	.
	31-5, 141		.	.	.	.	.	.	.	.	.	.	.	.	.	.	.	.	.	.	.	.	.	.	.	.	.
	31-CC	G	.	.	.	.	C	C	A	R	.	.	C	.	A	.	.	.	.	.	.	F	.	F	C	R	R
Tithonian	32-1, 136	M	.	.	.	.	R	R	A	R	.	.	R	.	R	.	.	.	.	.	.	R	.	.	C	.	.
	32-1, 140	VP	.	.	.	.	R	.	F	R	.	.	.	.	.	.	.	.	.	.	.	.	.	R	F	.	.
	32-2, 10	P	.	.	.	.	.	.	F	.	.	.	.	.	.	.	.	.	.	.	.	R	.	R	R	.	.
	32-2, 40	VP	.	.	.	.	.	.	.	R	.	.	.	.	.	.	.	.	.	.	.	.	.	.	.	.	.
	32-2, 64		.	.	.	.	.	.	.	.	.	.	.	.	.	.	.	.	.	.	.	.	.	.	.	.	.
	32-2, 69		.	.	.	.	.	.	.	.	.	.	.	.	.	.	.	.	.	.	.	.	.	.	.	.	.
	32-2, 70	P	.	.	.	.	R	R	R	F	.	.	.	.	.	.	.	.	.	.	.	.	.	R	.	.	.
	32-2, 100	P	.	.	.	.	C	R	C	C	.	.	.	.	.	.	.	.	.	.	.	.	.	.	.	.	.
	32-2, 140	P	.	.	.	.	.	.	.	C	.	.	.	.	.	.	.	.	.	.	.	.	.	.	.	.	.
	32-3, 10	P	.	.	.	.	F	R	R	A	.	.	.	.	.	.	.	.	.	.	.	.	.	.	.	.	.
	32-3, 40	P	.	.	.	.	R	.	.	C	.	.	.	.	.	.	.	.	.	.	.	.	.	.	.	.	.
	32-3, 70	P	.	.	.	.	R	.	.	F	.	.	.	.	.	.	.	.	.	.	.	.	.	.	.	.	.
	32-3, 120	P	.	.	.	.	R	.	.	C	.	.	.	.	.	.	.	.	.	.	.	.	.	.	.	.	.
	32-3, 146	P	.	.	.	.	.	R	R	A	.	.	.	.	.	.	.	.	.	.	.	.	.	.	.	.	.

Table 5 (continued).

Age	Sample	Preservation	Calcisphere sp. indet.	*Ethmorhabdus hauterivianus*	*Watznaueria biporta*	*Cruciellipsis cuvillieri*	*Microstaurus quadratus*	*Crucibiscutum salebrosum*	*Manivitella pemmatoidea*	*Haquis ellipticus*	*Rhagodiscus nebulosus*	*Diazomatolithus lehmanii*	*Tubodiscus verenae*	*Haquis circumradiatus*	*Assipetra infracretacea*	*Axopodorhabdus dietzmannii*	*Grantarhabdus coronadventis*	*Retecapsa angustiforata*	*Retecapsa crenulata*	*Retecapsa surirella*	*Rotelapillus laffittei*	*Speetonia colligata*	*Tegumentum striatum*	*Vagalapilla matalosa*	*Vagalapilla* sp.
	27-1, 140		.	.	.	.	.	.	.	.	.	.	.	.	.	.	.	.	.	.	.	.	.	.	.
	27-2, 57	VP	.	.	.	.	.	.	.	.	.	.	.	.	.	.	.	.	.	.	.	.	.	.	.
	27-2, 71		.	.	.	.	.	.	.	.	.	.	.	.	.	.	.	.	.	.	.	.	.	.	.
	27-2, 109		.	.	.	.	.	.	.	.	.	.	.	.	.	.	.	.	.	.	.	.	.	.	.
	27-2, 142	P	.	.	.	.	.	.	.	.	.	.	.	.	.	.	.	.	.	.	.	.	.	.	.
late	28-1, 70	P	.	.	.	R	.	.	R	R	.	.	.	.	.	.	.	.	.	.	.	.	.	.	.
Valanginian–	28-1, 71	P	.	.	.	R	.	.	.	.	.	.	.	R	.	.	.	.	.	.	.	.	.	.	.
Hauterivian	28-1, 99	M	.	.	R	.	.	.	R	.	.	.	.	.	.	.	.	.	.	R	.	.	.	.	.
	28-1, 145	P	.	.	.	.	.	.	.	.	.	.	.	.	.	.	.	.	.	.	.	.	.	.	.
	28-2, 07		.	.	.	.	.	.	.	.	.	.	.	.	.	.	.	.	.	.	.	.	.	.	.
	28-2, 59		.	.	.	.	.	.	.	.	.	.	.	.	.	.	.	.	.	.	.	.	.	.	.
	28-2, 112	P	.	.	R	R	.	.	R	F	.	.	.	.	.	.	.	.	.	.	.	.	.	.	.
	28-2, 121		.	.	.	.	.	.	.	.	.	.	.	.	.	.	.	.	.	.	.	.	.	.	.
	28-2, 128	G	.	R	R	F	.	C	F	R	.	R	R	R	R	R	R	R	R	R	R	R	F	R	R
	28-3, 48		.	.	.	.	.	.	.	.	.	.	.	.	.	.	.	.	.	.	.	.	.	.	.
	28-3, 103		.	.	.	.	.	.	.	.	.	.	.	.	.	.	.	.	.	.	.	.	.	.	.
	28-3, 110	P	.	.	.	R	.	.	.	.	.	.	.	R	.	.	.	.	.	.	.	.	.	.	.
	28-4, 10		.	.	.	.	.	.	.	.	.	.	.	.	.	.	.	.	.	.	.	.	.	.	.
	29-1, 134	P	.	.	.	.	.	.	.	R	.	.	.	.	.	.	.	.	.	.	.	.	.	.	.
	29-1, 140	VP	.	.	.	.	.	.	.	.	.	.	.	.	.	.	.	.	.	.	.	.	.	.	.
Valanginian	29-2, 38	P	.	.	.	.	.	.	.	.	.	.	.	.	.	.	.	.	.	.	.	.	.	.	.
	29-2, 80	P	.	.	.	R	.	.	R	F	.	R	R	.	.	.	.	.	.	.	.	.	.	.	.
	29-3, 30		.	.	.	.	.	.	.	.	.	.	.	.	.	.	.	.	.	.	.	.	.	.	.
	29-3, 130	P	.	.	R	R	.	.	R	R	.	R	R	.	.	.	.	.	.	.	.	.	.	.	.
	29-3, 138	M	.	.	.	R	.	.	.	.	.	.	R	.	.	.	.	.	.	.	.	.	.	.	.
	30-1, 104		.	.	.	.	.	.	.	.	.	.	.	.	.	.	.	.	.	.	.	.	.	.	.
	30-2, 17	P	.	.	R	F	.	.	.	.	.	.	R	.	.	.	.	.	.	.	.	.	.	.	.
	30-2, 60	M	.	.	F	R	.	C	R	R	R	R	R	.	.	.	.	.	.	.	.	.	.	.	.
	30-2, 130	M	.	.	F	C	.	C	.	R	.	.	.	.	.	.	.	.	.	.	.	.	.	.	.
	30-3, 90	VP	.	.	R	F	.	.	.	R	.	.	.	.	.	.	.	.	.	.	.	.	.	.	.
	30-3, 140	G	R	.	F	R	.	C	R	.	R	.	.	.	.	.	.	.	.	.	.	.	.	.	.
	30-4, 20	P	.	.	F	F	.	.	.	R	.	.	.	.	.	.	.	.	.	.	.	.	.	.	.
	30-4, 140	VP	R	.	.	.	.	.	.	.	.	.	.	.	.	.	.	.	.	.	.	.	.	.	.
Berriasian	31-2, 40		.	.	.	.	.	.	.	.	.	.	.	.	.	.	.	.	.	.	.	.	.	.	.
	31-2, 80		.	.	.	.	.	.	.	.	.	.	.	.	.	.	.	.	.	.	.	.	.	.	.
	31-2, 122	M	F	R	R	F	R	F	.	R	.	.	.	.	.	.	.	.	.	.	.	.	.	.	.
	31-2, 129	G	R	.	.	R	.	R	R	.	.	.	.	.	.	.	.	.	.	.	.	.	.	.	.
	31-3, 10	P	.	.	.	.	R	.	.	.	.	.	.	.	.	.	.	.	.	.	.	.	.	.	.
	31-3, 40	P	F	.	.	R	.	.	.	.	.	.	.	.	.	.	.	.	.	.	.	.	.	.	.
	31-3, 41	P	.	R	R	.	.	.	.	.	.	.	.	.	.	.	.	.	.	.	.	.	.	.	.
	31-3, 80		.	.	.	.	.	.	.	.	.	.	.	.	.	.	.	.	.	.	.	.	.	.	.
	31-3, 140		.	.	.	.	.	.	.	.	.	.	.	.	.	.	.	.	.	.	.	.	.	.	.
	31-4, 40		.	.	.	.	.	.	.	.	.	.	.	.	.	.	.	.	.	.	.	.	.	.	.
	31-4, 60	P	F	.	.	.	.	.	.	.	.	.	.	.	.	.	.	.	.	.	.	.	.	.	.
	31-4, 80	P	.	.	.	.	.	.	.	.	.	.	.	.	.	.	.	.	.	.	.	.	.	.	.
	31-4, 120		.	.	.	.	.	.	.	.	.	.	.	.	.	.	.	.	.	.	.	.	.	.	.
	31-5, 10		.	.	.	.	.	.	.	.	.	.	.	.	.	.	.	.	.	.	.	.	.	.	.
	31-5, 50		.	.	.	.	.	.	.	.	.	.	.	.	.	.	.	.	.	.	.	.	.	.	.
	31-5, 80		.	.	.	.	.	.	.	.	.	.	.	.	.	.	.	.	.	.	.	.	.	.	.
	31-5, 135		.	.	.	.	.	.	.	.	.	.	.	.	.	.	.	.	.	.	.	.	.	.	.
	31-5, 141		.	.	.	.	.	.	.	.	.	.	.	.	.	.	.	.	.	.	.	.	.	.	.
	31-CC	G	R	.	.	.	.	.	.	.	.	.	.	.	.	.	.	.	.	.	.	.	.	.	.
Tithonian	32-1, 136	M	.	.	.	.	.	.	.	.	.	.	.	.	.	.	.	.	.	.	.	.	.	.	.
	32-1, 140	VP	.	.	.	.	.	.	.	.	.	.	.	.	.	.	.	.	.	.	.	.	.	.	.
	32-2, 10	P	.	.	.	.	.	.	.	.	.	.	.	.	.	.	.	.	.	.	.	.	.	.	.
	32-2, 40	VP	.	.	.	.	.	.	.	.	.	.	.	.	.	.	.	.	.	.	.	.	.	.	.
	32-2, 64		.	.	.	.	.	.	.	.	.	.	.	.	.	.	.	.	.	.	.	.	.	.	.
	32-2, 69		.	.	.	.	.	.	.	.	.	.	.	.	.	.	.	.	.	.	.	.	.	.	.
	32-2, 70	P	.	.	.	.	.	.	.	.	.	.	.	.	.	.	.	.	.	.	.	.	.	.	.
	32-2, 100	P	.	.	.	.	.	.	.	.	.	.	.	.	.	.	.	.	.	.	.	.	.	.	.
	32-2, 140	P	.	.	.	.	.	.	.	.	.	.	.	.	.	.	.	.	.	.	.	.	.	.	.
	32-3, 10	P	.	.	.	.	.	.	.	.	.	.	.	.	.	.	.	.	.	.	.	.	.	.	.
	32-3, 40	P	.	.	.	.	.	.	.	.	.	.	.	.	.	.	.	.	.	.	.	.	.	.	.
	32-3, 70	P	.	.	.	.	.	.	.	.	.	.	.	.	.	.	.	.	.	.	.	.	.	.	.
	32-3, 120	P	.	.	.	.	.	.	.	.	.	.	.	.	.	.	.	.	.	.	.	.	.	.	.
	32-3, 146	P	.	.	.	.	.	.	.	.	.	.	.	.	.	.	.	.	.	.	.	.	.	.	.

Table 5 (continued).

Age	Sample	Preservation	*Watznaueria* sp. indet.	*Biscutum dubium*	*Biscutum erismatum*	*Vagalapilla stradneri*	*Watznaueria barnesae*	*Watznaueria britannica*	*Watznaueria fossacincta*	*Watznaueria manivitae*	*Zeugrhabdotus* sp. 1	Podorhabdid indet.	Retecapsid indet.	*Cretarhabdus conicus*	*Cyclagelosphaera margerelii*	*Zeugrhabdotus erectus*	*Axopodorhabdus cylindratus*	*Biscutum ellipticum*	*Ethmorhabdus gallicus*	*Stephanolithion bigotii*	*Conusphaera mexicana minor*	*Zeugrhabdotus cooperi*	*Pickelhaube furtiva*	*Zeugrhabdotus embergeri*	*Cyclagelosphaera argoensis*	*Lithraphidites carniolensis*	*Microstaurus chiastius*
Tithonian	32-4, 01	P	.	.	.	.	R	F	.	A	.	.	R	.	.	.	.	.	.	.	.	.	.	.	.	.	.
	32-4, 20	VP	.	.	.	.	.	.	.	F	.	.	.	.	.	.	.	.	.	.	.	.	.	.	.	.	.
	32-4, 50	P	.	.	.	.	R	C	R	A	.	.	.	.	.	.	.	.	.	.	.	.	.	.	.	.	.
	32-4, 80	P	.	.	.	.	R	R	R	C	.	.	.	.	.	.	.	.	.	.	R	.	.	.	.	.	.
	32-4, 100	P	.	.	.	.	C	A	.	C	.	.	F	.	.	.	.	.	.	.	.	.	R	.	.	.	.
	32-4, 140	P	.	.	.	.	F	F	F	A	.	.	.	.	.	.	.	.	.	.	.	.	.	.	.	.	.
	32-CC	M	.	.	.	.	C	C	C	C	.	.	R	.	F	.	.	.	.	.	R	.	.	.	.	.	.
	33-1, 01	G	.	.	R	R	C	C	C	R	R	R	R	.	R	R	.	R	?	.	R	.	.	.	.	.	.
	33-1, 05	G	.	.	R	R	A	C	C	C	F	F	R	.	R	R	.	.	?	.	.	R	.	.	.	.	.
l. Kimm.–e. Tith.	33-1, 10	G	.	.	R	R	A	C	C	C	R	F	F	R	R	F	?	.	.	R	R	.	.	.	.	.	.
	33-1, 15	G	.	R	R	R	A	A	C	C	C	F	C	R	F	F	?	R	?	R	.	.	.	.	.	.	.
	33-1, 19	G	.	.	R	.	A	C	C	C	F	F	R	R	R	R	.	.	.	.	.	.	.	.	.	.	.
	33-1, 25	M	.	R	R	R	C	C	F	F	R	R	R	.	.	.	.	.	.	.	.	.	.	.	.	.	.
	33-1, 59	P	F	.	.	.	.	.	.	.	.	.	.	.	.	.	.	.	.	.	.	.	.	.	.	.	.

Tithonian (Sections 27-261-33-1, 5 cm, to -31-3, 41 cm)

The base of this interval is defined by the highest occurrence of *Stephanolithion bigotii*, which indicates an early Tithonian age. The top is marked by the lowest occurrence of *Cruciellipsis cuvillieri*. The nannofossil taxon most useful for defining the Jurassic/Cretaceous boundary, *Nannoconus*, is not present in the 261 section due to provincialism (see below). Determination of the exact position of the Jurassic/Cretaceous boundary was further impeded by poor preservation and barren intervals in this part of the section. The species *C. cuvillieri* has a first occurrence in the latest Tithonian (Bralower et al., 1989) and is used here to approximate the Jurassic/Cretaceous boundary.

The lower part of this interval (27-261-32-4, 140 cm, to -32-3, 10 cm) is characterized by the numerical dominance of large specimens (about 20 μm) of *Watznaueria manivitae*. The abundance of this species is indicative of a Tithonian age, with numbers declining sharply toward the top of the stage. The decline in abundance of *W. manivitae* (and also *W. britannica* and *W. barnesae*) followed by a distinct increase in the abundance of *W. fossacincta*, indicates the proximity of the Jurassic/Cretaceous boundary (Cooper, 1985). Sample 27-261-32-2, 10 cm, includes the first occurrence of a new coccolith species, *Cyclagelosphaera argoensis*, which ranges up into the Valanginian at Site 261. The occurrence of *Conusphaera mexicana minor* (last occurrence, late Tithonian) in the lower part of this interval indicates a Tithonian age. This interval also includes the first occurrences of *Microstaurus chiastius, Lithraphidites carniolensis, Pickelhaube furtiva, Zeugrhabdotus embergeri*, and *Ethmorhabdus hauterivianus*, all of which have first occurrences in the Latest Jurassic (Bralower et al., 1989).

These assemblages generally are poorly preserved and display considerable etching and consequent low diversities, but retain components that indicate a Tithonian age. In the Tethyan area, this time period is characterized by an evolutionary radiation event that included the appearance and diversification of the nannoconid group (Bown et al., in press). This radiation coincided with the first consistent occurrence of nannofossil-generated pelagic carbonates (Roth, 1986; Bown and Ozcan, in press). Many of the features of the Tethyan radiation were not recorded during this interval at Site 261, indicating the strong biogeographic distinctions evident at this time. Although preservation is poor this does not explain the absence of solution resistant Tethyan taxa, such as *Nannoconus* and *C. mexicana mexicana*.

Berriasian (Sections 27-261-31-3, 40 cm, to -30-2, 130 cm)

This interval ranges from the lowest occurrence of *Cruciellipsis cuvillieri*, used here to approximate the Jurassic/Cretaceous boundary, to the lowest occurrence of *Tubodiscus verenae*, which has a first occurrence at the base of the Valanginian. The Early Cretaceous age of this interval is indicated by the dominance of *W. fossacincta* along with the occurrence of typically Cretaceous taxa, such as *Ethmorhabdus hauterivianus, Cruciellipsis cuvillieri, Manivitella pemmatoidea*, and *Haqius ellipticus*. The first occurrence of *Crucibiscutum salebrosum* in Sample 27-261-31-2, 129 cm, and *Rhagodiscus nebulosus* in Sample 27-261-30-3, 140 cm, confirms a definite (possibly late) Berriasian age (Jakubowski, 1987; Bralower et al., 1989) for the upper part of this interval. The *Sollasites*-type morphology of the *Crucibiscutum salebrosum* specimens from Samples 27-261-31-2, 129 cm, to 27-261-30-2, 60 cm, is identical to those observed in the lower part of the Valanginian interval at Site 765.

Valanginian (Sections 27-261-30-2, 60 cm, to -28-2, 128 cm)

This interval is defined by the first and last occurrence of *Tubodiscus verenae*, which has a restricted range in the Valanginian (Bralower, 1987; Bralower et al., 1989). The occurrence of *Tegumentum striatum* in Sample 27-261-28-2, 128 cm, is indicative of a Valanginian to Early Hauterivian age (Crux, 1989; Mutterlose, this volume).

Most assemblages in the lower part of this interval are moderately to poorly preserved and of low diversity, compared to coeval intervals in the Tethyan and Boreal areas. A more diverse and well-preserved Valanginian assemblage can be seen in Sample 27-261-28-2, 128 cm. The occurrence of *Vagalapilla matalosa* in this interval is by far the earliest record of this species; it had previously been reported as occurring first in the late Barremian (Applegate and Bergen, 1988; Crux, 1989).

Table 5 (continued).

Age	Sample	Preservation	Calcisphere sp. indet.	*Ethmorhabdus hauterivianus*	*Watznaueria biporta*	*Cruciellipsis cuvillieri*	*Microstaurus quadratus*	*Crucibiscutum salebrosum*	*Manivitella pemmatoidea*	*Haqius ellipticus*	*Rhagodiscus nebulosus*	*Diazomatolithus lehmanii*	*Tubodiscus verenae*	*Haqius circumradiatus*	*Assipetra infracretacea*	*Axopodorhabdus dietzmannii*	*Grantarhabdus coronadventis*	*Retecapsa angustiforata*	*Retecapsa crenulata*	*Retecapsa surirella*	*Rotelapillus laffittei*	*Speetonia colligata*	*Tegumentum striatum*	*Vagalapilla matalosa*	*Vagalapilla* sp.
Tithonian	32-4, 01	P	.	.	.	.	.	.	.	.	.	.	.	.	.	.	.	.	.	.	.	.	.	.	.
	32-4, 20	VP	.	.	.	.	.	.	.	.	.	.	.	.	.	.	.	.	.	.	.	.	.	.	.
	32-4, 50	P	.	.	.	.	.	.	.	.	.	.	.	.	.	.	.	.	.	.	.	.	.	.	.
	32-4, 80	P	.	.	.	.	.	.	.	.	.	.	.	.	.	.	.	.	.	.	.	.	.	.	.
	32-4, 100	P	.	.	.	.	.	.	.	.	.	.	.	.	.	.	.	.	.	.	.	.	.	.	.
	32-4, 140	P	.	.	.	.	.	.	.	.	.	.	.	.	.	.	.	.	.	.	.	.	.	.	.
	32-CC	M	.	.	.	.	.	.	.	.	.	.	.	.	.	.	.	.	.	.	.	.	.	.	.
	33-1, 01	G	.	.	.	.	.	.	.	.	.	.	.	.	.	.	.	.	.	.	.	.	.	.	.
	33-1, 05	G	.	.	.	.	.	.	.	.	.	.	.	.	.	.	.	.	.	.	.	.	.	.	.
l. Kimm. e. Tith.	33-1, 10	G	.	.	.	.	.	.	.	.	.	.	.	.	.	.	.	.	.	.	.	.	.	.	.
	33-1, 15	G	.	.	.	.	.	.	.	.	.	.	.	.	.	.	.	.	.	.	.	.	.	.	.
	33-1, 19	G	.	.	.	.	.	.	.	.	.	.	.	.	.	.	.	.	.	.	.	.	.	.	.
	33-1, 25	M	.	.	.	.	.	.	.	.	.	.	.	.	.	.	.	.	.	.	.	.	.	.	.
	33-1, 59	P	.	.	.	.	.	.	.	.	.	.	.	.	.	.	.	.	.	.	.	.	.	.	.

Upper Valanginian to Hauterivian (Sections 27-261-28-2, 121 cm, to -27-2, 57 cm)

This interval ranges from the highest occurrence of *Tubodiscus verenae* to the upper part of Core 27-261-27, where the last productive nannofossil sample was found. The last occurrence of *T. verenae* indicates a late Valanginian age. The continued presence of *Cruciellipsis cuvillieri* infers an age no younger than Late Hauterivian (Bralower, 1987).

Paleoenvironmental and Paleobiogeographic Implications

Nannoplankton distribution in the present-day oceans is known to be controlled by a number of major factors, the most important being light intensity, temperature, water depth, nutrient concentration, and salinity (Tappan, 1980). Provincialism in the fossil record has long been recognized and is particularly well-developed in the Upper Jurassic to Lower Cretaceous interval (e.g., Applegate et al., 1989; Cooper, 1989; Crux, 1989; and Mutterlose, 1989). At this time, nannoplankton distribution defined a discrete northern, mid- to high-latitude Boreal Realm, a low-latitude Tethyan Realm, and a less well-documented southern, mid- to high-latitude Austral Realm (Cooper, 1989; Crux, 1989; Wise, 1988). These biogeographic realms are defined by endemic species distributions, differing stratigraphic ranges, and contrasting assemblage compositions. The cause(s) of these biogeographic delimitations in the Jurassic and Cretaceous is problematic. The Mesozoic Earth appears to have been ice-free, global temperature gradients were low, climate was equable, and atmospheric and oceanic circulation was sluggish. It is against this background of global equability and high "greenhouse"-induced temperatures that the Boreal and Tethyan biogeographic floral and faunal provinces are set. Nannofossil distributions are explained in terms of temperature (Mutterlose, 1989), transgression/regression (Crux, 1989), physical barriers (Applegate et al., 1989), water depth (Applegate et al., 1989), and nutrients (Roth and Krumbach, 1986). A number of these explanations can be tested using the nannofossil data recovered from Sites 261 and 765, which are located far from the European/North Atlantic region where most of the data for this interval have been gathered.

Sites 261 and 765 occupied a position on the Argo Abyssal Plain at about 35°S during the Late Jurassic-Early Cretaceous (Ogg et al., this volume), which places them at the probable southern limit of the low-latitude Tethyan Realm and within the influence of the southern high-latitude Austral Realm. The sites were separated from the European-proto North Atlantic area at this time by the large Neotethys Ocean.

Most of the nannofossil assemblages recovered from the Upper Jurassic–Lower Cretaceous sequences of the Argo Abyssal Plain differ in varying degrees from coeval assemblages in the Boreal and Tethyan areas. The assemblages display features characteristic of both the Tethyan Realm (e.g., the presence of *Tubodiscus verenae*) and the Boreal Realm (e.g., the abundance of *Crucibiscutum salebrosum*), along with endemic attributes not observed elsewhere. The most striking contrast is the complete lack of nannoconids, which dominated Tethyan assemblages and progressively infiltrated Boreal assemblages from the late Tithonian to the mid-Cretaceous.

Boreal affinities are indicated by the following:

1. The absence of *Nannoconus* and *Conusphaera mexicana mexicana* in the Tithonian.
2. The absence of *Calcicalathina oblongata, Nannoconus,* and other Tethyan taxa in the Berriasian-Hauterivian.
3. The presence of *Crucibiscutum salebrosum* in the Berriasian-Hauterivian.

Tethyan affinities are shown by the following:

1. The presence of *Watznaueria manivitae* in the Tithonian.
2. The presence of *Cruciellipsis cuvillieri, Eiffellithus windii, Rhagodiscus nebulosus, Speetonia colligata,* and *Tubodiscus verenae* in the Berriasian to Valanginian.

Nannofloral features that are unique to these sites include:

1. Assemblages dominated by *W. manivitae* in the Tithonian.

2. High abundances of *Zeugrhabdotus cooperi* in the Tithonian.

3. The presence of *Cyclagelosphaera argoensis* in the Tithonian to Valanginian.

4. The rarity of *Rhagodiscus asper* and *Diazomatolithus lehmanii*.

5. The presence of *Vagalapilla matalosa* and *Repagulum parvidentatum* in the Valanginian and Hauterivian.

The mixed nature of the nannofloras suggests that the area was transitional between the low latitude (Tethyan) and high latitude (?Austral) provinces, allowing for the coexistence of certain taxa from both areas, perhaps at the limit of their ecological tolerance. There is also complete ecological exclusion of certain Tethyan forms, most notably *Nannoconus*. The calpionellid microplankton group, which has a comparable distribution to *Nannoconus* at this time, is also absent from the Argo sites. The exclusion of *Nannoconus* from this area cannot be satisfactorily explained by water depth, as *Nannoconus* is found at deep water sites in the Atlantic Ocean (e.g., Bralower et al., 1989). In addition, all of the Lower Cretaceous carbonate on the Argo Abyssal Plain has slope or shelf provenance. Most likely, the distribution of *Nannoconus* was controlled by latitudinal temperature differences (see also Mutterlose, 1989). Lower temperatures and a lack of warm ocean currents from the subtropical-tropical Tethyan Realm prevented *Nannoconus* (and other Tethyan species) from living in this area. Certain Tethyan species appear to have been more tolerant of cooler temperatures, e.g., *C. cuvillieri, S. colligata, T. verenae,* and were able to survive at higher latitudes. Positive evidence of cooler temperatures is demonstrated by the presence of abundant *C. salebrosum,* which had a bipolar distribution at this time (Mutterlose, this volume). Tethyan influence (via ocean currents and transgressions), as seen in the North Sea through the Lower Cretaceous (Crux, 1989), was not observed to the same extent in the Argo sites. The absence of certain Boreal taxa, e.g., *Sollasites arcuatus, Micrantholithus speetonensis,* and *Tegulalithus septentrionalis,* suggests that these forms were restricted to the northern high latitude province. The nannofloral features unique to these sites may represent southern temperate biogeographic characters, which typified the Austral Realm at this time.

While the results here have been interpreted in terms of wider biogeographic distribution patterns, these cannot be confirmed until sufficient data are available from other Austral regions.

In addition to control exerted by latitudinal temperature variations, evidence also exists to suggest the influence of water depth. Applegate et al. (1989), described abyssal assemblages from the North Atlantic that included continental shelf/slope taxa found commonly only in redeposited horizons, i.e., turbidites. These shelf indicators included *Lithraphidites carniolensis, Micrantholithus,* and *Pickelhaube furtiva*. These observations are confirmed in the sections described here, as both *L. carniolensis* and *P. furtiva* are found in sediments interpreted as turbidites with continental margin provenance. These taxa may be restricted to areas having higher nutrient conditions, such as nearshore environments.

MICROFOSSIL CORRELATION

Detailed nannofossil biostratigraphy was performed on the lower cores of Sites 765 and 261. Age determinations and the correlation presented below therefore differ from those originally presented in Ludden, Gradstein, et al. (1990), and Proto Decima (1974). Other microfossil data from the lower cores of Site 261, originally described in Veevers, Heirtzler, et al. (1974), have been reinterpreted. The biostratigraphic information for the upper cores of Site 765 was taken from Ludden, Gradstein, et al. (1990). These data have been incorporated into Figures 2, 10, and 24.

Calcareous Nannofossils

The assemblages observed in the basal 25 cm of Site 261 contain the distinctive Jurassic index species, *Stephanolithion bigotii,* and are not comparable with any seen in Site 765. These assemblages indicate a Kimmeridgian-early Tithonian age.

Above the *S. bigotii* interval at Site 261, nannofossil assemblages are characterized by high abundances of large *Watznaueria manivitae* coccoliths along with other taxa that indicate a Tithonian age. This distinctive nannofloral feature also was observed in the lowest nanno-fossil-bearing sediments at Site 765 (123-765C-62R, 13 cm, to -61R-3, 3 cm). These Tithonian intervals correlate well.

The intervals from 123-765C-58R-2, 10 cm, to -56R-3, 142 cm, at Site 765 and 27-261-31-3, 40 cm, to -27-2, 57 cm, at Site 261 have been dated as Berriasian to Hauterivian and contain comparable nannofossil assemblages, including the Lower Cretaceous marker species, *Cruciellipsis cuvillieri, Crucibiscutum salebrosum,* and *Tubodiscus verenae*.

The remaining Mesozoic cores at Site 261 are barren of nannofossils. The upper Cores 27-261-4 to -1 contain Miocene, Pliocene, and Quaternary nannofossils (Proto Decima, 1974). A relatively complete nannoplankton succession from Late Cretaceous through Holocene is present at Site 765, with the nannofossils occurring in redeposited calcareous sediments (Ludden, Gradstein, et al. 1990).

Palynology

Palynological data from Site 261 is limited to an interval in the Lower Cretaceous (Wiseman and Williams, 1974) and isolated references to Upper Jurassic dinoflagellates from Core 27-261-32 in bio-stratigraphic discussions (Veevers, Heirtzler, et al., 1974, pp. 136, 139, 683). Dinoflagellates from Cores 27-261-14 to -21 indicate an Aptian age (*O. operculata* Zone), and from Cores 27-261-22 to -26 indicate a Barremian age (*M. australis* Zone) (Wiseman and Williams, 1974; Helby et al., 1987; A. McMinn, pers. comm., 1988). Both these Lower Cretaceous dinoflagellate zones are also present at Site 765 within similar thicknesses of sediments (Sections 123-765C-40R-4, 140 cm, to -54-CC) (Ludden, Gradstein, et al., 1990; Helby and McMinn, this volume).

The oldest dinocyst assemblages from Site 765 were found in Sections 765C-59R-4 and -59R-5, and dated as Berriasian, lower *Batioladinium reticulatum* Zone (Helby and McMinn, this volume).

Benthic Foraminifers

At Site 261, Cores 27-261-29 to -35 yield diverse and abundant assemblages of calcareous and agglutinated benthic foraminifers, which were interpreted as being a mixture of Upper Jurassic and Lower Cretaceous taxa (Kutznetsova, 1974). Similar assemblages were also found in the basal cores at Site 765 and are taken as *in-situ* taxa of Late Jurassic and Early Cretaceous age (Kaminski, Gradstein, et al., this volume). Many taxa were found to have stratigraphic ranges quite different from published data, and thus biostratigraphic dating was problematic (Kaminski, Gradstein, et al., this volume).

At Site 261, benthic foraminifers indicate a Turonian age for Cores 27-261-7 and -8, and a Coniacian-lower Campanian age for Cores 27-261-5 and -6 (M. Kaminski, pers. comm., 1988).

Radiolarians

The radiolarian biostratigraphy for Sites 261 and 765 is presented in Baumgartner (this volume). Biostratigraphic dating

proved difficult due to the paucity or absence of (Tethyan) species used in published zonations.

The lowest radiolarian assemblage recovered from Site 765 is from Sample 123-765C-62R-1, 53–56 cm, and includes the species *Sethocapsa cetia* and *Holocryptocanium barbui*. This was dated as late Berriasian–early Valanginian in Ludden, Gradstein, et al. (1990) and was used to constrain the age of basement. However, this radiolarian assemblage correlates with Zone D of Baumgartner (1984), which ranges from late Tithonian to earliest Valanginian in the Mediterranean-Tethys region. The co-occurrence of this radiolarian assemblage with *Watznaueria manivitae*-dominated nannofossil assemblages dated as Tithonian thus is not incompatible and may indicate the sample is of late Tithonian age.

CORRELATION OF SITES 765 AND 261

Sedimentary successions at Sites 765 and 261 are correlated on the basis of age and lithology (Fig. 24). The lower sequence at both sites (Cores 123-765C-62R through -34R and 27-261-33 through -10) consists of Upper Jurassic–Lower Cretaceous sediments subdivided into four lithologic units (L1–L4). Upper Cretaceous–Cenozoic sediment makes up the upper sequence at both sites (Cores 123-765C-33R through 1R, 123-765B-41X through -1H, and 27-261-9 through -1) and is subdivided into three lithologic units (U1–U3). Equivalent lower sequence units at both sites are of roughly equal thickness, but upper sequence units are more than three times thicker at Site 765.

Similarities in lithologic patterns at the two sites reflect regional factors, such as paleoceanographic conditions, changes in sea level and sediment supply, and tectonic evolution of the Australian margin. Dissimilarities are mainly attributable to the greater proximity of Site 765 to the continental margin and to concomitant differences in the position of the CCD and in the nature and amount of material eroded from the margin and redeposited on the abyssal plain at the two sites. Lithologies at Sites 765 and 261 differ most dramatically at the contact with igneous basement. Sediment at Site 261 (filling cracks in the basalt and directly overlying the highest basalt) is calcareous, whereas the basal 150 cm at Site 765, directly in contact with the basalt, is noncalcareous. The other major difference between the sites is the greater amount of redeposited calcareous sediment at Site 765, most notably in the Upper Cretaceous and younger section.

Lower Sequence

Silty Claystone (Site 765) and Limestone and Marl (Site 261)

Basal units at Sites 765 and 261 are dissimilar in many respects, but may be stratigraphically equivalent: they occur between volcanic basement and overlying sediments that correlate well, both lithologically and biostratigraphically. The basal (L1) unit at Site 261 is limestone and marl; it contains distinctive nannofossil assemblages that indicate a Kimmeridgian-early Tithonian age. Unit L1 at Site 765 is silty claystone and includes no fossils that provide definitive age control or constraints on the rate of sedimentation.

Major differences between the two basal units include disparities in calcareous and detrital contents and in apparent rates of sedimentation. L1 sediments at Site 261 contain abundant nannofossils and lesser calcispheres and other calcareous biotics, whereas the silty claystone at Site 765 includes virtually no primary calcareous material. Site 765 sediments contain more abundant coarse detritus (mainly quartz and volcanic lithic clasts) than is found at Site 261. Unit L1 at Site 765 is five times thicker than L1 at Site 261 and contains evidence of slow (perhaps discontinuous) sedimentation, such as manganese nodules and manganese-coated detrital grains, that is not seen at Site 261. Sediments at both sites are reddish-brown and accumulated in an oxidizing depositional environment.

Differences in carbonate content of the basal sediments at the two sites most likely reflect Site 765's greater proximity to the Australian margin. The CCD shallows as it approaches the continental margin; for example, in the northeastern Indian Ocean, the present-day level is more than 5000 m deep 500 km offshore, but decreases to less than 3500 m along the margin (Berger and Winterer, 1974). The position of the CCD in world oceans during the Late Jurassic is poorly constrained, but appears to have been relatively shallow. A level of about 3500 m has been proposed for the Atlantic Ocean during the Tithonian (Jansa et al., 1979), and a level of less than 3000 m has been inferred for this time period in the equatorial Pacific (Lancelot, Larson, et al., 1990). Estimates of the CCD in the Indian Ocean during the Late Jurassic, based solely on data from Site 261, are 3400 to 3800 km (van Andel, 1975; Sclater et al., 1977). Given a relatively high global CCD, and the shallowing of the CCD toward the continental margin, sediments at Site 261, 250 km west of the nearest margin, could have accumulated above the CCD, while coeval sediments at Site 765, less than 75 km from the margin, accumulated below it.

Other differences between the basal units also reflect the position of the sites relative to the continental margin and the CCD, and possible differences in the age of volcanic basement. The greater abundance of silt- and sand-sized detritus at Site 765 is explained by the closer continental margin and less dilution by background sediment (clay only at Site 765 vs. a considerable percentage of more rapidly accumulating pelagic carbonate at Site 261). It is arguable that proximity to the margin also contributed to the greater thickness of the basal sediments at Site 765, but other factors may have been more important. Magnetic anomaly data suggest that oceanic crust (and thus basal sediments) at Site 765 should be older than those at Site 261 (Fullerton et al., 1989; Sager et al., this volume). No conclusive biostratigraphic or radiometric evidence to prove this contention was obtained at Site 765 (Kaminski, Baumgartner, et al., this volume; Ludden, this volume). However, the sediments immediately above Unit L1 at both sites are dated as Tithonian, contain distinctive nannofloral assemblages dominated by *W. manivitae*, and appear to correlate well. The greater thickness of sediment underlying these correlated intervals at Site 765 (silty claystone) may be interpreted as follows: (1) Cores 123-765C-61R and -62R are Tithonian (i.e. equivalent to or slightly younger than the basal core of Site 261), but more corrosive dissolution has removed the nannofloral evidence, i.e., *W. manivitae;* or (2) Cores 123-765C-61R and -62R correspond, at least in part, to the *S. bigotii* interval at Site 261, dated as Kimmeridgian/early Tithonian, and may be older, based on the greater thickness of sediment and the low sedimentation rate. We favor the second hypothesis. Our interpretation of a low sedimentation rate at Site 765 is based on lithologic evidence such as the presence of manganese nodules, rather than interpolation from sedimentation rate curves, which are unreliable for this interval due to a lack of any well constrained micropaleontological data.

Inoceramid Sediment (Site 765) and Nannofossil Claystone (Site 261)

Unit L2 at Site 765, inoceramid sediment, is correlated with Unit L2 at Site 261, nannofossil claystone, on biostratigraphic and lith-ologic grounds. Both units contain distinctive nannofossil assemblages characterized by abundant *Watznaueria manivitae* and are dated as Tithonian. The units also have numerous lithologic similarities. Both exhibit features indicative of slow, discontinuous sedimentation, such as manganese nodules and winnowed concentrations of calcareous grains, and contain inoceramid prisms riddled with pits (possible fungal microborings). Sediments at

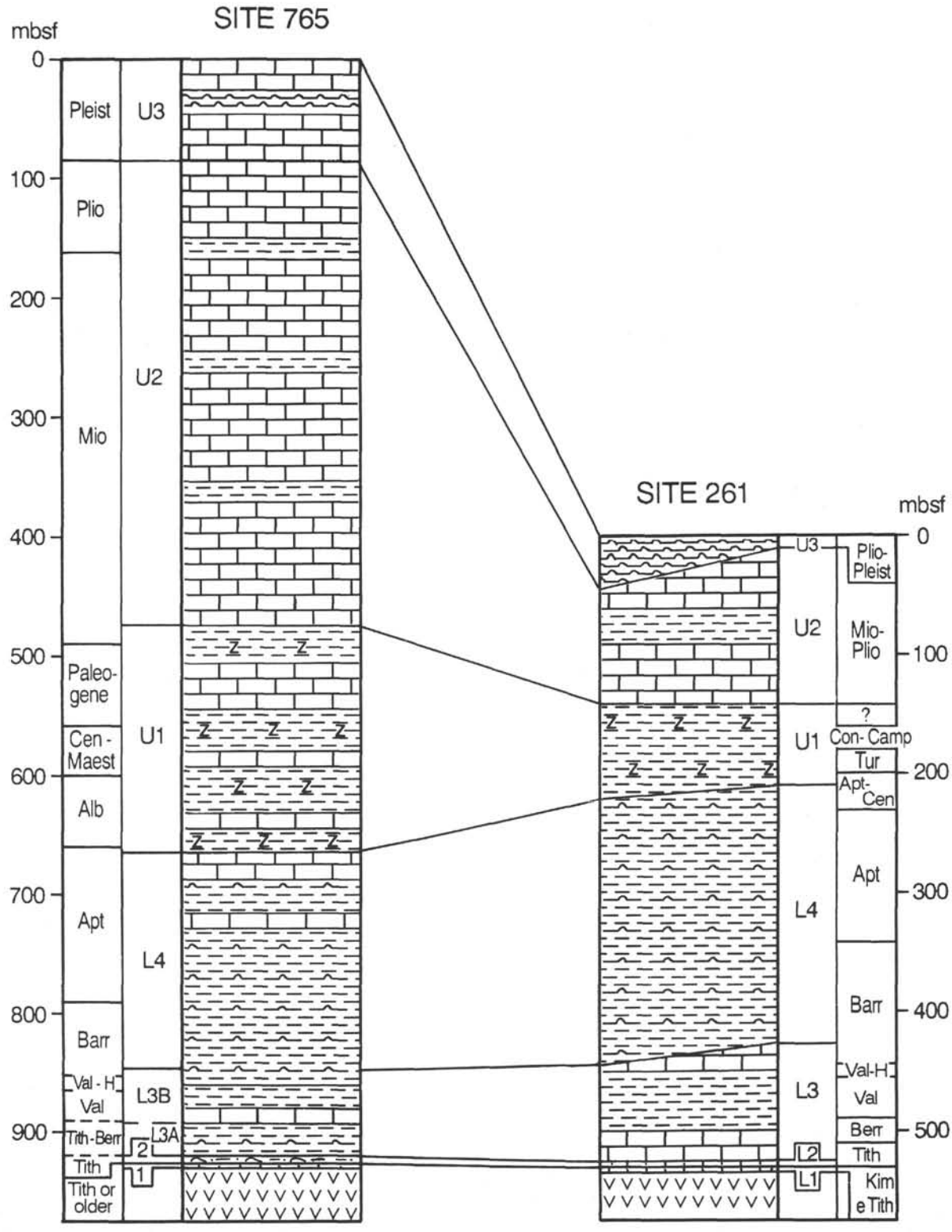

Figure 24. Lithostratigraphic and biostratigraphic correlation of Sites 765 and 261. Lithologic symbols same as in Figure 2.

both sites are reddish-brown, denoting accumulation in an oxic environment, and include relatively abundant, but strongly etched, calcareous grains, indicating deposition below the lysocline but above the CCD. Last, layers rich in calcisphere debris (calcite needles) that have an identical and distinctive microtexture of cemented clasts in a less-cemented matrix occur at both sites (intervals 123-765C-61R-5, 54-62 cm, and 27-261-31-2, 40-74 cm).

Differences between the L2 units include the size and condition of the calcareous material. There are many more sand- and

coarse silt-sized grains (whole mollusk shells, shell fragments, inoceramid prisms, and whole calcispheres) at Site 765, whereas nannofossils are the dominant calcareous grain at Site 261. Obvious volcanic detritus, such as volcanic lithic clasts and glassy fragments, is also more abundant at Site 765. These disparities reflect Site 765's position nearer the continental margin. Although the relative abundance and pervasive distribution of calcareous grains at both sites indicate sedimentation took place above the CCD, nannofossils are more numerous, diverse, and better preserved at Site 261. This suggests Unit L2 sediments were deposited farther above the CCD at Site 261 than at Site 765, as was the case during deposition of the underlying (L1) sediments.

Calcareous Sediment and Noncalcareous Claystone (Sites 765 and 261)

The L3 units at both sites correlate well paleontologically and lithologically. L3 sediments at Site 765 are Tithonian?-Barremian, and at Site 261 are Tithonian-Barremian. Calcareous turbidites, which also contain considerable clay and siliceous biogenic material, characterize the L3 units and are intercalated with noncalcareous background sediment at both sites. The turbidites consist mainly of smectite and nannofossils; silt and sand grains include radiolarians, calcispheres, inoceramid prisms, calcareous and agglutinated foraminifers, quartz, glauconite, and claystone clasts. Calcispheres in these sediments show a wide variety of test types (wall thickness and texture) in contrast to the more homogeneous forms found in the underlying unit. Some, but not all, inoceramid prisms are pitted (bored?). Analyses indicate the same range of carbonate (7%–42%) in the turbidites at Sites 765 and 261. Sediment intercalated between the turbidites is reddish-brown smectite claystone and includes thin layers of radiolarite and bentonite.

Differences between the L3 units at the two sites include a thicker overall section of calcareous turbidites at Site 261, but some thicker and coarser grained individual turbidites at Site 765. Calcareous turbidites occur through an interval of about 34 m at Site 765 and overlie a 27-m section that contains only a few turbidites, all of which lack primary calcareous material. Calcareous components may originally have been present in these turbidites, but subsequently were removed by diagenesis. Calcareous turbidites occur throughout unit L3 at Site 261, an interval at least 70 m thick. Discrete graded turbidites 1 to 3 m thick occur at Site 765. Although calcareous layers this thick occur at Site 261, they are not graded throughout and represent a series of thin turbidites amalgamated by bioturbation rather than the deposit of a single event. One-third of the calcareous turbidites at Site 765 contain at least several centimeters of sandstone, and some turbidites include sandstone layers 20 to 100 cm thick; maximum clast size is about 2 mm. At Site 261, turbidites are mostly fine-grained; the coarsest material is silt and fine sand that forms layers 1 cm or less thick.

Similarities between turbidites at the two sites indicate similar sources, while differences reflect the greater proximity of Site 765 to the continental margin. Turbidites at both sites were derived from outer shelf, slope, or rise sediments that accumulated above the CCD, but below the photic zone, and include a volcanic component; however, turbidites are more "proximal" (thicker and coarser grained) at Site 765. We suggest that most Site 765 turbidites were derived from the south (Wombat and northern Exmouth plateaus), possibly via Swan Canyon, whereas thinner, finer grained, but more numerous turbidites reaching Site 261 came from both the south and east (Scott Plateau). Suitable source materials occur along both continental margins. Triassic-Lower Jurassic volcanic rocks make up much of the Wombat Plateau (von Rad and Exon, 1983) and Middle to Upper Jurassic volcanic and volcaniclastic rocks are widely exposed along the Scott Plateau (Hinz et al., 1978; Stagg and Exon, 1981). A condensed interval of nannofossil-calcisphere chalk with radiolarians accumulated on the Wombat Plateau during the Neocomian (Haq, von Rad, et al., 1990) and provides an example of the sort of pelagic carbonate material probably deposited all along the northwest Austral- ian outer shelf and slope at this time and redeposited in these turbidites.

Other differences between L3 sediments at the two localities also relate, though less directly, to Site 765's position closer to the continental margin. Turbidites are more distinct and contain more obvious sedimentary structures (i.e., Bouma sequences) at Site 765, a result both of coarser grain size and less intense bioturbation. Bioturbation is pervasive at Site 261 and has disturbed many contacts between turbidites and background sediment, but is much less evident at Site 765, perhaps at least in part because individual turbidites here are thicker. Site 765 turbidites have mostly sharp contacts and contain discrete burrows only in their uppermost few centimeters. Nannofossil assemblages are better preserved and more diverse in Site 765 turbidites, a result of subtle differences in sediment redeposited at the two sites or, more likely, of greater dissolution of components after deposition in the thinner turbidites at Site 261. Last, although radiolarite and bentonite layers occur at both sites, these margin-derived sediments are thicker and more abundant at Site 765.

Radiolarian Claystone (Sites 765 and 261)

Unit L4 consists of radiolarian claystone which is dated as Barremian-Aptian and is of similar thickness at both sites. Lower cores contain alternating centimeter- to decimeter-thick red and green layers, whereas green and gray shades predominate in the higher cores. The color shift reflects a change from oxic to more reduced depositional and/or diagenetic conditions, at least in part caused by greatly increased sedimentation rates during the Aptian. Elongate dark mottles (probable flattened burrows) are abundant at both sites. L4 microfaunas consist mostly of radiolarians and lesser palynomorphs and arenaceous foraminifers; pollen is notable, particularly in the Aptian, and indicates increased influx from continental sources. Intervals of black claystone that have high organic contents occur in both sections and are broadly correlative (Aptian). These sediments may be a local expression of one or more episodes of reduced oxygen content in world oceans that are thought to have occurred during the mid-Cretaceous (e.g., Jenkyns, 1986). Authigenic manganese carbonate forms micronodules and replaces radiolarians at both sites.

Differences between L4 sediments again are attributable to Site 765's greater proximity to the margin. Radiolarite layers are thicker and more abundant at Site 765. Calcareous turbidites are abundant in the upper part of the unit at Site 765, and noncalcareous sandy turbidites occur infrequently throughout the lower cores. Obvious (sandy and/or calcareous) turbidites were not observed at Site 261, but the high sedimentation rates in the L4 units (Fig. 5) are unlikely for purely pelagic claystones. This suggests that much of the claystone at both sites was redeposited by gravity flows.

Upper Sequence

Zeolitic Claystone (Sites 765 and 261)

Unit U1 consists of zeolitic clay at Site 261 and is of Aptian-Upper Cretaceous age. Similar zeolitic claystone, intercalated with calcareous sediment (mostly turbidites), makes up Unit U1 at Site 765 and is of Albian to Miocene age. The claystones are variegated in color, but are dominantly brown to orange, indicating oxic depositional conditions as a result of slow sedimentation rates. Palygorskite clay, often associated with slow sedimentation, occurs at both sites but is more common at Site 261.

Microfaunas in these claystones are relatively sparse, largely arenaceous foraminifers and minor radiolarians. The zeolite (clinoptilolite) found at both sites denotes very low silica concentrations during diagenesis and reflects the relative paucity of radiolarians in these sediments. Unit U1 is roughly three times as thick at Site 765 as at Site 261. This discrepancy is explained by the occurrence of calcareous turbidites at Site 765 and their absence at Site 261; the amount of claystone at the two sites is roughly equivalent. Unit U1 turbidites include the first significant appearance of notably older reworked biotic components in the Argo Abyssal Plain sequence.

Calcareous Sediment (Sites 765 and 261)

Unit U2 at both sites is Miocene-Pliocene and consists mainly of calcareous sediment redeposited by gravity flows and intercalated with noncalcareous claystone. Calcareous sediments at both sites are chiefly turbidites that are less than 2 m thick, graded, and composed of nannofossil and lesser foraminifer ooze. Thicker (to 42 m) debris flows and complex sequences (thought to have formed during single depositional events) occur at Site 765 and are particularly abundant in the lower Miocene and upper Pliocene sections. At Site 261, a single debris flow deposit (at least 20 cm thick) was recovered. The turbidites in Unit U2 have the highest carbonate contents of any of the units at both sites. Noncalcareous background sediment makes up about 10%–20% of Unit U2 at both sites and is greenish gray in contrast to the brownish colors dominant in underlying Unit U1. This color change most likely reflects the shift to much more rapid sedimentation during the Neogene (Fig. 5).

Differences between the U2 units at the two sites include the three times greater thickness of the section at Site 765 and the presence of older components (i.e., clasts containing Jurassic nannofossils) and exotic clasts (volcanic lithics) at Site 765; no such clasts were observed at Site 261. Both differences reflect Site 765's position closer to the continental margin, from which the redeposited sediments were derived.

Siliceous Ooze (Sites 765 and 261)

Unit U3 is of Quaternary age at Site 765 and Pliocene-Quaternary age at Site 261 and includes siliceous ooze at both sites. At Site 765, the ooze is intercalated with abundant layers of redeposited calcareous sediment; calcareous layers also occur at Site 261, but are thin and rare. The ooze is clayey and greenish gray at both sites and contains glass that probably was derived from the Indonesian volcanic arc to the north. Unit U3 is more than three times as thick at Site 765 as at Site 261.

DISCUSSION

Basal Sediment Age and Implications

The Deep Sea Drilling Project first drilled a site on the Argo Abyssal Plain (Site 261) in 1972 to test the suggestion of Veevers et al. (1971) that this ocean basin was established in pre-Cretaceous time. This notion had been countered by Falvey (1972), who proposed, based on seafloor magnetic anomalies, that the opening of the Argo Abyssal Plain took place no earlier than Late Cretaceous (Santonian). The age of the basal sediments at Site 261, principally determined by calcareous nannofossils, was found to be Late Jurassic (Oxfordian to Tithonian); the older date has been used in paleogeographic and tectonic reconstructions (Veevers, Heirtzler, et al., 1974). This age determination has been the principal tie-point for all subsequent seafloor magnetic anomaly interpretation on the Argo Abyssal Plain and the Gascoyne and Cuvier Abyssal plains to the southwest (e.g., Heirtzler et al., 1978; Larson, 1975; Fullerton et al., 1989). The most recent magnetic anomaly interpretation for the Argo Abyssal Plain (Fullerton et al., 1989; Sager et al., this volume) mapped a complete set of anomalies from M26 to M16, trending N70°E. This suggests that spreading along the northwestern Australian margin began prior to M26 (late Oxfordian) and pre-dated spreading along the margin to the southwest.

In 1988, to obtain a thicker and older sequence of Jurassic sediments, Leg 123 scientists drilled Site 765 between the M25 and M26 anomalies, nearer the continental margin. Dating the basal sediments at Site 765 proved to be problematic, due to inconclusive biostratigraphic, magnetostratigraphic, and radiometric evidence. The age was originally stated as late Berriasian-Valanginian, based on a radiolarian assemblage that was recovered 4.2 m above basement and on the interpretation of a rapid sedimentation rate for the basal sediments (Ludden, Gradstein, et al., 1990). Our reinterpretation of the biostratigraphic and sedimentologic information indicates that the basal sediments were deposited slowly and are of Late Jurassic (Kimmeridgian?–Tithonian) age.

Problems remain in reconciling interpretations of magnetic lineations and the sediment record from the Argo Abyssal Plain. The most recent consideration of the magnetic anomaly data is that of Sager, et al. (this volume). These authors concluded that reversal sequence M26-M16 is still the best model for the lineations and that basement at Site 765 should be Oxfordian; they suggested that the discrepancy between the age of the seafloor indicated by magnetic anomalies and the biostratigraphic age of the oldest sediments overlying basement was due to spotty sedimentation in the young Argo Basin. The modified age determination we propose for the basal sediments at Site 765 reduces this discrepancy and is more compatible with the age determined for the basal sediments at Site 261. Our data support a sequence of tectonic evolution that led to spreading of the Argo Abyssal Plain in the Late Jurassic (late Oxfordian/Kimmeridgian), followed by spreading of the Gascoyne and Cuvier abyssal plains to the southwest in the Early Cretaceous (early Valanginian, M10). The successive opening of these adjacent abyssal plains may be part of the same large-scale tectonic event, with rifting propagating time-transgressively to the west and culminating in the complete breakup of Australia and Greater India.

Depositional History of the Argo Basin

Patterns of sedimentation across the Argo Abyssal Plain have been influenced most strongly by changes in sea level, position of the CCD, and configuration of the adjacent continental margins. The Argo Abyssal Plain has been below the CCD for most of its history, and redeposited sediments emplaced by gravity flows dominate the sedimentary succession. Since its inception in the Late Jurassic, the Argo Basin has been notably sediment-starved. The Australian continent is relatively flat, low-lying, and arid, and has produced little terrigenous detritus (Cook, 1977). An extensive series of marginal basins (the Browse, Canning, and Carnarvon basins and their constituent sub-basins) has flanked northwestern Australia since the Mesozoic and provided a sink for most of the terrigenous material that has been generated. Thus, sediment redeposited on the abyssal plain has come largely from the outer shelf and continental slope and rise of Australia, rather than from the continent itself (Cook, 1977); variations in composition and rates of emplacement of this sediment reflect eustatic fluctuations, as will be discussed below.

Lower Sequence

The basal sediments (Units L1 and L2) were slowly deposited. Sediments are more calcareous but finer grained at Site 261 due to local parameters such as proximity of the margin (Site 261 is more than twice as far from the nearest margin as Site 765). Sediments at both sites are dominantly pelagic, contain a distinc-

tive biotic assemblage of large coccoliths (*W. manivitae*), calcispheres, and inoceramid debris, and accumulated close to or just below the level of the CCD.

The Argo basal sediments, particularly at Site 765, have many similarities with Jurassic condensed sequences described from the Tethyan region (e.g., Jenkyns, 1986). The Tethyan sequences contain closely packed shells (largely ammonites) that are highly corroded and bored, as well as ferromanganese nodules, and columnar sessile foraminiferal colonies. Fe-Mn oxyhydroxides coat shells, fill borings, and form crusts and pavements on sediment surfaces. Sedimentation rates estimated for these sequences (0.5-6.5 m/my) are equivalent to those inferred for the Argo sediments. The Tethyan sediments were deposited in shallower water than prevailed in the Argo Basin (i.e., above the Aragonite Compensation Depth) but in a similar, largely nondepositional setting characterized by current winnowing, carbonate dissolution, and encrustation by Fe-Mn oxyhydroxides.

Carbonate content profiles at the two Argo sites differ as a result of basin geometry (proximity of the margin), but also may reflect global changes in the CCD with time. Sediments at Site 261 decrease, relatively steadily, in carbonate content upward through the basal 5 m and contain essentially no autochthonous carbonate above the base of Core 27-261-31. Carbonate content at Site 765 traces a parabolic curve; it increases above Section 123-765C-62R-3, reaches a maximum in Section 123-765C-62R-1, and then decreases upward, declining to nearly zero above Section 123-765C-61R-3. As discussed previously, volcanic basement (and thus, immediately overlying sediments) at Site 765 may be older than at Site 261, perhaps as old as Oxfordian. Many authors (e.g., Garrison and Fischer, 1969; Winterer and Bosellini, 1981) have proposed a sharp global decline in CCD levels during the Late Jurassic in response to the proliferation of calcareous nannoplankton at that time. The upward increase in carbonate content seen in the basal sediments at Site 765 could reflect such a global shift in position of the CCD.

Thin, current-emplaced deposits (such as reworked bentonites and, perhaps, some calcisphere concentrations) are sparsely distributed through the oldest abyssal plain sediments, but consistent turbidite deposition is not recorded until the latest Tithonian–Berriasian. Calcareous turbidites make up just over half the Argo sediment deposited from that time into the Hauterivian (Unit L3); however, sedimentation rates for this period are still relatively low (7 m/m.y. or less).

Unit L3 turbidites contain a mix of clay and calcareous and siliceous microfossils; the microfossils are pelagic or deep-water benthic forms. Similar composition characterizes most turbidites throughout the Argo sedimentary succession and denotes derivation from the continental rise, slope, or outer shelf, below the photic zone but above the CCD. Minor constituents of the Lower Cretaceous turbidites, such as quartz and pollen, most likely derived from the Australian continent itself, but little evidence exists for important continental input into this part of the basin plain succession. Deposits of the Barrow Delta, which prograded north along the west Australian margin through the Early Cretaceous, have a continental provenance (i.e., Boote and Kirk, 1989). These sediments form thick accumulations in sub-basins of the Carnarvon Basin and also occur on the Exmouth Plateau, although they thin drastically from south to north (Haq, von Rad, et al., 1990). Barrow Group sediments are clay-rich, but the clay is largely kaolinite; clay in the Argo turbidites is dominantly smectite. Thus, most material eroded from the Australian landmass in Early Cretaceous time was trapped in marginal basins and did not reach the abyssal plain.

Lower Cretaceous turbidites in the Argo Basin were generated from multiple sources along the continental margin, not just the Exmouth Plateau to the south. Seismic profiles in Buffler (1990) show Mesozoic sediments of uniform thickness across the abyssal plain onlapping and infilling a basement topography of considerable relief. No evidence exists of south-north thinning away from the Exmouth margin as is seen in the Neogene sequences (discussed below). The lower units at Site 261 are generally as thick or thicker than equivalent units at Site 765; this is explained by deposition at Site 261 of turbidites derived from both south and east basin margins. The eastern margin consists of the Scott Plateau, a high through Jurassic time that began to subside during the Early Cretaceous (Stagg and Exon, 1981). The Plateau could have contributed both smectite and pelagic carbonate to the basin; it contains abundant Jurassic volcanic rocks (Hinz et al., 1978; Stagg and Exon, 1981) and pelagic sediment should have accumulated along its steep basinward slopes.

Accumulation of abundant calcareous turbidites on the Argo Abyssal Plain during the Neocomian appears due to two linked factors: sea level and CCD. Two pronounced eustatic lowstands have been proposed for the latest Berriasian-Valanginian (Haq et al., 1987). Evidence that these global events were felt along the west Australian margin has been presented by Wiseman (1979), who inferred on biostratigraphic grounds an early Neocomian sea-level fall of more than 200 m in the northern Carnarvon Basin.

Lowered sea levels should increase redeposition of pelagic calcareous material. Lowstands correlate with increased generation of siliciclastic turbidites (i.e., Shanmugam and Moiola, 1982), but the reverse has been demonstrated for calciclastic turbidites derived from shallow-water carbonate banks (Droxler and Schlager, 1985). Although the Argo turbidites are calcareous, they consist mostly of pelagic carbonate material, not shallow bank-derived detritus. Lowstands of sea level are associated with depression of the CCD (Kennett, 1982); such depression would place more of the continental slope and rise above the CCD and thus increase the area in which pelagic carbonate ooze could accumulate. Rapidly deposited carbonate ooze is unstable (i.e., Buchbinder et al., 1988). Increased generation of pelagic calcareous turbidites during times of lowered sea level is seen throughout the Argo sedimentary succession (further discussion below).

Volcanogenic input is notable through much of the Argo Abyssal Plain sequence, but is particularly evident in Unit L3. Bentonites occur throughout this interval and are also found in correlative sediments on the Wombat Plateau (Site 761) and eastern Gascoyne Abyssal Plain (Site 766) (Thurow and von Rad, this volume). The greater abundance of bentonite layers at Sites 761, 765, and 766, compared to Site 261, supports notions of a southerly source, such as the Wallaby or northwestern Exmouth plateaus (von Rad et al., 1989) for the original ash. Bentonites at these sites may have had a common volcanic source; however, specific bentonite layers cannot be correlated between the sites (Thurow and von Rad, this volume). The other major volcanic component in Argo sediments is smectite, the dominant clay in both turbidites and background sediment throughout the lower sequence (Units L1 through L4). Smectite may have been derived from the spreading system itself, Lower Cretaceous volcanic features (such as those proposed as sources for the bentonites), and/or older (Triassic–Jurassic) volcanics and volcaniclastics exposed along the northwestern Australian margin (i.e., Wombat and Scott plateaus).

Radiolarians are an important constituent of Unit L3 and L4 sediments, especially at Site 765. They occur in calcareous turbidites and as current-deposited radiolarites that lack a calcareous component; they also occur, much more sparsely, disseminated in the background claystone. Their abundance in Lower Cretaceous sediments reflects the development of favorable oceanographic conditions, such as upwelling along the northwest Australian margin, at this stage in the evolution of the Argo Basin (Baumgartner, this volume).

Unit L4 at both sites is thick and consists predominantly of claystone. Calcareous turbidites are virtually absent from uppermost Hauterivian and younger Cretaceous sediments at Site 261 and are rare through the Barremian and lower Aptian at Site 765. The uppermost (Aptian) part of Unit L4 yields sedimentation rates of about 20 m/m.y., the highest recorded on the Argo Abyssal Plain throughout the Mesozoic. Such rates are atypically high for pelagic sedimentation and suggest turbidity currents or other redeposition processes were important in the generation of this unit. The increased importance of pollen (relative to dinoflagellates) in palynomorph assemblages in these sediments indicates greater input from continental sources (Ludden, Gradstein, et al., 1990). High sedimentation rates are recorded across the eastern Indian Ocean during the Aptian and are interpreted as a response to increased magmatism and tectonism in Australia at this time (Cook, 1977).

Sedimentary structures diagnostic of turbidite deposition are generally lacking in Unit L4 sediments, but this may be a function of the predominantly fine grain size and noncalcareous nature of the redeposited material. Fine-grained marl turbidites in the Lower Cretaceous section would be difficult to recognize without their anomalous carbonate content, which contrasts strongly with the noncalcareous nature of the background sediment. The lack of primary calcareous material in most Unit L4 turbidites suggests a source below the CCD and may also indicate a rise in CCD in the Argo basin during this interval. A sharp rise in CCD during the Barremian has been proposed for the Atlantic Ocean (Jansa et al., 1979).

Calcareous turbidites reappear in the upper (Aptian) part of Unit L4 at Site 765. Resumption of calcareous turbidite deposition may reflect additional fluctuations in sea level and concomitant changes in the CCD (Dumoulin, this volume); several eustatic lowstands have been inferred during the Aptian (Haq et al., 1987). Unlike the Neocomian calcareous turbidites, which occur across the abyssal plain, Aptian calcareous turbidites were not found at Site 261. This appears to indicate that the eastern margin source inferred during the Neocomian no longer existed, or at least no longer provided pelagic carbonate to this part of the basin, and that turbidites generated from the southern margin did not reach past Site 765 to Site 261, as they did during the Neogene (see below).

Upper Sequence

Above Unit L4, a significant shift occurs in sedimentation patterns that coincides with the transition from juvenile to mature ocean described by Veevers and Johnstone (1974), von Rad et al. (1989), and others. This transition involves increased, and more calcareous, sedimentation along the Australian margin, as a result of establishment of "mature" (thermohaline) circulation in the Indian Ocean. This change resulted in increased deposition of calcareous turbidites on the Argo Abyssal Plain, but turbidites are much thicker and more numerous at Site 765. Seismic profiles in Buffler (1990) show a shift in the Upper Cretaceous from sedimentary units deposited uniformly across the abyssal plain to sequences dominated by redeposited sediments that thin strongly from south to north away from the Exmouth Plateau margin. Subsequently, all the upper lithologic units are three to four times as thick at Site 765 as at Site 261, where chiefly distal turbidites were emplaced.

The Upper Cretaceous-Paleogene strata (Unit U1) have low sedimentation rates (0.8–2.0 m/m.y.), indicating a return to starved, largely pelagic, sedimentation. Low sedimentation rates during this time period are a world-wide phenomenon (Ludden, Gradstein, et al., 1990). High global sea levels flooded continental margins, diminished coastal relief, and led to an expanded zone of sediment trapping around continents.

The Neogene to Holocene strata (Units U2 and U3) are characterized by high sedimentation rates (16–26 m/m.y.), reflecting sedimentation dominated by calcareous turbidites and debris flows. This interval of mass flow sedimentation was initiated around 26 m.y. ago and is probably related to sharply declining global sea levels (Haq et al., 1987). Such a large eustatic decrease produced undercutting of the continental margin and downcutting of marginal canyons, such as Swan Canyon just south of Site 765. Downcutting is evident in the abundance of older, reworked fossil components in Neogene turbidites at Site 765; such obviously reworked components were not found in the redeposited sediments of the lower sequence.

Patterns of Neogene sedimentation at both sites fit models that have been proposed for abyssal plain deposits based on studies of modern examples (i.e., Pilkey, 1987). Calcareous turbidites are more abundant in Unit U2 at Site 261 than in any other upper sequence unit at this site and make up the same proportion of the unit as at Site 765 (80%–90%). Overall thickness of Unit U2 at Site 261 is much less, however, and debris flows are much rarer and less spectacular than at the more "proximal" (to the continental margin) Site 765. Turbidites make up 80%-90% of the sediment column on most modern abyssal plains, and plains with major sediment entry points at one end show strong proximal-distal differences in amount and thickness of coarse sediment layers (Pilkey, 1987).

Siliceous ooze forms the background sediment at the top of both sections. The reappearance of abundant siliceous biotics (largely absent from both background and redeposited sediment since the Aptian) reflects the northward movement of the Australian margin into the zone of equatorial high productivity (Cook, 1977).

SUMMARY

Our analysis of available biostratigraphic and sedimentologic data confirms the Late Jurassic (Kimmeridgian–Tithonian) age previously proposed for basal sediments at Site 261 (Veevers, Heirtzler, et al., 1974) and indicates that basal sediments at Site 765 are also Late Jurassic (Kimmeridgian?–Tithonian) in age, not Early Cretaceous (late Berriasian–Valanginian) as stated by Ludden, Gradstein, et al. (1990). Marl that directly overlies basement at Site 261 contains nannofossils of late Kimmeridgian-early Tithonian age and is succeeded by claystone bearing a distinctive nannofossil assemblage of Tithonian age. At Site 765, age-diagnostic microfossils were not obtained from sediment immediately above basement, but Tithonian nannofossils occur 150 cm above the highest basalt. Correlation of these Tithonian horizons, and sedimentologic evidence that the basal sediment at Site 765 accumulated slowly, suggests that this basal sediment is Tithonian or older (?Kimmeridgian) in age and could be older than the basal sediment at Site 261. This reinterpretation is more compatible with seafloor magnetic anomaly data and proposed models of tectonic evolution for the northeast Indian Ocean (e.g. Sager et al., this volume).

Biogeographic interpretation of the nannofossil data suggests that the Argo Basin occupied a position transitional between the Tethyan and Austral nannofloral realms. A cool water regime is suggested by the absence of thermophyllic Tethyan forms, such as *Nannoconus*, and the presence of taxa which display bipolar distribution, such as *Crucibiscutum salebrosum* (see also Baumgartner et al., this volume).

The sediment sequence recovered from the Argo Abyssal Plain is dominated by turbidites derived from bathyal or deeper regions along the Australian continental margin. These turbidites contain calcareous and siliceous biotics and abundant volcanogenic smectite; calcareous content increases upward within the section. Turbidites were deposited primarily at times of global lowstands in

sea level: Valanginian, Aptian, and Neogene. Little obviously terrigenous material has accumulated on the abyssal plain; most of this detritus has been trapped in marginal basins that flank northwest Australia.

Sedimentation patterns across the Argo Abyssal Plain shifted in the mid-Cretaceous. Prior to this time, a sediment cover of uniform thickness was deposited across the plain and turbidites were derived from both eastern and southern continental margins. From the Late Cretaceous onward, three times as much sediment accumulated at Site 765 as at Site 261, and this sediment was overwhelmingly derived from the southern margin. Neogene sediments at both sites fit models proposed (i.e., Pilkey, 1987) for sedimentation on basin plains with one main sediment entry point; turbidites compose 80%–90% of the sediment and show strong proximal-distal differences in turbidite abundance and thickness.

ACKNOWLEDGMENTS

Financial support for this work was provided by a grant from the U.S. Scientific Advisory Committee (USSAC) and a research fellowship from the Natural Environment Research Council (NERC). For technical assistance, we are grateful to James Davy, Richard Emanuel, Eugenio Gonzales, and Jonathan Krupp. We thank our fellow Leg 123 scientists and the ship's and drilling crews on board the *JOIDES Resolution* for their helpfulness and cooperation.

REFERENCES

Applegate, J. L., and Bergen, J. A., 1988. Cretaceous calcareous nannofossil biostratigraphy of sediments recovered from the Galacia margin, ODP Leg 103. *In* Boillet, G., Winterer, E. L., et al., *Proc. ODP, Sci. Results,* 103: College Station, TX (Ocean Drilling Program), 293–326.

Applegate, J. L., Bergen, J. A., Covington, J. M., and Wise, S. S., 1989. Lower Cretaceous calcareous nannofossils from continental margin drill sites off North Carolina (DSDP Leg 93) and Portugal (ODP Leg 103): a comparison. *In* Crux, J. A., and Van Heck, S. E., (Eds.), *Nannofossils and Their Applications:* Chichester (Ellis Horwood), 212–222.

Barron, E. H., Saltzman, E., and Price, D. A., 1984. Occurrence of *Inoceramus* in the South Atlantic and oxygen isotopic paleotemperatures in Hole 530A. *In* Hay, W. W., Sibuet, J.-C., et al., *Init. Repts. DSDP,* 75, Pt. 2: Washington (U.S. Govt. Printing Office), 893–904.

Baumgartner, P. O., 1984. A Middle Jurassic-Early Cretaceous low-latitude radiolarian zonation based on unitary associations and age of Tethyan radiolarites. *Eclogae Geol. Helv.,* 77:729–837.

Berger, W. H., and Winterer, E. L., 1974. Plate stratigraphy and the fluctuating carbonate line. *In* Hsü, K. J., and Jenkyns, H. C. (Eds.), *Pelagic Sediments: On Land and Under the Sea.* Int. Assoc. Sedimentol. Spec. Pub., 1:11–48.

Bernoulli, D., Garrison, R. E., and McKenzie, J., 1978. Petrology, isotope geochemistry, and origin of dolomite and limestone associated with basaltic breccia, Hole 373A, Tyrrhenian Basin. *In* Hsü, K., Montadert, L., et al., *Init. Repts. DSDP,* 42 (Pt.1): Washington (U.S. Govt. Printing Office), 541–558.

Bode, G. W., 1974a. Carbon and carbonate analyses, Leg 27. *In* Veevers, J. J., Heirtzler, J. R., et al., *Init. Repts. DSDP,* 27: Washington (U.S. Govt. Printing Office), 499–502.

_____, 1974b. Grain-size analyses, Leg 27. *In* Veevers, J. J., Heirtzler, J. R., et al., *Init. Repts. DSDP,* 27: Washington (U.S. Govt. Printing Office), 503–506.

Boote, D.R.D., and Kirk, R. B., 1989. Depositional wedge cycles on evolving plate margin, western and northwestern Australia. *AAPG Bull.,* 73:216–243.

Bouma, A. H., 1962. *Sedimentology of Some Flysch Deposits:* Amsterdam (Elsevier).

Bown, P. R., 1987. Taxonomy, evolution, and biostratigraphy of late Triassic–Early Jurassic calcareous nannofossils. *Spec. Pap. Palaeontol.,* 38:1–118.

Bown, P. R., Burnett, J. A., and Gallagher, L. T., in press. Calcareous nannofossil evolution. *Mem. Sci. Geol.*

Bown, P. R., Cooper, M.K.E., and Lord, A. R., 1988. A calcareous nannofossil biozonation scheme for the early to mid Mesozoic. *Newsl. Stratigr.,* 20(2):91–114.

Bown, P. R., and Ozcan, S., in press. Calcareous nannofossil biostratigraphy and correlation across the Jurassic/Cretaceous boundary. *Mem. Sci. Geol.*

Bralower, T. J., 1987. Valanginian to Aptian calcareous nannofossil stratigraphy and correlation with the M-sequence magnetic anomalies. *Mar. Micropaleontol.,* 11:293–310.

Bralower, T. J., Monechi, S., and Thierstein, H. R., 1989. Calcareous nannofossil zonation of the Jurassic/Cretaceous boundary interval and correlation with the geomagnetic polarity time scale. *Mar. Micropaleontol.,* 14:153–235.

Buchbinder, B., Benjamini, C., Mimran, Y., and Gvirtzman, G., 1988. Mass transport in Eocene pelagic chalk on the northwestern edge of the Arabian platform, Shefela area, Israel. *Sedimentology,* 35:257–274.

Buffler, R. T., 1990. Underway geophysics. *In* Ludden, J. N., Gradstein, F. M., et al., *Proc. ODP, Init. Repts.,* 123: College Station, TX (Ocean Drilling Program), 13–25.

Cook, H. E., Zemmels, I., and Matti, J. C., 1974. X-ray mineralogy data, eastern Indian Ocean—Leg 27, Deep Sea Drilling Project. *In* Veevers, J. J., Heirtzler, J. R., et al., *Init. Repts. DSDP,* 27: Washington (U.S. Govt. Printing Office), 535–548.

Cook, P. J., 1974. Phosphate content of sediments from Deep-Sea Sites 259-263, eastern Indian Ocean. *In* Veevers, J. J., Heirtzler, J. R., et al., *Init. Repts. DSDP,* 27: Washington (U.S. Govt. Printing Office), 455–462.

_____, 1977. Mesozoic-Cenozoic sediments of the eastern Indian Ocean. *In* Heirtzler, J. R., Bolli, H. M., Davies, T. A., Saunders, J. B., and Sclater, J. G. (Eds.), *Indian Ocean Geology and Biostratigraphy:* Washington (Am. Geophys. Union), 119–150.

Cooper, M.K.E., 1985. Nannofossils across the Jurassic/Cretaceous boundary in the Tethyan Realm. *In* Michelsen, O., and Zeiss, A. (Eds.), *Proc. Int. Symp. Jurassic Stratigr.,* 2:429–443.

_____, 1989. Nannofossil provincialism in the Late Jurassic-Early Cretaceous (Kimmeridgian to Valanginian) period. *In* Crux, J. A., and Van Heck, S. E. (Eds.), *Nannofossils and Their Applications:* Chichester (Ellis Horwood), 223–246.

Crux, J. A., 1989. Biostratigraphy and paleogeographical applications of Lower Cretaceous nannofossils from north-western Europe. *In* Crux, J. A., and Van Heck, S. E. (Eds.), *Nannofossils and Their Applications:* Chichester (Ellis Horwood), 143–211.

Davies, T. A., and Kidd, R. B., 1977. Sedimentation in the Indian Ocean through time. *In* Heirtzler, J. R., Bolli, H. M., Davies, T. A., Saunders, J. B., and Sclater, J. G. (Eds.), *Indian Ocean Geology and Biostratigraphy:* Washington (Am. Geophys. Union), 61–85.

Droxler, A. W., and Schlager, W., 1985. Glacial versus interglacial sedimentation and turbidite frequency in the Bahamas. *Geology,* 13:799–802.

Falvey, D. A., 1972. Seafloor spreading in the Wharton Basin (northeast Indian Ocean) and the breakup of eastern Gondwanaland. *APEA J.,* 12:86–88.

Fullerton, L. G., Sager, W. W., and Handschumacher, D. W., 1989. Late Jurassic-Early Cretaceous evolution of the eastern Indian Ocean adjacent to northwest Australia. *J. Geophys. Res.,* 94(B3):2937–2953.

Garrison, R. E., and Fischer, A. G., 1969. Deep-water limestones and radiolarites of the Alpine Jurassic. *In* Friedman, G. M. (Ed.), *Depositional Environments in Carbonate Rocks, A Symposium.* Spec. Publ.—Soc. Econ. Paleont. Mineral., 14:20–56.

Garrison, R. E., Hein, J. R., and Anderson, T. F., 1973. Lithified carbonate sediment and zeolitic tuff in basalts, Mid-Atlantic Ridge. *Sedimentology,* 20:399–410.

Garrison, R. E., and Kennedy, W. J., 1977. Origin of solution seams and flaser structure in Upper Cretaceous chalks of southern England. *Sediment. Geol.,* 19:107–137.

Golubic, S., Perkins, R. D., and Lukas, K. J., 1975. Boring microorganisms and microborings in carbonate substrates. *In* Frey, R. W. (Ed.), *The Study of Trace Fossils:* New York (Springer-Verlag), 229–259.

Hallam, A., 1975. *Jurassic Environments:* Cambridge (Cambridge University Press).

Haq, B. U., Hardenbol, J., and Vail, P. R., 1987. Chronology of fluctuating sea levels since the Triassic. *Science*, 235:1156–1167.

Haq, B. U., von Rad, U., O'Connell, S., et al., 1990. *Proc. ODP, Init. Repts.*, 122: College Station, TX (Ocean Drilling Program).

Hein, J. R., and Koski, R. A., 1987. Bacterially mediated diagenetic origin for chert-hosted managanese deposits in the Franciscan Complex, California Coast Ranges. *Geology*, 15:722–726.

Heirtzler, J. R., Cameron, P., Cook, P. J., Powell, T., Roeser, H.A., Sukardi, S., and Veevers, J. J., 1978. The Argo Abyssal Plain. *Earth Planet. Sci. Lett.*, 41:21–31.

Helby, R., Morgan, R., and Partridge, A. D., 1987. A palynological zonation of the Australian Mesozoic. *In* Jell, P. A. (Ed.), *Studies in Australian Mesozoic Palynology*. Mem. Assoc. Australas. Paleontol., 4:1–94.

Hinz, K., Beiersdorf, H., Exon, N. F., Roeser, H. A., Stagg, H. M. J., and von Stackelberg, U., 1978. Geoscientific investigations from the Scott Plateau off northwest Australia to the Java Trench. *BMR J. Aust. Geol. Geophys.*, 3:319–340.

Jakubowski, M., 1987. A proposed Lower Cretaceous calcareous nannofossil zonation scheme for the Moray Firth area of the North Sea. *Abh. Geol. Bundesanst (Austria)*, 39:99–119.

Jansa, L. F., Enos, P., Tucholke, B. E., Gradstein, F. M., and Sheridan, R. E., 1979. Mesozoic and Cenozoic sedimentary formations of the North American Basin; western North Atlantic. *In* Talwani, M., Hay, W., and Ryan, W.B.F. (Eds.), *Deep Sea Drilling Results in the Atlantic Ocean: Continental Margins and Paleoenvironment*. Am. Geophys. Union, Maurice Ewing Ser., 3:1–57.

Jenkyns, H. C., 1986. Pelagic environments. *In* Reading, H. G. (Ed.), *Sedimentary Environments and Facies* (2nd ed.): Oxford (Blackwell Scientific), 343–397.

Kang, J.-K., and Hein, J. R., 1988. Textural characteristics of hydrogenetic and hydrothermal Fe-Mn crusts. *Eos*, 69:1271. (Abstract)

Kauffman, E. G., 1976. Deep-sea Cretaceous macrofossils: Hole 317A, Manihiki Plateau. *In* Jackson, E. D., Schlanger, S. O., et al., *Init. Repts. DSDP*, 33: Washington (U.S. Govt. Printing Office), 503–535.

Kelts, K., and Arthur, M. A., 1981. Turbidites after 10 yr of deep-sea drilling—wringing out the mop? *In* Warme, J. E., Douglas, R. G., and Winterer, E. L. (Eds.), *The Deep Sea Drilling Project: A Decade of Progress*. Spec. Publ.—Soc. Econ. Paleont. Mineral., 32:91–127.

Kennett, J., 1982. *Marine Geology:* Englewood Cliffs, NJ (Prentice-Hall).

Kutznetsova, K. I., 1974. Distribution of benthonic foraminifera in Upper Jurassic and Lower Cretaceous deposits at Site 261, DSDP Leg 27, in the eastern Indian Ocean. *In* Veevers, J. J., Heirtzler, J. R., et al., *Init. Repts. DSDP*, 27: Washington (U.S. Govt. Printing Office), 637–682.

Lancelot, Y., Larson, R. L., et al., 1990. *Proc. ODP, Init. Repts.*, 129: College Station, TX (Ocean Drilling Program).

Larson, R. L., 1975. Late Jurassic seafloor spreading in the eastern Indian Ocean. *Geology*, 3:69–71.

Ludden, J. N, Gradstein, F. M. , et al., 1990. *Proc. ODP, Init. Repts.*, 123: College Station, TX (Ocean Drilling Program).

Masters, B. A., and Scott, R. W., 1979. Calcispheres and nannoconids. *In* Fairbridge, R. W., and Jablonski, D. (Eds.), *The Encyclopedia of Paleontology:* Stroudsburg (Dowden, Hutchinson, and Ross), 167–170.

McKnight, B. K., 1974. Heavy mineral content of sediments from Deep Sea Drill Sites 259–263, eastern Indian Ocean. *In* Veevers, J. J., Heirtzler, J. R., et al., *Init. Repts. DSDP*, 27: Washington (U.S. Govt. Printing Office), 523–534.

Mutterlose, J., 1989. Temperature-controlled migration of calcareous nannofossils in the north-west European Aptian. *In* Crux, J. A., and Van Heck, S. E. (Eds.), *Nannofossils and Their Applications:* Chichester (Ellis Horwood), 122–142.

Oertli, H. J., 1974. Lower Cretaceous and Jurassic ostracods from DSDP Leg 27—a preliminary account. *In* Veevers, J. J., Heirtzler, J. R., et al., *Init. Repts. DSDP*, 27: Washington (U.S. Govt. Printing Office), 947–966.

Perch-Nielsen, K., 1985. Mesozoic calcareous nannofossils. *In* Bolli, H. M., Saunders, J. B., and Perch-Nielsen, K. (Eds.), *Plankton Stratigraphy:* Cambridge (Cambridge University Press), 329–426.

Peterson, L. C., and Prell, W. L., 1985. Carbonate preservation and rates of climatic change; an 800 k.y. record from the Indian Ocean. *In* Sundquist, E. T., and Broecker, W. S. (Eds.), *The Carbon Cycle and Atmospheric CO_2: Natural Variations, Archean to Present:* Am. Geophys. Union Monogr., 32:251–269.

Pilkey, O. H., 1987. Sedimentology of basin plains. *In* Weaver, P.P.E., and Thompson, J. (Eds.), *Geology and Geochemistry of Abyssal Plains*. Geol. Soc. Spec. Publ. London, 31:1–12.

Potter, P. E., Maynard, J. B. , and Pryor, W. A., 1984. *Sedimentology of Shale:* New York (Springer-Verlag).

Proto Decima, F., 1974. Leg 27 calcareous nannoplankton. *In* Veevers, J. J., Heirtzler, J. R., et al., *Init. Repts. DSDP*, 27: Washington (U.S. Govt. Printing Office), 589–622.

Renz, G. W., 1974. Radiolaria from Leg 27 of the Deep Sea Drilling Project. *In* Veevers, J. J., Heirtzler, J. R., et al., *Init. Repts. DSDP*, 27: Washington (U.S. Govt. Printing Office), 769–842.

Robinson, P. T., Thayer, P. A., Cook, P. J., and McKnight, B. K., 1974. Lithology of Mesozoic and Cenozoic sediments of the eastern Indian Ocean, Leg 27, Deep Sea Drilling Project. *In* Veevers, J. J., Heirtzler, J. R., et al., *Init. Repts. DSDP*, 27: Washington (U.S. Govt. Printing Office), 1001–1048.

Roth, P. H., 1978. Cretaceous nannoplankton biostratigraphy and oceanography of the northwestern Atlantic Ocean. *In* Benson, W. E., Sheridan, R. E., et al., *Init. Repts. DSDP*, 44: Washington (U.S. Govt. Printing Office), 731–759.

_____, 1983. Jurassic and Lower Cretaceous calcareous nannofossils in the western North Atlantic (Site 534): biostratigraphy, preservation, and some observations on biogeography and paleoceanography. *In* Sheridan, R. E., Gradstein, F. M., et al., *Init. Repts. DSDP*, 76: Washington (U.S. Govt. Printing Office), 587–621.

_____, 1986. Mesozoic palaeoceanography of the North Atlantic and Tethys oceans. *In* Summerhayes, C. P., and Shackleton, N. J. (Eds.), *North Atlantic Palaeoceanography*. Geol. Soc. Spec. Publ., 21:299–320.

Roth, P. H., Medd, A. W., and Watkins, D. K., 1983. Jurassic calcareous nannofossil zonation, an overview with new evidence from Deep Sea Drilling Project Site 534A. *In* Sheridan, R. E., Gradstein, F. M., et al., *Init. Repts. DSDP*, 76: Washington (U.S. Govt. Printing Office), 573–579.

Roth, P. H., and Krumbach, K. R., 1986. Middle Cretaceous calcareous nannofossil biogeography and preservation in the Atlantic and Indian Oceans: implications for paleoceanography. *Mar. Micropaleontol.*, 10:235–266.

Scholle, P. A., Arthur, M. A., and Ekdale, A. A., 1983. Pelagic environments. *In* Scholle, P. A., Bebout, D. G., and Moore, C. H. (Eds.), *Carbonate Depositional Environments*. AAPG Mem., 33:620–691.

Sclater, J. G., Abbott, D., and Thiede, J., 1977. Paleobathymetry and sediments of the Indian Ocean. *In* Heirtzler, J. R., Bolli, H. M., Davies, T. A., Saunders, J. B., and Sclater, J. G. (Eds.), *Indian Ocean Geology and Biostratigraphy:* Washington (Am. Geophys. Union), 25–59.

Shanmugam, G., and Moiola, R. J., 1982. Eustatic control of turbidites and winnowed turbidites. *Geology*, 10:231–235.

Stagg, H.M.J., and Exon, N. F., 1981. Geology of the Scott Plateau and Rowley Terrace, off northwestern Australia. *Bur. Miner. Resour. Aust. Bull.*, 213:1–53.

Stow, D.A.V., and Miller, J., 1984. Mineralogy, petrology, and diagenesis of sediments at Site 530, southeast Angola Basin. *In* Hay, W. W., Sibuet, J.-C., et al., *Init. Repts. DSDP*, 75: Washington (U.S. Govt. Printing Office), 857–873.

Stow, D.A.V., and Piper, D.J.W., 1984. Deep-water fine-grained sediments: facies models. *In* Stow, D.A.V., and Piper, D.J.W. (Eds.), *Fine-Grained Sediments: Deep-Water Processes and Facies:* Oxford (Blackwell), 611–645.

Tappan, H., 1980. *The Paleobiology of Plant Protists:* San Francisco (W. H. Freeman).

Tassé, N., and Hesse, R., 1984. Origin and significance of complex authigenic carbonates in Cretaceous black shales of the western Alps. *J. Sediment. Petrol.*, 54:1012–1027.

Thayer, P. A., Hostettler, J., and Smith, S., 1974. Grain-size distribution of sediments from the eastern Indian Ocean: Deep Sea Drilling Project, Leg 27. *In* Veevers, J. J., Heirtzler, J. R., et al., *Init. Repts. DSDP*, 27: Washington (U.S. Govt. Printing Office), 507–522.

Thiede, J., and Dinkelman, M. G., 1977. Occurrence of *Inoceramus* remains in late Mesozoic pelagic and hemipelagic sediments. *In* Supko, P. R., Perch-Nielsen, K., et al., *Init. Repts. DSDP*, 39: Washington (U.S. Govt. Printing Office), 899–910.

Thierstein, H. R., 1981. Late Cretaceous nannoplankton and the change at the Cretaceous/Tertiary boundary. *In* Warme, J. E., Douglas, R. G., and Winterer, E. L. (Eds.), *The Deep Sea Drilling Project: A Decade of Progress*. Spec. Publ.—Soc. Econ. Paleont. Mineral., 32:355–394.

van Andel, T. H., 1975. Mesozoic-Cenozoic calcite compensation depth and the global distribution of calcareous sediments. *Earth Planet. Sci. Lett.*, 26:187–194.

Veevers, J. J., Heirtzler, J. R., et al., 1974. *Init. Repts. DSDP*, 27: Washington (U.S. Govt. Printing Office).

Veevers, J. J., and Johnstone, M. H., 1974. Comparative stratigraphy and structure of the western Australian margin and the adjacent deep ocean floor. *In* Veevers, J. J., Heirtzler, J. R., et al., *Init. Repts. DSDP*, 27: Washington (U.S. Govt. Printing Office), 571–585.

Veevers, J. J., Jones, J. G., and Talent, J. A., 1971. Indo-Australian stratigraphy and the configuration and dispersal of Gondwanaland. *Nature*, 229:383–388.

von Rad, U., and Exon, N. F., 1983. Mesozoic–Cenozoic sedimentary and volcanic evolution of the starved passive margin off northwest Australia. *AAPG Mem.*, 34:253–281.

von Rad, U., Thurow, J., Haq, U., Gradstein, F., and Ludden, J., et al., 1989. Triassic to Cenozoic evolution of the NW Australian continental margin and the birth of the Indian Ocean (preliminary results of ODP Legs 122 and 123). *Geol. Rundsch.*, 78:1189–1210.

Wendt, J., 1974. Encrusting organisms in deep-sea manganese nodules. *In* Hsü, K. J., and Jenkyns, H. C. (Eds.), *Pelagic Sediments: On Land and Under the Sea*. Spec. Publ. Int. Assoc. Sedimentol., 1:437–447.

Winterer, E. L., and Bosellini, A., 1981. Subsidence and sedimentation on Jurassic passive continental margin, southern Alps, Italy. *AAPG Bull.*, 65:394–421.

Wise, S. S., 1988. Mesozoic-Cenozoic history of calcareous nannofossils in the region of the southern ocean. *Palaeogeogr., Palaeoclimatol., Palaeoecol.*, 67:157–179.

Wiseman, J. F., 1979. Neocomian eustatic changes—biostratigraphic evidence from the Carnarvon Basin. *APEA J.*, 19:66–73.

Wiseman, J. F., and Williams, A. J., 1974. Palynological investigation of samples from Sites 259, 261, and 263, Leg 27. *In* Veevers, J. J., Heirtzler, J. R., et al., *Init. Repts. DSDP*, 27: Washington (U.S. Govt. Printing Office), 915–924.

Date of initial receipt: 28 May 1990
Date of acceptance: 15 May 1991
Ms 123B-156

APPENDIX

List of nannofossil species mentioned in the text, arranged in alphabetical order by generic epithets.

Assipetra infracretacea (Thierstein, 1973) Roth, 1973
Axopodorhabdus cylindratus (Noel, 1965) Wind and Wise, 1977
Axopodorhabdus dietzmannii (Reinhardt, 1965) Wind and Wise, 1983
Biscutum dubium (Noel, 1965) Grun *in* Grun et al., 1974
Biscutum ellipticum (Gorka, 1957) Grun *in* Grun and Allemann, 1975
Biscutum erismatum (Wind and Wise, 1977) Grun and Zweili, 1980
Calcicalathina oblongata (Worsley, 1971) Thierstein, 1971
Conusphaera mexicana mexicana Trejo, 1969
Conusphaera mexicana minor (Trejo, 1969) Bown and Cooper, 1989
Crepidolithus perforata (Medd, 1979) Grun and Zweili, 1980
Cretarhabdus conicus, Bramlette and Martini, 1964
Crucibiscutum salebrosum (Black, 1971) Jakubowski, 1986
Cruciellipsis cuvillieri (Manivit, 1966) Thierstein, 1971
Cyclagelosphaera argoensis Bown (this volume)
Cyclagelosphaera margerelii Noel, 1965
Diazomatolithus lehmanii Noel, 1965
Discorhabdus ignotus (Gorka, 1957) Perch-Nielsen, 1968
Eiffellithus windii Applegate and Bergen, 1989
Ethmorhabdus gallicus Noel, 1965
Ethmorhabdus hauterivianus (Black, 1971) Applegate et al. *in* Covington and Wise, 1987
Grantarhabdus coronadventis (Reinhardt, 1966) Grun *in* Grun and Allemann, 1975
Haquis circumradiatus (Stover, 1966) Roth, 1978
Haquis ellipticus (Grun *in* Grun and Allemann, 1975) Bown, this volume
Hexapodorhabdus cuvillieri Noel, 1965
Lithraphidites carniolensis Deflandre, 1963
Lotharingius crucicentralis (Medd, 1971) Grun and Zweili, 1980
Manivitella pemmatoidea (Reinhardt, 1966) Thierstein, 1977
Micrantholithus hoschultzi (Reinhardt, 1966) Thierstein, 1971
Micrantholithus obtusus Stradner, 1963
Micrantholithus speetonensis Perch-Nielsen, 1979
Microstaurus chiastius (Worsley, 1971) Grun *in* Grun and Allemann, 1975
Nannoconus Kamptner, 1931
Pickelhaube furtiva (Roth, 1983) Applegate et al. *in* Covington and Wise, 1987
Podorhabdus grassei Noel, 1965
Repagulum parvidentatum (Deflandre and Fert, 1954) Forchheimer, 1972
Retecapsa angustiforata Black, 1971
Retecapsa crenulata (Bramlette and Martini, 1964) Grun *in* Grun and Allemann, 1975
Retecapsa surirella (Deflandre and Fert, 1954) Grun *in* Grun and Allemann, 1975
Rhagodiscus asper (Stradner, 1963) Reinhardt, 1967
Rhagodiscus nebulosus Bralower *in* Bralower et al., 1989
Rotelapillus laffittei (Noel, 1957) Noel, 1973
Sollasites Black, 1967
Sollasites arcuatus Black, 1971
Speetonia colligata Black, 1971
Stephanolithion bigotii bigotii Deflandre, 1939
Tegulalithus septentrionalis (Stradner, 1963) Crux, 1986
Tegumentum striatum (Black, 1971) Crux, 1989
Tubodiscus verenae Thierstein, 1973
Vagalapilla matalosa (Stover, 1966) Thierstein, 1973
Vagalapilla stradneri (Rood et al., 1971) Thierstein, 1973
Watznaueria barnesae (Black *in* Black and Barnes, 1959) Perch-Nielsen, 1968
Watznaueria biporta Bukry, 1969
Watznaueria britannica (Stradner, 1963) Reinhardt, 1964
Watznaueria fossacincta (Black, 1971) Bown *in* Bown and Cooper, 1990
Watznaueria manivitae Bukry, 1973
Zeugrhabdotus cooperi Bown (this volume)
Zeugrhabdotus embergeri (Noel, 1958) Perch-Nielsen, 1985
Zeugrhabdotus erectus (Deflandre, 1958) Reinhardt, 1965

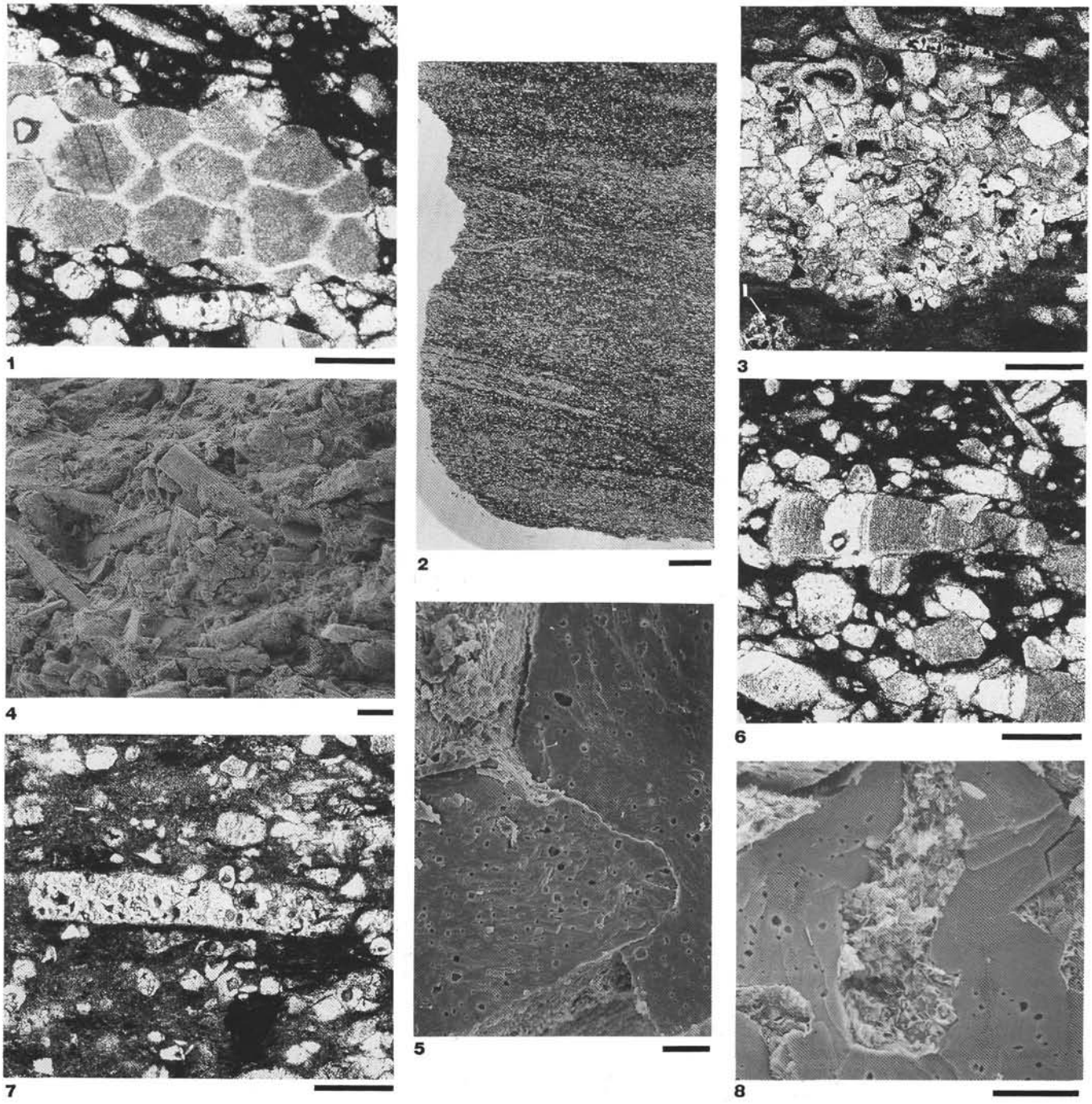

Plate 1. Microtextures of inoceramid sediment and inoceramid prisms. 1, 2, 3, 6, and 7 are photomicrographs; 5 and 8 are high-magnification SEM photographs; scale bars = 10 μm; 1, 2, 4, 5, and 6, Sample 123-765C-62R-1, 131–134 cm. **1.** Inoceramid shell fragment with prisms still articulated. Scale bar = 0.5 mm. **2.** Abundant inoceramid prisms, locally concentrated into lenses and laminae. Scale bar = 2 mm. **3.** Detail of inoceramid prism lens; elongate prisms largely oriented parallel to bedding. Prism in lower left (I) has highly irregular outline and appears to be etched; Sample 123-765C-61R-5, 51–55 cm; scale bar = 0.5 mm. **4.** Low-magnification SEM photograph of inoceramid prism concentration; view perpendicular to bedding plane. Some elongate prisms are at high angle to overall fabric; scale bar = 150 μm. **5.** Sutured, interpenetrative contact between inoceramid prisms in concentrated lens. **6.** Sample shown in **5**; note overly close packing and interpenetrative grain-grain contacts. Elongate inoceramid prism in center contains clouded (organic inclusion-rich) bands. Scale bar = 0.5 mm. **7.** Inoceramid prism with abundant irregular pits (probable microborings); Sample 123-765C-61R-5, 51–55 cm; scale bar = 0.5 mm. **8.** Cylindrical, clay-filled pit with bulbous termination in inoceramid prism; straight segments of pit outline may have been modified by secondary etching (Sample 123-765C-61R-5, 74–76 cm).

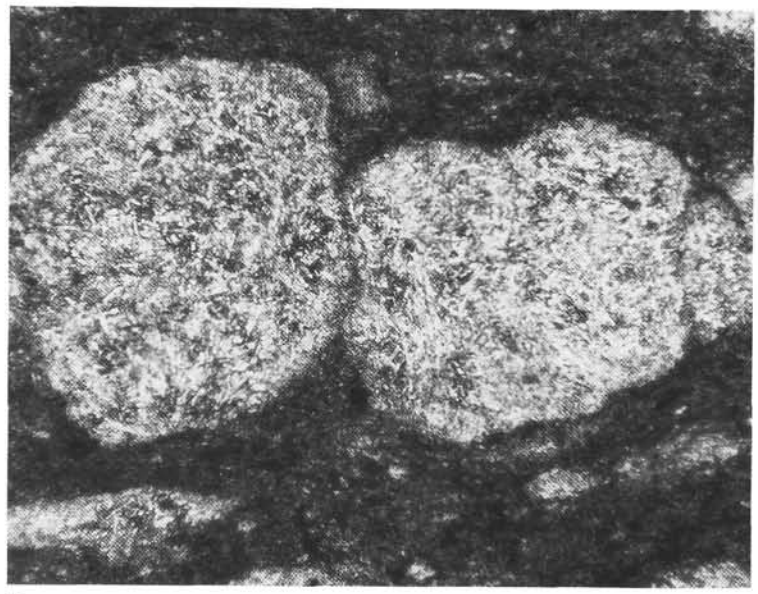

1

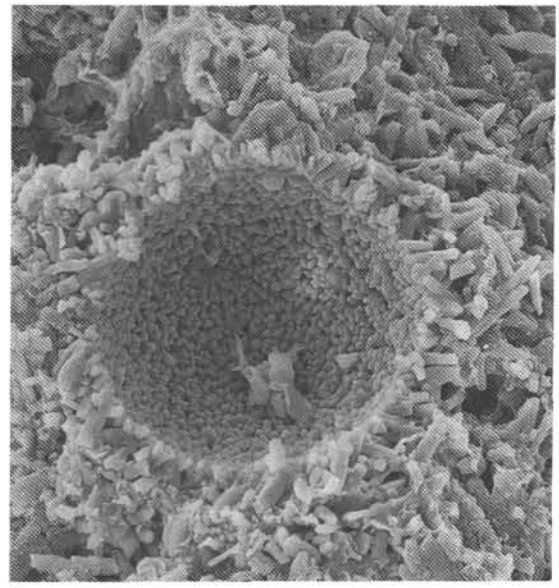

2

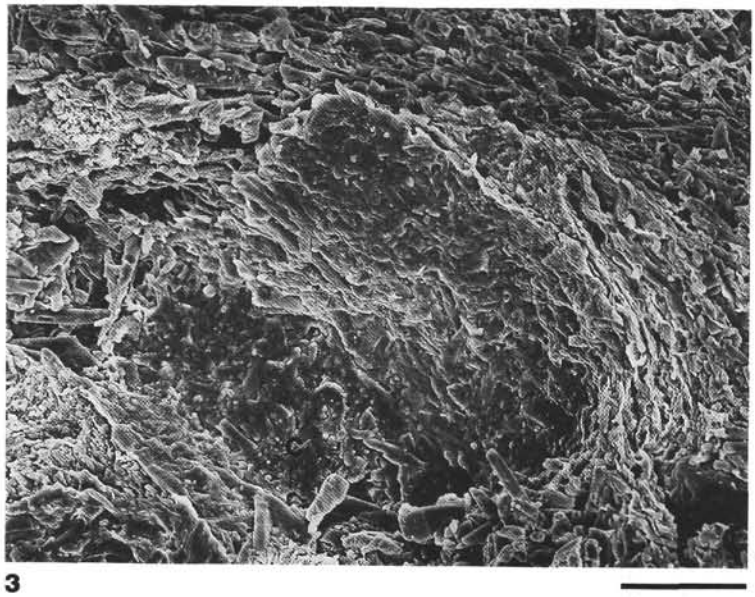

3

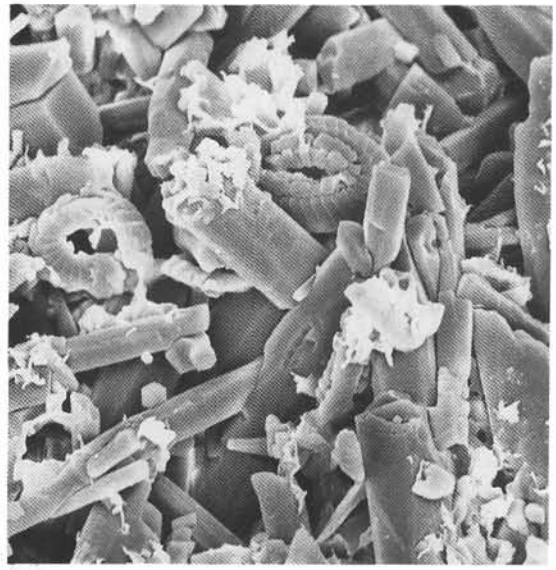

4

Plate 2. Microtextures of layers rich in calcispheres and calcite needles derived from the breakdown of calcisphere tests (1, 2, and 4, Sample 27-261-32-2, 49–52 cm; 3, Sample 123-765C-61R-5, 55–57 cm. **1.** Photomicrograph with crossed nicols of clasts rich in calcite needles; scale bar = 0.1 mm. **2.** SEM micrograph of calcisphere test, illustrating breakdown into discrete needles. Scale bar = 15 µm. **3.** High-magnification SEM photograph of needle-rich clast. More clay-rich, less well-cemented matrix wraps around needle-rich, better-cemented clast, which contains recrystallized coccoliths (C). Scale bar = 15 µm. **4.** SEM micrograph of matrix shown in **1**. Abundant needles consist of low magnesian calcite; coccoliths are *Watznaueria* sp. Scale bar = 4 µm.

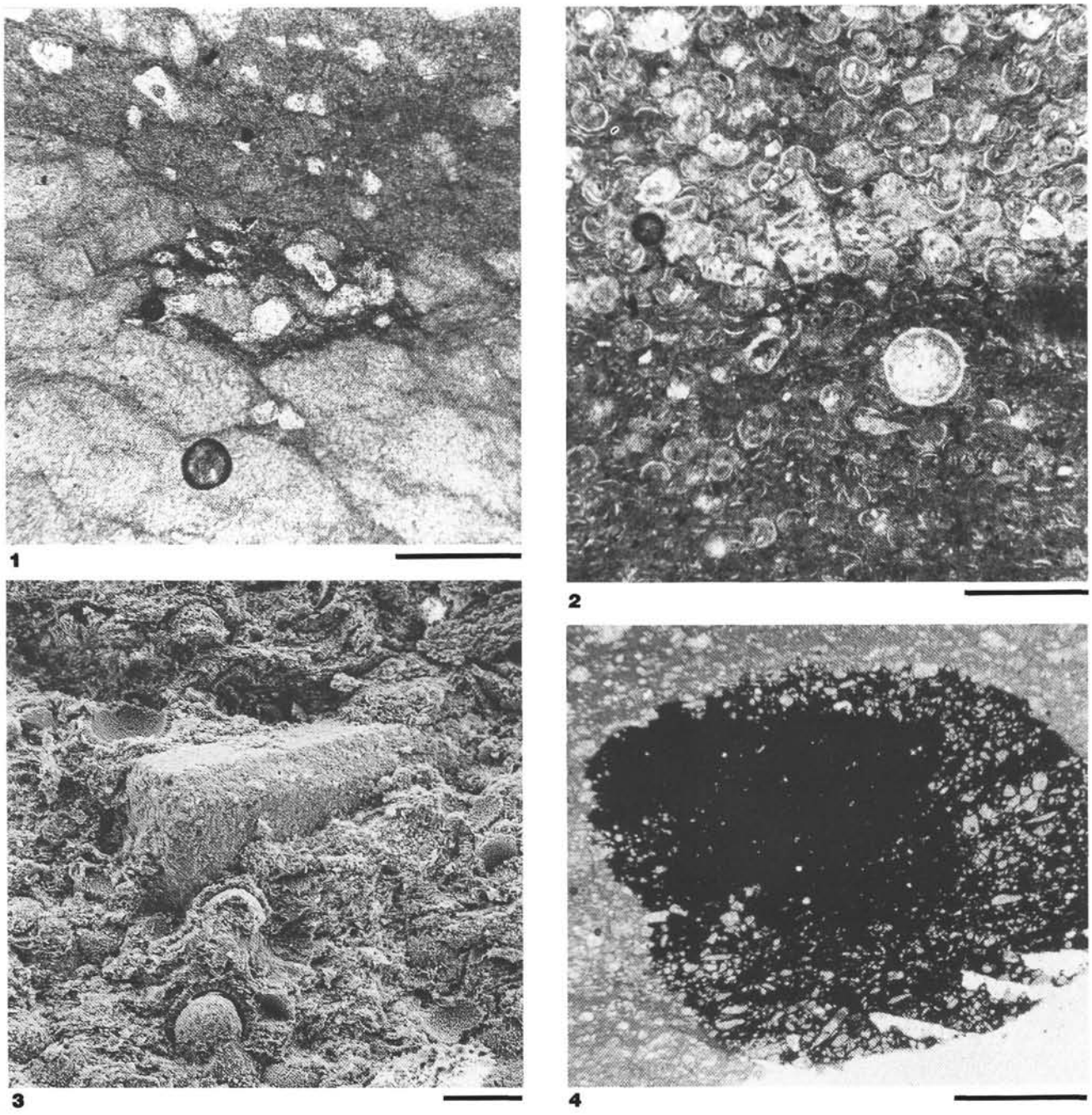

Plate 3. Microtextures in inoceramid sediment unit; 1, 2, and 4 are photomicrographs. **1.** Layer rich in clasts made of calcite needles (calcisphere debris) shows irregular (burrowed) upper surface. Sample 123-765C-61R-5, 57–59 cm; scale bar = 0.2 mm. **2.** Calcisphere-rich layer overlies muddier zone. Sample 123-765C-61R-4, 21–25 cm; scale bar = 0.2 mm. **3.** SEM micrograph of calcisphere-rich lens shown in **2**; inoceramid prism in center. Scale bar = 50 µm. **4.** Manganese nodule encloses inoceramid prisms and has partially replaced some prisms; texture indicates nodule grew in place. Sample 123-765C-62R-2, 91–95 cm; scale bar = 1.0 mm.

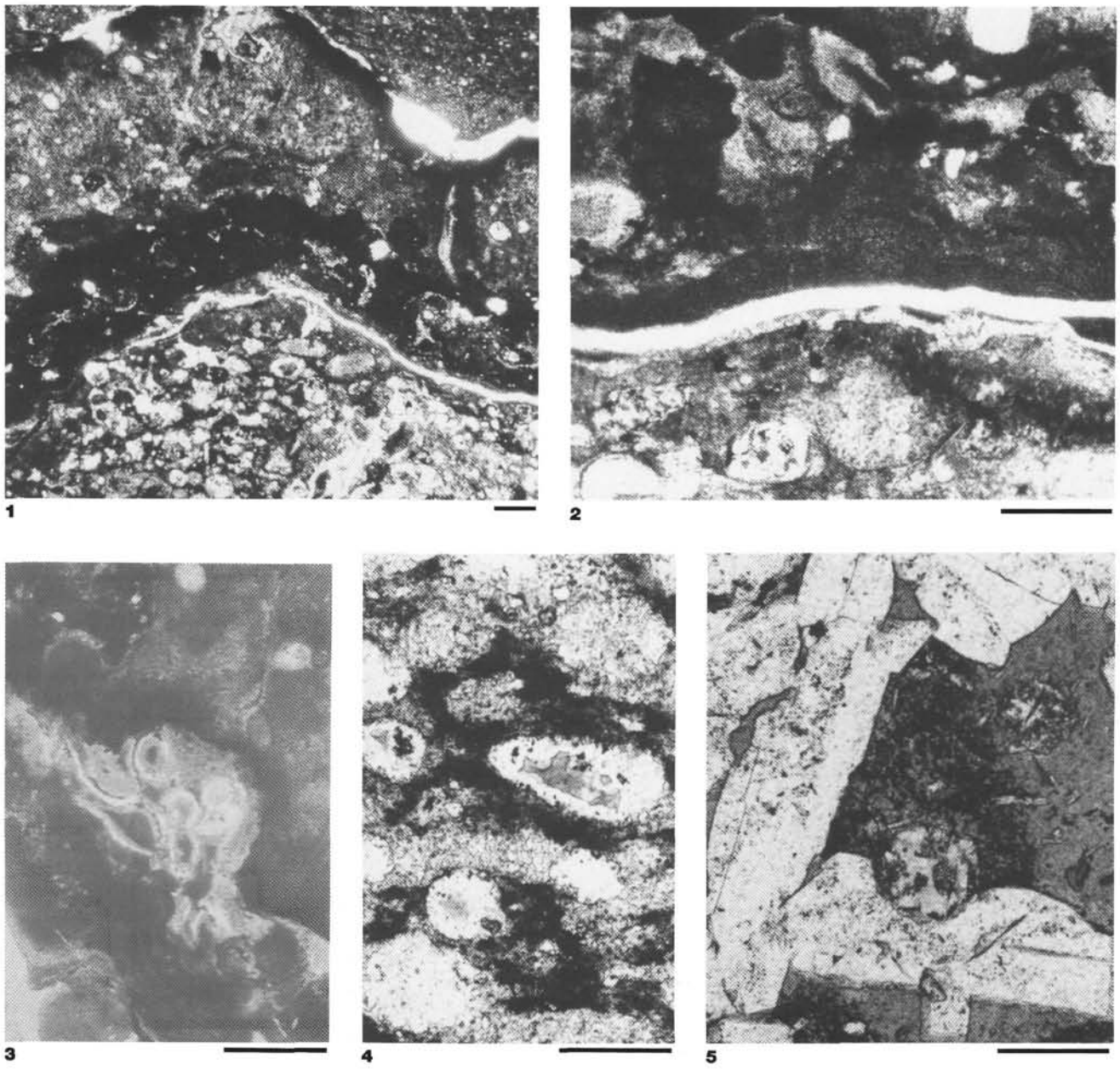

Plate 4. Photomicrographs of features of radiolarian claystone facies; scale bars equal 0.2 mm. **1.** Ferromanganese crust shown in text Figure 6; crust overlies sand rich in calcitized radiolarians and contains detrital material and microfossils (Sample 123-765C-61R-2, 94–95 cm). **2.** Close-up of lower part of crust shown in **1**; lowest layer has well-developed colloform texture. **3.** Sessile arenaceous foraminifer (*Ammolagena clavata*) attached to upper surface of crust shown in **1**. **4.** Radiolarians recrystallized to microcrystalline quartz and filled with chalcedony cement (Sample 123-765C-53R-5, 71–75 cm). **5.** Pyritized radiolarians in micronodules of manganese carbonate surrounded by large, euhedral crystals of barite (Sample 123-765C-52R-1, 114–116 cm).

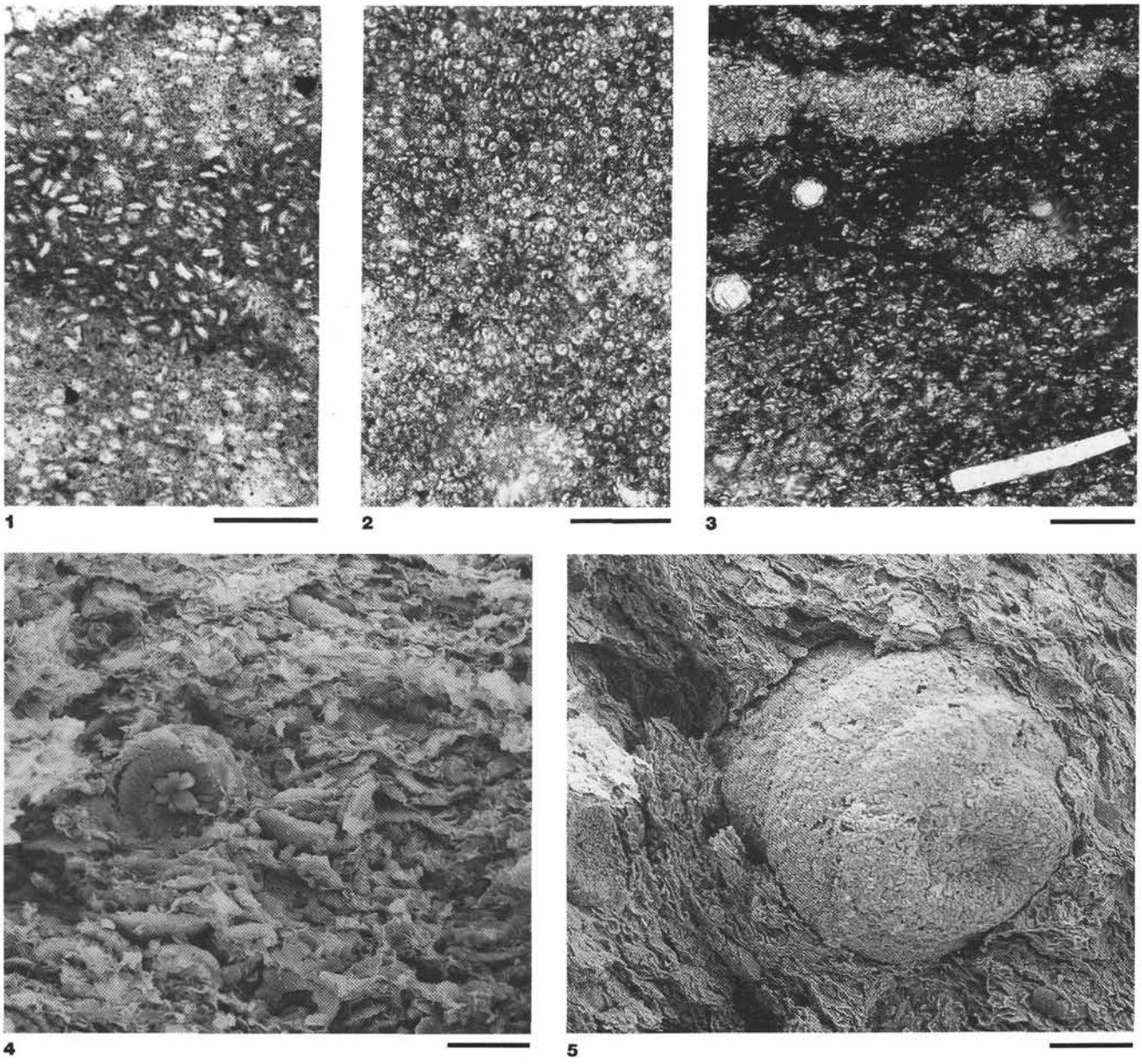

Plate 5. Microtextures of brown nannofossil claystone (Tithonian). 1, 2, and 3 are photomicrographs; scale bars equal 0.1 mm (Sample 27-261-32-3, 146–150 cm). 4 and 5 are high-magnification SEM photographs; scale bars equal 10 and 30 μm, respectively. **1.** Abundant robust coccoliths (*Watznaueria manivitae*) well-aligned parallel to bedding, in side view. **2.** As for **1**, but plane view. **3.** Coccoliths concentrated into microlens. Spheres in left center are calcispheres filled with sparry calcite cement; elongate form in lower right is phosphatic debris. **4.** *Watznaueria manivitae* in distal and side view, etched and overgrown. View perpendicular to bedding; note that coccoliths are predominantly aligned parallel to clay fabric (Sample 27-261-32-4, 0–1 cm). **5.** Agglutinated foraminifer (*Glomospira charoides*) (right) and calcisphere fragment (left) (Sample 27-261-32-4, 100–101 cm).